Monocyte / Macrophage Activation and Traffic Mediates HIV and SIV – Associated Peripheral Neuropathy

Author: Jessica Robyn Lakritz

MONOCYTE / MACROPHAGE ACTIVATION AND TRAFFIC MEDIATES HIV AND SIV – ASSOCIATED PERIPHERAL NEUROPATHY

JESSICA ROBYN LAKRITZ

A dissertation submitted to the Faculty of the department of Biology in partial fulfillment of the requirements for the degree of Doctor of Philosophy

Boston College
Morrissey College of Arts and Sciences
Graduate School

September 2016

MONOCYTE / MACROPHAGE ACTIVATION AND TRAFFIC MEDIATES HIV AND SIV – ASSOCIATED PERIPHERAL NEUROPATHY

Jessica Robyn Lakritz

Advisor: Tricia Helen Burdo, Ph.D.

Abstract

Human immunodeficiency virus-associated peripheral neuropathy (HIV-PN) continues to be a prevalent comorbidity of HIV infection, despite virologic control due to effective antiretroviral therapy (ART). Symptoms include bilateral tingling, numbness, and pain in distal extremities. Severity of symptoms is associated with a loss of intraepidermal nerve fiber density (IENFD) in the feet. Damage to the dorsal root ganglia (DRG) has also been observed in post-mortem tissue analysis from patients with HIV-PN. Treatment options are limited due to a lack of understanding of the disease pathogenesis. Chronic monocyte activation and accumulation of macrophages in peripheral nervous system (PNS) tissues has been reported but few studies have directly demonstrated the role of monocyte/macrophage activation and traffic in the pathogenesis of HIV-PN. The central hypothesis of this thesis is that monocyte activation and traffic mediates PNS neuronal damage.

We addressed this hypothesis in several ways. In chapter 2, we describe pathology seen in a rapid disease progression animal model of HIV-PN. We found that an early loss of IENFD preceded a loss of small diameter DRG neurons. In chapter 3, we associated DRG pathology with an accumulation of inflammatory macrophages surrounding DRG neurons. Increased monocyte traffic to the DRG was associated with severity of DRG pathology and with a loss

of IENFD. In chapter 4, we directly tested the impact of monocyte traffic on DRG pathology by blocking leukocyte traffic with an anti-VLA-4 antibody, natalizumab. Blocking cell traffic reduced accumulation of macrophages in the DRG and improved pathology. Next we treated animals with methylglyoxal-bis-guanylhydrazone (MGBG) to specifically target myeloid cells and reduce their activation. MGBG treatment improved DRG pathology and reduced accumulation of macrophages in tissues. Having demonstrated the role of monocyte traffic and activation, we aimed to identify signaling proteins and inflammatory proteins associated with PNS pathology. We found elevated monocyte chemoattractants in DRG tissue and elevated markers of monocyte activation in plasma that were associated with a loss of IENFD.

Together, these studies demonstrate that systemic monocyte activation, macrophage accumulation in DRG tissue, and monocyte traffic plays a major role in SIV-PN pathogenesis. These studies provide novel insight into immune mechanisms that impact neuronal loss during SIV infection. Thus, modulating macrophage activation and reducing monocyte traffic may have therapeutic benefits to patients suffering from or at risk of developing HIV-PN.

TABLE OF CONTENTS

LIST OF TABLES

LIST OF FIGURES

LIST OF ABBREVIATIONS

AIDS	acquired immunodeficiency syndrome
ANI	asymptomatic neurocognitive impairment
ART	antiretroviral therapy
ATN	antiretroviral neurotoxicity
ATP	adenosine triphosphate
AZT	azidothymidine
BrdU	bromodeoxyuridine
CA	capsid
cART	combined antiretroviral therapy
CCL*X*	C-C motif ligand *X*
CCR*X*	C-C motif receptor *X*
CD*X*	cluster of differentiation marker *X*
CDRG	cervical dorsal root ganglia
CGRP	calcitonin gene-related protein
CMV	cytomegalovirus
CNS	central nervous system
CVC	cenicriviroc
CVD	cardiovascular disease
CXCL*X*	C-X-C motif chemokine ligand *X*
CXCR*X*	C-X-C motif chemokine receptor *X*
d4T	stavudine
ddC	zalcitabine
ddI	didanosine
dNTP	deoxynucleotide
DPI	days post-infection
DRG	dorsal root ganglia
DSP	distal symmetric polyneuropathy
ELISA	enzyme linked immunosorbent assay
FIV	feline immunodeficiency virus
H&E	hematoxlyin and eosin
HAART	highly active antiretroviral therapy
HAD	HIV-associated dementia
HAND	HIV-associated neurocognitive disorders
HIV	human immunodeficiency virus
HTLV	human T-lymphotropic virus
IB4	Isolection B4
IENFD	intraepidermal nerve fiber density
IFN	interferon
IHC	immunohistochemistry
IL	interleukin
IN	integrase
INs	integration inhibitors
LAV	lymphadenopathy-associated virus

LDRG	lumbar dorsal root ganglia
LTR	long terminal repeats
MA	matrix
MGBG	methylglyoxal bis(guanylhydrazone)
MIP	macrophage inflammatory protein
MND	mild neurocognitive disorder
MNGC	multinucleated giant cell
MRP-14	migratory inhibitory factor-related protein 14
NBF	neutral buffered formalin
NC	nucleocapsid
NF	neurofilament
NGF	nerve growth factor
NgR	nogo-66 receptor
NK	natural killer
NNRTI	non-nucleoside reverse transcriptase inhibitors
NRTI	nucleoside/nucleotide reverse transcriptase inhibitors
PEP	post-exposure prophylaxis
PI	protease inhibitor
PIC	pre-intregration complex
PCR	polymerase chain reaction
PML	progressive multifocal leukoencephalopathy
PN	peripheral neuropathy
PNS	peripheral nervous system
PR	protease
PrEP	pre-exposure prophylaxis
RANTES	regulated on activation, normal T cell expressed and secreted
RT	reverse transcriptase
SAIDS	simian acquired immunodeficiency syndrome
SAMDC	S-adenosylmethionine decarboxylase
SAMHD1	sterile alpha motif- and HD domain-containing protein 1
SDRG	sacral dorsal root ganglia
SIV	simian immunodeficiency virus
SIVE	SIV-associated encephalitis
SN	sensory neuropathy
SP	substance P
Tat	trans-activator of transcription
TDRG	thoracic dorsal root ganglia
Th*X*	type *X* T helper
TNF	tumor necrosis factor
TNFRSF9	tumor necrosis factor receptor superfamily 9
VCAM-1	vascular cell adhesion molecule 1
VLA-4	very late antigen 4
VPR	viral protein R
VPX	viral protein X
VPS	vacuolar protein sorting
WPI	weeks post-infection

ACKNOWLEDGEMENTS

I feel extremely fortunate to have worked under Dr. Tricia Burdo during my time at Boston College. Trish is a very driven scientist and has taught me how to pursue scientific inquiry, work efficiently, and have fun while doing so. I appreciate the fact that she respected and valued my opinions and treated me as an equal. She always had helpful suggestions for troubleshooting experiments or to help interpret data. She created a wonderful working environment and knew when and how much to push me. On a personal level, she has also been a wonderful role model as a woman in science. I admire her ability to balance family and work, and excel at both. Going forward, I'm sure that I can always reach out to her for career or personal advice. The process of earning a Ph.D. was certainly made easier and more enjoyable due to Trish's wonderful mentoring and the relationship we formed.

I would also like to thank Dr. Kenneth Williams. He has served as a second mentor to me, as well as a collaborator. He has provided great advice for experiments, data interpretation, and my future career. I am also grateful for his willingness to share lab equipment with me. I would also like to thank members of his lab including Dr. Josh Walker, Dr. Jamie Schaffer, and Jaclyn Mallard for helping out with an experiment and teaching me a new techniques. I would also like to thank Dr. Patrick Autissier for assisting with flow cytometry. He improved my flow cytometry skills greatly and has always been helpful with analyzing and running samples for me.

I would also like to thank all of the undergraduate students that have worked with me over the years. They made lab work more enjoyable, kept me on my toes, and helped me generate data faster than I ever could alone. Thank you to Ayman Bodair, Neil Shah, Jinal Ghandi, Jake Robinson, Guy Guenthner, Samshita Yalamanchili, and Cherry Au.

Thank you to the other members of my committee. Dr. Welkin Johnson has always been supportive and provided helpful comments during committee meetings. I have had the pleasure of working with Dr. Andrew Miller. He is a wonderful pathologist who never hesitated on answering questions. This thesis relied very heavily on pathology analysis, and thus this would these experiments would not have been possible without his help. Thank you to Dr. Thomas Seyfried for serving as a reader on my thesis committee.

I would also like to thank my friends and family. My parents have been very supportive of me pursuing my passion in science. They raised me to be inquisitive, driven, and to value education. I could not have reached this point without their support. Finally, I want to thank my fiancée (soon to be husband), Zachary Kublin. Zach has provided me with more support and encouragement than I thought possible could come from a single person. He pushed me to send out “just one more application” to Boston College and has listened to so many practice presentations that he has become an expert on HIV peripheral neuropathy, despite not being a biologist. He has been cheering me on endlessly and has kept me sane throughout this journey.

CHAPTER I

Introduction: A literature review of the factors contributing to HIV and SIV associated peripheral neuropathy.

LITERATURE REVIEW

I. Human Immunodeficiency Virus

a. A brief history of the HIV epidemic

Since the human immunodeficiency virus (HIV) epidemic began in the 1980's, almost 71 million people worldwide have been infected, resulting in 34 million deaths. Currently, there are estimated to be 36.7 million people infected with HIV, living across 160 countries. Despite advances in treatment and prevention, there were 2.1 million new infections in 2015. Treatment compliance and availability remains problematic. Less than half of those infected with HIV are on antiretroviral therapy and 1.1 million individuals died from acquired immune deficiency syndrome (AIDS)-related illnesses in 2015 (Figure 1.1) [4].

The virus was first reported in the United States in 1981 when four, young, gay men in Los Angeles were reported to have a rare lung infection called *Pneumocytosis carinii pneumonia* and other rare infections, suggesting a new form of cellular immunodeficiency [5]. By the end of 1981, 270 individuals, all in the gay population, had similar reports of severe immunodeficiency and 121 of those individuals died. A few years later, a retrovirus from a family of human T-cell leukemia viruses (HTLV) named Lymphadenopathy Associated Virus (LAV) by one group and human T-lymphotropic virus type III (HTLV-III) by another, was identified as the cause of AIDS [8, 9]. A few years later the virus was renamed HIV to eradicate confusion of multiple names of the same virus causing AIDS, as well as to better describe its biological function [10].

In 1987, the first HIV antiretroviral, azidothrymidine (AZT) was FDA approved for treatment of HIV [11]. However, it was quickly determined that AZT had many side

effects, and that it was ineffective in extending time to death [12]. A decade later, new classes of antiretroviral drugs were discovered and it was determined that combination therapy with multiple classes of drugs, instead of monotherapy was effective to extend life, reduce plasma viral load, and restore immune function [13, 14]. These new and effective classes of drugs ushered in the era of highly active antiretroviral therapy (HAART) and combined antiretroviral therapy (cART). Currently there are six classes of HIV antiretroviral drugs including non-nucleoside reverse transcription inhibitors (NNRTIs), nucleoside reverse transcriptase inhibitors (NRTIs), protease inhibitors (PIs), fusion inhibitors, entry inhibitors, and integrase inhibitors (INs). There are 25 HIV drugs on the US market, many of which are used in combination with others. Additionally, great strides have been made in HIV prevention including post- and pre- exposure prophylaxis (PEP and PrEP) [15].

b. HIV structure and life cycle

The HIV-1 genome consists of nine open reading frames, which encode 15 proteins. Gag, Pol, and Env polyproteins are present in all retroviruses, HIV included. The Gag polyprotein is cleaved into four proteins: MA (matrix), CA (capsid), NC (nucelocapsid), and p6. These four Gag proteins, along with two Env proteins, gp120 and gp41, make up the core and outer membrane of the virion particle. There are three Pol proteins that perform essential enzymatic steps that allow HIV to replicate. These three proteins are PR (protease), RT (reverse transcriptase), and IN (integrase). The remaining six proteins are accessory proteins that aid in gene regulation and particle assembly. Also included in the HIV viral particle is an RNA molecule [16].

The HIV-1 envelope is covered in spikes that are composed of trimmers of heterodimers made of gp120 and gp41 [17]. Gp120 binds to CD4 expressed on host immune cells, typically T helper cells and macrophages [18]. After initial binding, there is a conformational change that allows for binding to a host co-receptor, either C-C chemokine receptor type 5 (CCR5) and sometimes CXC chemokine receptor type 4 (CXCR4) [19]. Binding to the co-receptor initiates a second conformational change that allows for gp41's fusion peptide to enter the host cell's membrane [20].

Once the virus has fused and entered the host cell, the inner cone-shaped shell made of CA must uncoat to release replication enzymes RT and IN and the genomic RNA [21]. Uncoating is aided by host factor TRIM5α [22]. After uncoating, reverse transcription takes place within the cytoplasm of the host cell, which results in a linear viral DNA molecule. Reverse transcription is inhibited by host restriction factor APOBEC3G [23], but Vif, an HIV-encoded accessory protein counteracts this inhibition [24].

The viral DNA is then transported into the nucleus of the host cell as a part of the pre-intergration complex (PIC) [25]. IN first cleaves off HIV's long terminal repeats (LTRs) and then joins the 3'hydroxyl ends of the viral DNA to the cut host DNA. This process is completed by the host's machinery and a stable provirus is established. Once integration is complete, the virus is transcribed with the help of Tat, which is essential for transcriptional elongation [26, 27], and Rev, which acts as an adaptor protein for mRNA export [28, 29]. Once the mRNA has been exported out of the nucleus, the mRNA is translated by the host's machinery.

Structural proteins CA, MA, and NC are cleaved from the precursor polypeptide Gag, which together form a viral-like particle at the plasma membrane of the host cell [30]. Gag and cellular E vacuolar protein sorting (VPS) proteins are responsible for viral budding [31, 32]. Once the viral particle has budded, it needs to mature in order to become infectious. Gag and Gag-Pol are cleaved into structural proteins and enzymes by PR [33]. The mature viral particle is now ready to infect another host cell and the cycle continues (Figure 1.2).

c. An evolutionary perspective of SIV and HIV

HIV type 1 (HIV-1) was identified to be the cause of the AIDS epidemic soon after it began in 1981. Genetic analysis of clinical samples from around the world has identified three subgroups of HIV-1: M, N, and O. The vast majority of HIV infections around the world are group M, while N and O are more rare [34]. Using molecular clock analysis, it is estimated that HIV-1 group M first appeared in humans in the 1920s, but has since diversified extensively [35, 36]. Additional lentiviruses in humans and monkeys have been identified including HIV-2 and several species-specific strains of simian immunodeficiency virus (SIV). HIV-2 was first found in 1989 in an individual living in West Africa and is still common in the region. HIV-2 is less pathogenic and less easily transmitted than HIV-1 [37]. Over 40 species-specific strains of SIV have been identified and characterized. Each of these strains is named after the species from which it was isolated.

HIV-2 is closely related to a strain of SIV isolated from sooty mangabeys (SIVsmm). It is believed that HIV-2 is a result of multiple cross-species transmission events from sooty mangabeys to humans [38]. HIV-1 is most closely related to a strain

of SIV isolated from chimpanzees (SIVcpz) [39, 40]. Different HIV-1 groups are interspersed amongst SIVcpz lineages, thus each group of HIV-1 most likely arose from a separate interspecies transmission event [41]. SIVcpz arose from a recombination event from SIVrcm (red-capped mangabeys) and SIVgsn (greater spot-nosed monkeys) [42, 43].

For the most part, these SIV lentiviruses are nonpathogenic in their natural hosts, although simian AIDS (SAIDS) has been observed in captive monkeys as a result of long-term infection with SIV [44, 45]. Soon after the discovery of HIV-1, SAIDS was observed in captive rhesus macaques in U.S. primate research facilities [46-48]. The pathogenic SIV infection is believed to be a result of cross-species transmission events from sooty mangabeys (SIVsm) to rhesus macaques (SIVmac) [49, 50]. Other species of macaques including pigtailed and cynomolgus macaques develop disease similar to HIV/AIDS in humans, presumably because they are also unnatural hosts to the virus [51]. SIV infection in these primate species results in severe immunodeficiency, progressive wasting, opportunistic infection, and death, which is what is observed with HIV/AIDS during human disease [52]. SIV-infected primates have since been used as model to understand HIV disease pathogenesis and test therapeutics to treat, prevent, and cure HIV infection in humans.

d. **Clinical progression of HIV infection during the pre-cART era**

There are four clinical stages of HIV infection (Figure 1.3) [2]. The earliest stage often begins when a single HIV virion infects an individual. Initial infection is followed by an eclipse phase, lasting about two weeks. During this phase, the virus is replicating

rapidly and spreading throughout the body, however an immune response and viremia are undetectable at this phase.

Acute infection occurs 2-4 weeks post infection (wpi). This phase is characterized by high viremia and sometimes results in flu-like symptoms. During this phase, the body begins to mount an immune response consisting of antibodies against viral proteins and a CD8+ (cluster of differentiation 8) T cell response against infected cells. There is also a decline in the number of CD4+ T cells that will later partially recover. The end of acute infection is marked by a sharp decline in viral load due partially to control by the host's immune system and by exhaustion of CD4+ target cells.

Both infected and uninfected CD4+ T cells die throughout HIV infection. Uninfected T cells die from apoptosis due to over expression of death ligands, direct cytotoxicity of HIV proteins, and activation-induced cell death due to elevated and persistent immune activation [53]. There are multiple ways that infected T cells can be killed [54]. Recently, it was found that the permissibility of the host cell dictates the death pathway. Quiescent T cells die via caspase-1 mediated pryoptosis due to abortive viral infection, while activated T cells die from caspase-3-mediated apoptosis [55].

Acute infection is followed by a period of clinical latency, also known as chronic HIV infection. This period of latency can last an average of 10 years, during which patients have little or no symptoms. The virus remains active but replicates at low levels, maintaining a steady level, known as the viral set point. During this phase, the number of CD4+ T cells continues to slowly decline due to viral infection.

Finally, without treatment, patients can progress to AIDS, which is severe immunodeficiency due to a low CD4 T cell count (typically less than 200 cells/μL of

blood). With AIDS, plasma viral load increases, as the host's immune system can no longer suppress viremia. Patients with AIDS usually succumb to opportunistic infections within 3 years of an AIDS diagnosis.

Today, cART regimens can prevent progression to AIDS. Recently, HIV-infected individuals have been urged to begin treatment as soon as they are diagnosed [56]. Previous guidelines had suggested to delay beginning cART until CD4 counts fell below a certain level [57]. When patients comply with their drug regimen, viral load can be undetectable and CD4 counts rise.

e. Complications in the modern cART era

Due to advances in cART, an HIV diagnosis is no longer considered a death sentence. In fact, HIV+ persons have a lifespan only slightly shorter than the general population [58]. HIV+ patients are living longer due to suppressed or undetectable viral loads and higher CD4 counts [58]. A longer time to death has resulted in a demographic shift in the HIV+ population. Today, more than 50% of the HIV+ population in the United States is over the age of 50 [59]. Living with HIV in the modern era comes with the risk of many comorbidities due life-long exposure to cART, chronic immune activation that does not resolve after viral replication is controlled, and increased age [60, 61].

Disorders that typically appear with advanced age in uninfected individuals, appear in HIV+ individuals at a younger age [62]. While the cause of the increased prevalence of these comorbidities is not completely understood, all are linked to chronic immune activation and an aging immune system – both of which are observed in HIV patients on cART [60, 61]. As the average age of the HIV+ population increases, premature aging has become evident in the past decade. Both aging and HIV infection

are associated with inflammatory phenotypes due to T cell exhaustion and mucosal barrier dysfunction [61, 63-65]. A selection of non-AIDS related comorbidities that are found in HIV-infected persons are discussed in more detail below. HIV-associated peripheral neuropathy (HIV-PN) is discussed in section II of this chapter.

i. Cardiovascular Disease

In developed countries, where use of cART is more prevalent, about 20% of HIV-associated deaths are due to cardiovascular disease (CVD) [66]. HIV+ patients have an increased prevalence and risk of CVD and fat accumulation in cardiac tissues [67, 68]. Inflammatory proteins released from activated monocytes are a major source of cardiac tissue damage [69, 70].

ii. Metabolic Syndrome

The increased risk of metabolic syndrome is largely due to use of metabolically toxic cART drugs that cause hypertriglyceridemia, low levels of high-density lipoprotein, and insulin resistance [71]. Adipose tissue distribution is also disrupted during HIV infection, also due to long-term cART usage [72]. Certain classes of antiretroviral therapy (ART) drugs have different metabolic side effects. PI's induce accumulation of lipids and free cholesterol and they also block glucose uptake in adipocytes [73, 74]. NRTI's alter mitochondria function and inhibit adenosine triphosphate (ATP) production by binding to mitochondrial DNA-polymerase γ [75]. Many of the drugs associated with metabolic dysfunction are no longer prescribed in developed countries because of their known side effects. However, many are still widely used in poorer countries [61].

iii. Low bone density

Evidence of low bone density in HIV+ patients has increased in recent years, due in part to an aging HIV+ population [76]. HIV+ patients are three times as likely to have a bone fracture than the general population [77]. The cause of low bone density in HIV+ patients is incompletely understood, but is likely multifactorial. Possible causes include traditional risk factors, increased age, nutritional deficiencies, cART regimen, and chronic inflammation [77].

iv. Cancer

In the pre-cART era, the most prevalent cancer types amongst HIV+ individuals were considered “AIDS-defining” and they included Kaposi sarcoma, cervical cancer, and non-Hodgkin’s lymphoma [78]. In the modern cART era, the prevalence of these cancers have decreased significantly as patients are not progressing to AIDS. However, about 10% of HIV-infected patients will develop non-AIDS defining cancers [79]. In particular HIV patients are at a much greater risk of developing anal or lung cancer and melanoma than the general population, but may actually be protected against other types such as prostate, breast, and colorectal cancers [78, 80]. The reason for this is not entirely understood, although increased risk factors such as tobacco and alcohol use and co-infections with cancer-causing viruses (such as human papillomavirus, hepatitis C, or Epstein-Barr virus) likely play a role [81].

v. Neurocognitive impairment

Before cART, more than half of HIV+ individuals suffered from severe neurocognitive impairment known as HIV-associated dementia (HAD) [82]. Today, the prevalence of HAD has significantly declined due to cART, but the prevalence of mild

neurocognitive disorder (MND) and asymptomatic neurocognitive impairment (ANI) has been increasing. Together, HAD, MND, and ANI, are known as HIV-associated neurocognitive disorders (HAND) [83]. Because neurons cannot be infected with virus, it is believed that damage to neurons occurs via indirect mechanisms. The pathogenesis of HAND is still not completely understood, although several studies have linked chronic immune activation in the periphery to the severity and presence of HAND [84-89]. Additionally, brain macrophages (microglia) serve as a reservoir for virus [90, 91]. Many ART drugs have difficulty crossing the blood-brain barrier and thus are present below therapeutic values in the central nervous system (CNS), allowing for viral replication and formation of reservoirs [92-94].

II. Peripheral Neuropathies

a. Overview of neuropathic pain and the peripheral nervous system

Peripheral neuropathic pain is defined as pain that is caused by a lesion or disease of the somatosensory nervous system [95]. It is estimated that over 20 million people in the United States suffer from peripheral neuropathy. Neuropathic pain varies in manifestation and cause. Over 100 types of peripheral neuropathies have been described. It can present as spontaneous and painful sensations, hyperalgesia (hypersensivity to a mild pain stimuli), or allodynia (pain that results from a normally non-painful stimuli). It is often caused by direct damage to the peripheral nerve and is usually a secondary effect to another condition such as diabetes or HIV infection [7].

The process of sensing and perceiving pain occurs in four steps. First, transduction occurs at the terminals of primary afferent nociceptors. Different stimuli

activate the nerve endings and a chemical or electochemical signal is sent to the central nervous system, which is known as transmission. The message is transmitted along the axon of the primary afferent neuron to the neuron's cell body located in the dorsal root ganglia (DRG). Primary afferent neurons are unipolar and receive sensory information from a long axon that terminates in the periphery, such as the skin. The DRG are clusters of sensory neuronal cell bodies that lie dorsal to the spinal column. In humans, there are 31 pairs (dorsal and ventral) of ganglia, named for the location along the spinal cord. In humans, there are 8 pairs of cervical nerves, 12 pairs of thoracic nerves, 5 pairs of lumbar and sacral nerves each, and 1 pair of coccyccygeal nerves. The neuron extends past the ganglia to the CNS through the dorsal nerve root and joins with nerves in the dorsal column white matter in the spinal cord (Figure 1.4). The pain signal is then modulated to reduce activity in the transmission system. Finally, perception occurs during which the pain message is integrated and perceived by the individual [96, 97].

b. HIV-associated peripheral neuropathies

HIV-PN continues to be the most common neurologic complication of HIV infection with studies reporting between one third and two thirds of the HIV population in the US being affected in the post-cART era [98]. The most common form of HIV-PN is distal symmetric polyneuropathy (DSP). Other patterns of neuropathy in HIV patients include inflammatory demyelinating polyneuropathy, progressive polyradiculopathy, mononeuropathy multiplex, autonomic neuropathy, and diffuse infiltrative lymphocytosis syndrome [99]. However, these other types of neuropathies are rare and are often associated with severe immunosuppression or an opportunistic infection [100].

While some patients diagnosed with HIV-DSP are asymptomatic, many present with bilateral pain, numbness, and tingling in the distal extremities. Before the use of ART, HIV-DSP was associated with a low CD4 T cell count and high viral load. However, in the post-ART era, HIV-DSP prevalence has increased and is no longer associated with these risk factors. More recent studies have shown that viral load is not related to HIV-DSP diagnosis in patients on ART and diagnosis may even be associated with high CD4 counts and advanced age [101].

HIV-DSP is clinically indistinguishable from antiretroviral toxic neuropathy (ATN). ATN is caused by neurotoxicity of certain classes ART drugs. NRTIs such as d-drugs (ddC, zalcitabine; ddI, didanosine; and d4T, stavudine) cause mitochondrial toxicity. This class of drugs interferes with the γ DNA polymerase which results in disruption of mitochondrial DNA synthesis and overall mitochondrial function [102, 103]. Abnormal mitochondria have been observed in the axons and Schwann cells in patients on ddC. Today, clinicians are urged to avoid prescribing these drugs with known neurotoxicity. Symptoms and pathology associated with HIV-DSP are still observed in patients with no history of taking neurotoxic d-drugs [101].

There is currently no FDA-approved drug treatment of HIV-DSP. Pain medications used to treat neuropathic pain such as anticonvulsants, topical treatments, antidepressants, and analgesics are often prescribed to treat HIV-DSP. However, clinical trials have shown that these drugs did not perform any better than placebo treatment [104].

Treatment of HIV-DSP is difficult partly because the pathogenesis is still poorly understood. Studies in humans with HIV-DSP have proven difficult because of several

confounding factors such as drug regimen, diabetes diagnosis, and nutritional deficiencies [98, 101, 105]. Importantly, very few studies have examined the pathogenesis of HIV-DSP in humans during the post-ART era [98, 106]. However, a “dying back” of axons in distal regions has been observed. Multiple types of nerve fibers are affected, including both small and large myelinated fibers. Notably, there is a reduction of small unmyelinated nerve fibers in distal regions. Reduction of intraepidermal nerve fiber density (IENFD) in distal regions has been associated with pain and can be used as an objective marker in the diagnosis of HIV-DSP [107, 108].

In addition to changes in nerve fiber density in the extremities, there are also changes at the DRG including increased cellular infiltration of inflammatory cells, neuronophagia, and increased frequency of Nageotte nodules (Figure 1.5) [6]. However, few studies have examined human DRG pathology in the post-ART era, contributing to a lack of understanding, and thus a lack of effective treatment for HIV-DSP. Instead, studies of HIV-DSP have relied mostly on SIV-infected macaque models and transgenic mouse models [109]. Currently, little is known about the pathophysiologic mechanisms that results in neuropathic pain during HIV infection with cART [107]. HIV is unable to directly infect neurons [110], and it is unclear to what extent HIV replication in surrounding cells has on neurodegeneration *in vivo.* There are two hypotheses regarding what is causing neuronal degeneration at the DRG; 1) Neuronal damage could result from direct damage from HIV viral proteins, or 2) from indirect damage from infected and/or activated monocytes/macrophages.

HIV proteins can cause neurodegeneration *in vitro*. When gp120, the HIV envelope glycoprotein, was applied to DRG cultures, neurodegeneration was observed

consisted of decreased neurite outgrowth and mitochondrial membrane depolarization [111]. Tat (trans-activator of transcription) has also been shown to be neurotoxic. Tat can bind to neuronal cell membranes and is cytotoxic to neurons due to it's ability to activate excitatory amino acid receptors [112]. Additionally, viral protein R (Vpr), an HIV regulatory protein, induces apoptosis in human neuronal cells [113]. However, despite the *in vitro* evidence, and *in vivo* evidence from transgenic mouse studies, it is unlikely that viral proteins are the sole cause of neurodegeneration. Central nervous system (CNS) and peripheral nervous system (PNS) damage occurs in patients despite effective ART when viral load is undetectable [101, 114]. These data suggest that viral proteins are not the main cause of damage to neurons.

A hallmark of HIV infection in the post-ART era is a systemic activation of monocytes, which puts patients at risk of neurocognitive disorders, cardiovascular disease, frailty, neuropathies, and other comorbidities [115]. Inflammatory macrophages secrete cytokines such as tumor necrosis factor α (TNF-α), interleukin (IL)-1β, IL-6, IL-8, and interferon (IFN)-α that are neurotoxic through various mechanisms [114]. Some of these cytokines (such as CXCL10, IL-1β, TNF-α, and IL-6) are produced in response to HIV proteins during early, acute infection that can exacerbate the immune response or be directly neurotoxic. Chemokines produced by macrophages, such as CXC chemokine ligand type 10 (CXCL10), can be directly neurotoxic and while others, such as C-C chemokine ligand type 5 and 2 (CCL5 and CCL2), can also recruit additional immune cells to the DRG and perpetuate the tissue-damaging inflammatory response [116-119]. When neurons were cultured with supernatants from HIV-activated macrophages, which contained these inflammatory cytokines and chemokines, there

was an increase in neuronal cell death compared to neurons cultured with supernatants from inactivated macrophages [120]. The vast majority of studies investigating neurotoxicity during HIV infection have focused on CNS neurons and microglia during HAND pathogenesis. Similar mechanisms may take place during PNS neurodegeneration; however, there are key differences between the PNS and CNS, such as the immune-privileged status of the CNS due to the blood-brain-barrier and the capacity of the PNS to regenerate.

Viral proteins likely play a role in initiating early inflammatory and neurotoxic events during acute infection (before ART initiation). Activated monocytes that persist throughout infection, even after ART initiation and suppression of viral replication, are most likely perpetuating neuroinflammation resulting in a reduction of IENFD and DRG pathology. A SIV-infected macaque model of HIV-DSP demonstrated a continued loss of IENFD after ART [121]. Another study found macrophage-mediated damage to the DRG and functional damage to small nerve fibers in distal regions [122]. Thus, the majority of PNS neurodegeneration likely results from neurotoxic cytokines and chemokines that continually recruit additional inflammatory monocytes to the DRG.

c. Animal models of HIV-peripheral neuropathy

Animal models of HIV are a powerful tool to study the pathogenesis of HIV-DSP because they are easily manipulated and free of confounding factors that are associated with human studies. Mice are frequently used in immunologic studies of infection. However, there is no murine equivalent of HIV and attempts to develop one have yet to succeed. Transgenic mice expressing HIV proteins have provided some

limited insight; particularly about the neurodegenerative properties of gp120 [123, 124]. This has also been demonstrated using neuronal cell culture models [111-113].

Unlike for mice, SIV occurs naturally. SIV is genetically similar to HIV, targets the same cell populations (CD4+ lymphocytes, and monocytes/macrophages) and uses the same cell receptors as HIV [109]. One group models HIV-DSP in pigtailed macaques where they dual infect with a neurovirulent molecular clone SIV/17E-Fr and with an immunosuppressive viral swarm SIV/Delta B670. Using this model, they have observed an influx of CD68+ macrophages to the DRG, similar to what is observed during HIV infection [125].

Rhesus macaques are the most common animal model to study HIV disease progression and pathogenesis. The pathogenesis of SIV in macaques is similar to that of HIV in humans. Infection with SIVmac251 results in AIDS progression within one to two years and an incidence of SIV encephalitis (SIVE) of 18% [126], as well as mild-moderate DRG pathology. CD8 lymphocyte depletion using a chimeric humanized mouse antibody of SIV infected rhesus macaques accelerates disease progression, with AIDS occurring at 3-4 months post-infection. Administration of this antibody during acute infection results in long-term depletion of CD8+ T cells and CD8+ natural killer (NK) cells. CD8 depleted animals also have a higher incidence of SIVE and DSP [127, 128]. CD8 depletion also allows for development of more severe pathology in the DRG including satellitosis, neuronophagia, and Nageotte nodules, similar to the histopathological findings in the DRG associated with HIV-DSP in human studies. CD3+ T cells in the DRG do not seem to be associated with DRG damage in the non-depleted or the depleted SIV infected animals, further validating the important role of

monocytes/macrophages. The CD8 depleted model recapitulates histopathological components of HIV-DSP and SIV-DSP in non-depleted animals, but allows for rapid disease progression and a higher incidence of SIV-DSP [128].

III. Immune regulation of the peripheral nervous system

a. Molecular signaling of pain and inflammation

Pain and inflammation are inherently linked. An appropriate pain sensation in response to a dangerous stimulus rightfully induces inflammation because pain is often associated with tissue damage (such as in the case of a burn or a cut). In such a case, an immune response is needed for debris removal and tissue repair. It is now widely accepted that cytokines and chemokines mediate both the immune response and pain sensation. Cytokines are a large and diverse class of small, secreted signaling proteins that regulate the immune response and cellular activities such as survival and differentiation. Neuronal cell bodies in the DRG upregulate inflammatory cytokines following peripheral nerve injury [129]. Additionally, DRG neurons express cytokine receptors on their surfaces so they can appropriately respond to cytokines in their environment [130, 131]. Thus, cytokines can facilitate pain signals from the periphery to the CNS [132, 133]. Additionally, chemokines, a sub-class of cytokines, are chemotactic and can recruit additional immune cells to the DRG to further exacerbate the state inflammation and pain sensation.

Damage to the peripheral nerve results in release of nerve growth factor (NGF), CXCL1, and other cytokines/chemokines that recruit neutrophils to the damaged nerve. Neutrophils release additional cytokines and chemokines, whose main role is to recruit

macrophages to the site of injury [134]. Large numbers of macrophages traffic to the site of nerve damage 24-48 hours after the initial insult to the axon. Macrophage chemotaxis is mainly mediated by CCL2, CCL3, and CCL5. These chemokines bind to CCR2 and CCR5, expressed on activated monocytes [135, 136]. The main role of macrophages during this stage is to phagocytose debris. First, they secrete matrix metalloproteases, such as MMP-9, which break down the blood-nerve barrier. Vasoactive mediators such as calcitonin gene-related peptide (CGRP) and substance P are released from injured nerves to cause vasodilation and upregulation of integrins on endothelial cells to recruit additional immune cells to the region [137, 138].

Following peripheral nerve injury, neuronal cell bodies in the DRG react to the distant injury. Satellite cells are activated and macrophages and T cells traffic into the DRG in response to chemotactic pro-inflammatory cytokines that are released by both DRG neurons and satellite cells. Fractalkine [139] and CCL2 [140] play a large role in recruiting macrophages to the DRG following damage to a distant axon. Activated macrophages linger in the DRG for months following injury long after the distant axon has been healed. Additionally, there is a loss of sensory DRG neurons after injury that continues to decline weeks to months following the initial injury [141].

Cytokine receptors such as CCR1, CCR4, CCR5, and CXCR4 are also present on neurons, thus cytokines that released by activated immune cells in the region may also act directly on neurons [142]. Additionally, during HIV infection, HIV proteins can interact with CCR5 and CXCR4 on DRG neurons [143]. Cytokines or HIV proteins interacting with receptors on neurons can result in direct neurotoxicity [111] or in

spontaneous nociceptor activation [144, 145]. Thus, cytokines and chemokines are capable of regulating both inflammation and pain sensation [141, 146, 147].

b. Peripheral nerve degeneration and regeneration

The PNS differs from the CNS in its ability to regenerate following injury. Following PNS axonal injury, axon segments distal from the site of injury remain intact for days in primates [148] and humans [149], whereas degeneration occurs much faster in smaller rodent models of nerve injury [150]. The process of nerve degeneration after injury is known as Wallerian degeneration.

The first step of Wallerian degeneration is granular disintegration of the cytoskeleton of the axon into fine debris [151, 152]. Following injury, the blood-nerve barrier begins to breakdown along the nerve, distal to the point of injury [153]. This allows for proteins in the blood and immune cells to have access to the nerve to facilitate degeneration, and later regeneration.

The first cell type to respond to PNS injury are Schwann cells, which make up over 90% of nucleated cells in the peripheral nerve [154]. Schwann cells form the myelin sheath around myelinated nerve fibers or ensheath small-diameter unmyelinated axons [155]. After nerve injury, Schwann cells dedifferentiate and proliferate [155, 156]. Dedifferentiated Schwann cells gain phagocytic ability and remove myelin debris after the axon has disintegrated [157]. Another major role of Schwann cells is secreting factors that promote axon regrowth and survival including laminins (a prevalent component of the extracellular matrix) and nerve growth factor [158]. The process of Schwann cells promoting a healthy and controlled degeneration and regeneration of nerves lasts only for a few weeks following injury; after which, the majority of Schwann

cells undergo apoptosis or atrophy [159]. However, before this occurs dedifferentiated Schwann cells also produce cytokines and chemokines including CCL2, IL-1β, and IL-1α, which play a major role in recruiting monocytes to the site of injury [160].

Monocytes are recruited to the site of injury in large numbers a few days after the initial insult [161] and macrophages follow chemotactic cues to the site of injury [156]. Macrophages are responsible for the majority of debris phagocytosis, further activation of Schwann cells, and producing factors that aid in axon regeneration [162-164]. Macrophages remain in the nerve for months, even after the nerve has healed. Eventually, macrophages are repelled against myelin by their expression of Nogo-66 receptor (NgR)1 and 2 (receptors for myelin-associated inhibitory proteins) and they re-enter circulation [165, 166]. Thus, functional Schwann cells and macrophages are required for proper Wallerian degeneration and axonal regrowth. However, over-activation or the inability to deactivate results in failure of this process, which could lead to chronic pain and lack of nerve regeneration.

IV. The role of monocytes and macrophages during HIV and SIV infection

a. Viral infection of monocytes and macrophages

HIV and SIV are able to productively infect monocytes and macrophages even though they are nondividing cells [167]. Macrophages can express the HIV entry receptor CD4 and coreceptors CXCR4 or CCR5 [168]. Macrophages are long-lived, largely resistant to cytopathic effects of the virus, and are present in nearly every tissue type. Therefore, macrophages serve as a vehicle for viral dissemination throughout the body and constitute viral reservoirs that are difficult to target with ART [169].

The viral life cycle in macrophages differs from that in T cells because of different host factors. The rate of reverse transcription is slower in macrophages than in T cells because of a smaller pool of deoxnucleotide (dNTP) molecules since macrophages are non-dividing cells, unlike T cells [170]. There are also macrophage-specific host restriction factors that interfere with viral reverse transcription. For example, sterile alpha motif domain and HD domain-containing protein 1 (SAMHD1) reduces the pool of intracellular dNTPs in macrophages [171]. However, SAMHD1 is degraded by viral protein x (Vpx), an HIV accessory protein [172]. Nuclear import is also different, in that it occurs independently of cell division in macrophages, unlike in T cells [173]. In T cells, viral assmebly occurs at the plasma membrane [174]. In macrophages, viral assembly takes place in late endosomes, although this is still a topic of debate [175].

The activation state of macrophages may also influence the permissability of the viral infection. Early HIV infection is associated with an increase in pro-inflammatory M1 macrophages which support a T helper type- (Th) 1 response. This activation state favors formation of viral reservoirs and increased viral transcription. During the later stages of infection, there is a shift from M1 towards M2 polarized macrophages, which restrict the expansion of the viral reservoir [176].

b. Chronic monocyte activation during HIV and SIV infection

Macrophages are part of the myeloid lineage, which originates in the bone marrow. Hematopoietic stem cells differentiate into monocytes that leave the bone marrow and enter blood circulation. There, they can become differentially activated. In healthy individuals approximately 80-90% of circulating monocytes are classical monocytes expressing CD14 (a receptor for bacterial LPS), but not CD16 (a receptor for

the Fc portion of IgG antibodies). During HIV infection, there is an increase in $CD14^{+}CD16^{+}$ (intermediate) and $CD14^{-}CD16^{+}$ (nonclassical) monocyte populations (Figure 1.6) [177]. This shift from $CD16^{-}$ monocytes to $CD16^{+}$ monocytes is associated with a faster rate of disease progression to AIDS [1].

Activated double positive ($CD14^{+}CD16^{+}$) monocytes have been implicated in the pathogenesis of HAND and other comorbidities of HIV infection, such as cardiovascular, renal, bone and liver dysfunction [177, 178]. The source of monocyte activation during chronic HIV infection is still debated [179]. One hypothesis is that during acute HIV infection, there is depletion of gut CD4+ T cells leading to microbial translocation out of the gut. LPS and sCD14 are elevated in plasma of HIV infected individuals, suggesting that monocytes are activated by bacterial products that escape from the gut [180]. Another hypothesis is that monocytes are activated by residual viremia. Immune activation is associated with viral blipping [181] and intermittent use of cART suggesting a link between viral replication and monocyte activation [182]. Another possible source of monocyte activation is from co-infections. Many HIV+ individuals are latently infected with human cytomegalovirus (CMV). CMV can infect and activate monocytes, which then spread the virus to other tissue types [183]. Latent viral herpes infections are also a source of monocyte activation in HIV+ patients on cART [179].

c. Macrophage polarization

Monocytes differentiate into mature macrophages when they enter tissues. Chemotactic signals direct monocytes to sites of infection and injury. Macrophages can be classified as either M1 or M2 polarized based on phenotype and activation signals. While this nomenclature is useful for discussion, it should be noted that M1 and M2

classification is not rigid, and there is evidence that macrophages can switch between the two phenotypes or have a range of intermediate phenotypes [184]. M1 macrophages are classically activated by INF-γ and secrete pro-inflammatory cytokines such as TNF-α, IL-1β, and IL-6 and chemokines such as CCL3, CCL4, and CCL5. M1 activation occurs during the early, acute phase of HIV infection, when there is a predominant Th1 T cell response. M2 macrophages are considered to be alternatively activated by Th2 cytokines and are involved in anti-inflammatory processes and tissue repair [176]. There is a shift from a Th1 to Th2 response during disease progression to AIDS [185]. Therefore, it has been proposed that a shift in macrophage phenotype also occurs with disease progression because macrophage polarization is dependent on the cytokine environment that is associated with Th1/Th2 expression profiles.

Summary

Despite advances in treatment and prevention of HIV, the AIDS still remains a worldwide epidemic [4]. Even though the lifespan of an HIV+ person is near that of the general population, they are at risk for a number of non-AIDS related comorbidities [58, 62]. The cause of these comorbidities has been attributed to viral protein toxicity to host cells, toxicity of long-term exposure of ART, and chronic immune activation that accompanies chronic HIV infection [61, 62].

HIV-PN is observed both in the absence of cART (during the early stages of the epidemic in the 1980s and in untreated animal models) and in the absence of viral replication (in patients with controlled viremia due to successful cART) [6]. Additionally, inflammatory and pain pathways use similar signaling proteins and receptors [7]. Thus,

we hypothesized that chronic immune activation is a driving force of HIV-PN associated tissue pathologies. Activated monocytes in peripheral blood and increased numbers of tissue macrophages in PNS tissues have been observed in HIV+ individuals with PN, but has not been extensively studied. In the series of studies presented here, we used an animal model of HIV-PN to investigate the role of monocyte activation and traffic to the DRG in developing HIV-PN associated tissue pathologies.

Figure 1.1

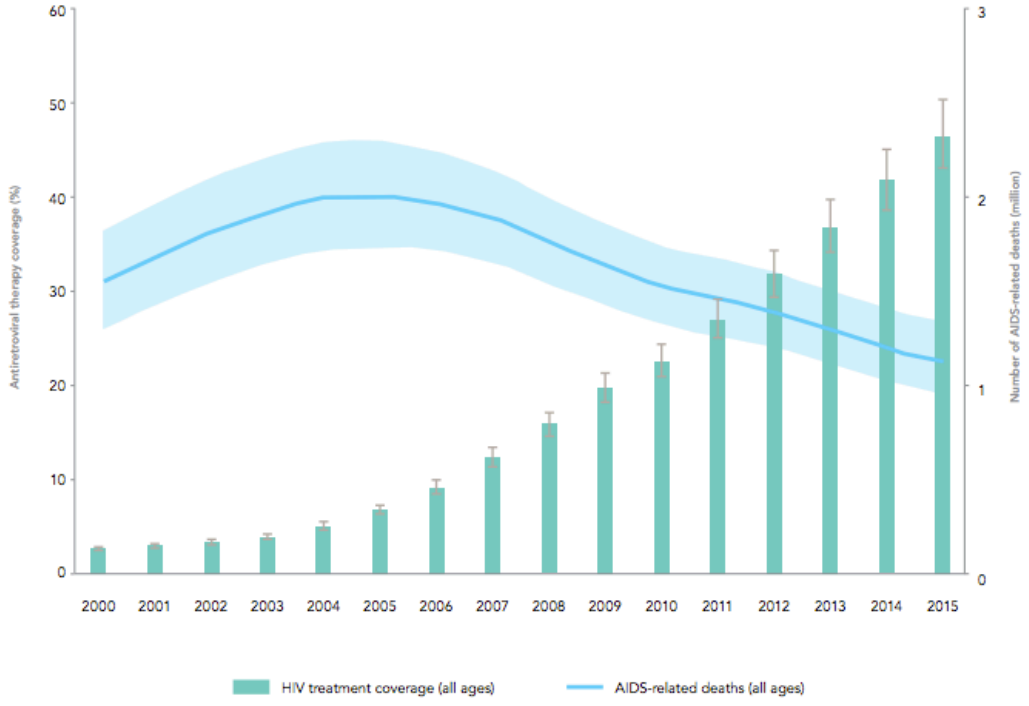
60
50
40
30
20
10
0
3
2
1
0
Antiretroviral therapy coverage (%)
Number of AIDS-related deaths (million)
2000
2001
2002
2003
2004
2005
2006
2007
2008
2009
2010
2011
2012
2013
2014
2015
HIV treatment coverage (all ages)
AIDS-related deaths (all ages)

Figure 1.1 Global antiretroviral therapy coverage and number of AIDS-related deaths.

The use of ART worldwide has increased since 2000 and there has been a 26% decline in AIDS-related deaths in 2015 since 2000 [4]. From reference [4].

Figure 1.2

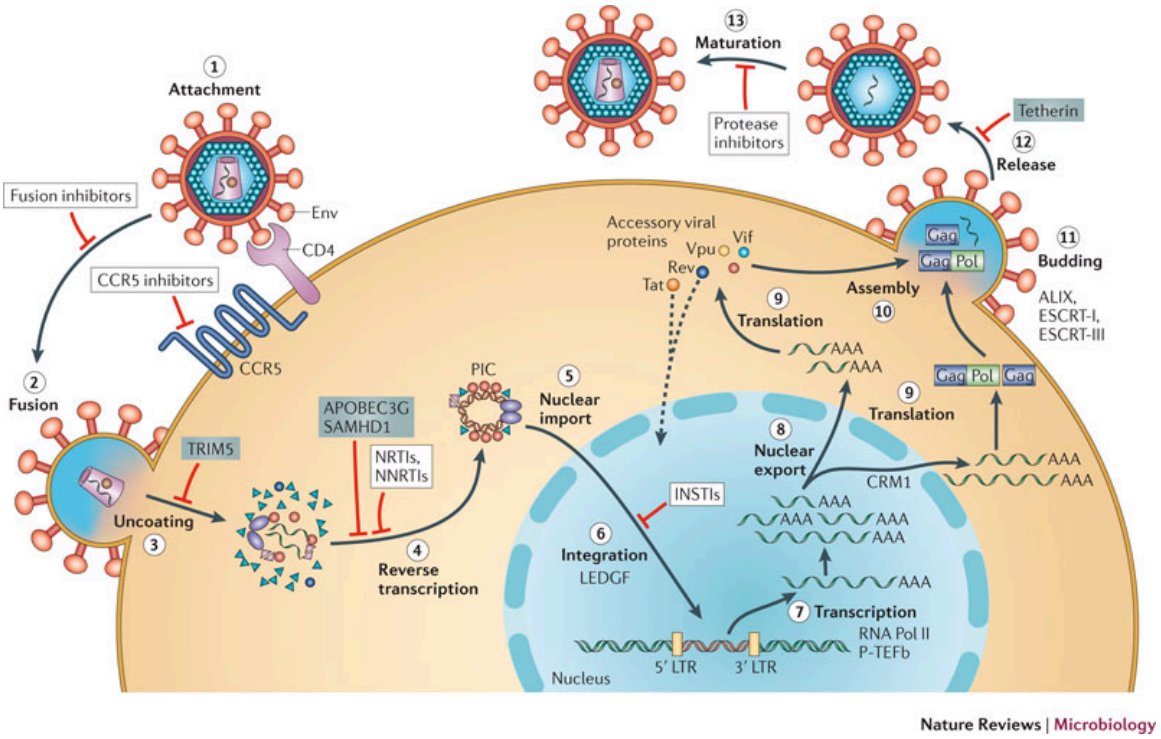
1 Attachment
Fusion inhibitors
Env
CD4
CCR5 inhibitors
CCR5
2 Fusion
TRIM5
Uncoating
3
APOBEC3G
SAMHD1
NRTIs,
NNRTIs
4 Reverse transcription
PIC
5 Nuclear import
6 Integration
LEDGF
INSTIs
7 Transcription
RNA Pol II
P-TEFb
5' LTR
3' LTR
Nucleus
8 Nuclear export
CRM1
9 Translation
AAA
Accessory viral proteins
Vpu
Vif
Rev
Tat
10 Assembly
Gag
Gag Pol
11 Budding
ALIX,
ESCRT-I,
ESCRT-III
12 Release
Tetherin
13 Maturation
Protease inhibitors
Nature Reviews | Microbiology

Figure 1.2 Schematic overview of the HIV-1 life cycle.

The HIV-1 life cycle consists of 13 steps. 1) Viral attachment to host receptors. 2) Fusion of the viral particle to the host cell. 3) The viral particle is uncoated in the cytoplasm of the host cell. 4) Viral RNA is reverse transcribed and forms the pre-integration complex (PIC). 5) PIC is imported into the nucleus. 6) Viral DNA is integrated in the host genome. 7) Viral genes are transcribed. 8) Viral mRNA is exported out of the nucleus. 9) Viral mRNA is translated into proteins. 10) The viral particle is assembled. 11) A new viral particle buds from the host cell. 12) The viral particle is released to form an immature viral particle. 13) The viral particle matures and is now able to repeat the cycle. From reference [3].

Figure 1.3

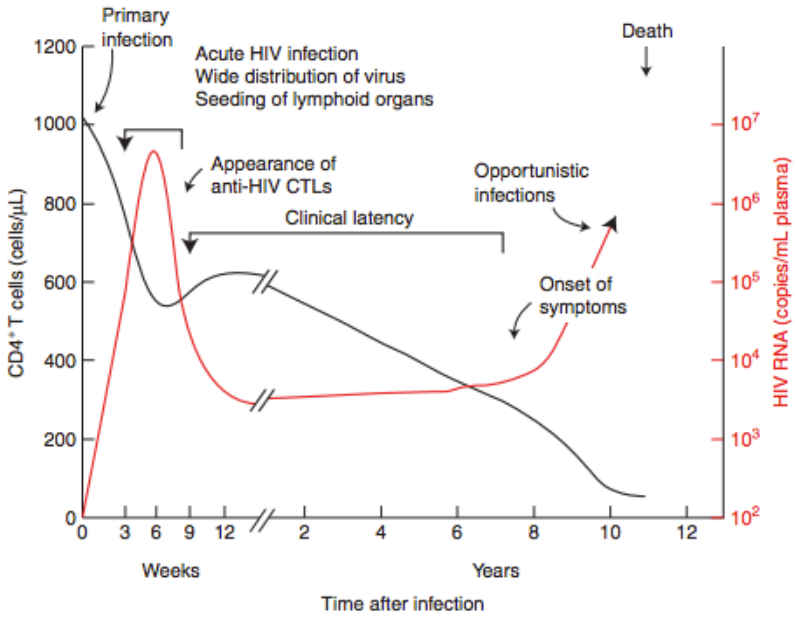
Primary infection
Acute HIV infection
Wide distribution of virus
Seeding of lymphoid organs
Death
Appearance of anti-HIV CTLs
Opportunistic infections
Clinical latency
Onset of symptoms
CD4+ T cells (cells/μL)
HIV RNA (copies/mL plasma)
1200
1000
800
600
400
200
0
10^7
10^6
10^5
10^4
10^3
10^2
0 3 6 9 12 2 4 6 8 10 12
Weeks
Years
Time after infection

Figure 1.3 Time course of typical HIV-1 infection.

During primary and acute infection, there is uncontrolled replication of the virus, which is associated with a loss of CD4+ T cells. Acute infection ends with a decline in plasma viral load. A long period of clinical latency is associated with a slow decline in CD4+ T cells. When CD4+ T cells are below 200cells/μl of blood the patient has progressed to AIDS which is associated with an increase in viral replication and opportunistic infections. From reference [2].

Figure 1.4

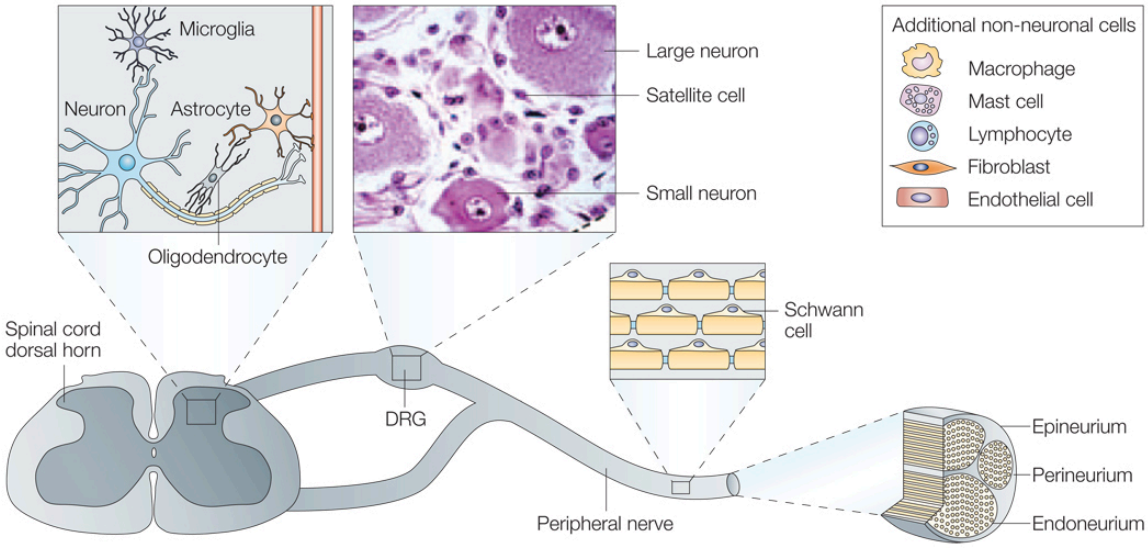
Microglia
Neuron
Astrocyte
Oligodendrocyte
Large neuron
Satellite cell
Small neuron
Additional non-neuronal cells
Macrophage
Mast cell
Lymphocyte
Fibroblast
Endothelial cell
Schwann cell
Spinal cord dorsal horn
DRG
Peripheral nerve
Epineurium
Perineurium
Endoneurium

Figure 1.4 Schematic overview of the dorsal root ganglia (DRG) and peripheral nervous system.

Sensory information is transmitted from peripheral nerves to the DRG. The DRG houses small and large neuronal cell bodies that are surrounded by satellite cells. Sensory information is then sent from the DRG to the dorsal horn of the spinal cord. From reference [7].

Figure 1.5

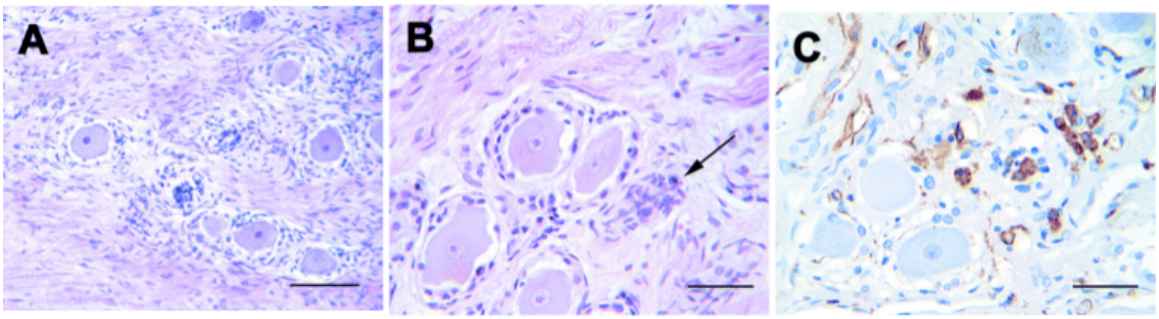

Figure 1.5 Dorsal root ganglia pathology associated with HIV infection.

A) Focal infiltration of macrophages and lymphocytes known as satellitosis. B) Infiltrating satellite cells for Nageotte nodules (arrow). C) Increased presence of CD68+ macrophages in the DRG of HIV+ individuals. Reprinted with permission from reference [6].

Figure 1.6

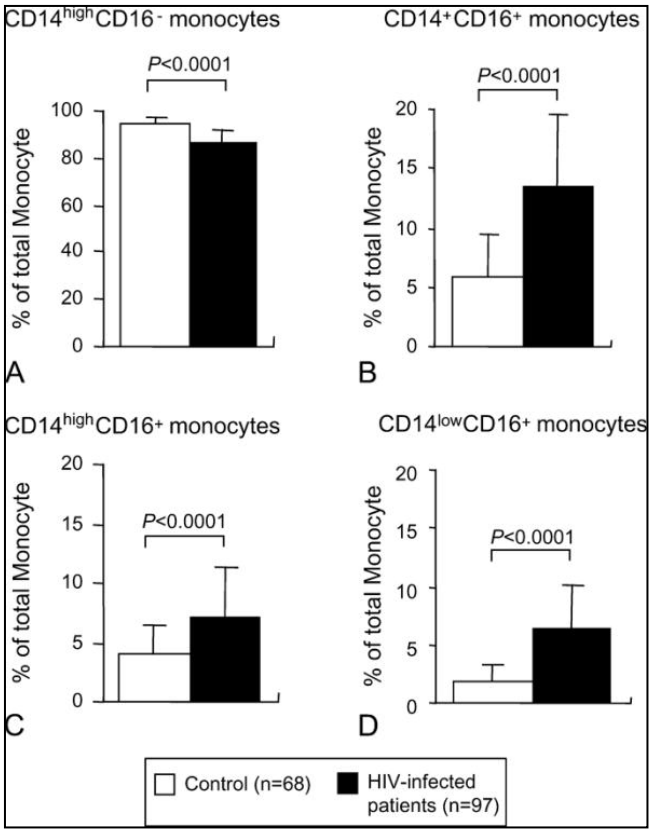
CD14highCD16- monocytes
CD14+CD16+ monocytes
P<0.0001
P<0.0001
% of total Monocyte
% of total Monocyte
100
80
60
40
20
0
20
15
10
5
0
A
B
CD14highCD16+ monocytes
CD14lowCD16+ monocytes
P<0.0001
P<0.0001
% of total Monocyte
% of total Monocyte
20
15
10
5
0
C
D
Control (n=68)
HIV-infected patients (n=97)

Figure 1.6 Increase in the CD16+ monocyte cell population during HIV infection. Monocyte populations were assessed by flow cytometry in HIV+ individuals and healthy HIV- individuals. Monocytes were divided into four distinct populations based on expression of CD14 and CD16. A) HIV+ patients had a smaller population of CD14+CD16- (classical) monocytes. B) both CD14+CD16+ and C) $CD14^{high}$ CD16+ and D) CD14-CD16+ monocyte populations were increased in HIV+ individuals compared to healthy controls. Reprinted with permission from reference [1].

REFERENCES:

1. Han, J., B. Wang, N. Han, Y. Zhao, C. Song, X. Feng, Y. Mao, F. Zhang, H. Zhao, and H. Zeng, *CD14(high)CD16(+) rather than CD14(low)CD16(+) monocytes correlate with disease progression in chronic HIV-infected patients.* Journal of acquired immune deficiency syndromes, 2009. **52**(5): p. 553-9.
2. Coffin, J. and R. Swanstrom, *HIV pathogenesis: dynamics and genetics of viral populations and infected cells.* Cold Spring Harbor perspectives in medicine, 2013. **3**(1): p. a012526.
3. Engelman, A. and P. Cherepanov, *The structural biology of HIV-1: mechanistic and therapeutic insights.* Nature reviews. Microbiology, 2012. **10**(4): p. 279-90.
4. UNAIDS. *Global AIDS updates*. World health forum 2016 May 2015 July 7, 2016]; Available from: http://www.who.int/entity/hiv/pub/arv/global-AIDS-update-2016.en.pdf?ua=1.
5. Gottlieb, M.S., R. Schroff, H.M. Schanker, J.D. Weisman, P.T. Fan, R.A. Wolf, and A. Saxon, *Pneumocystis carinii pneumonia and mucosal candidiasis in previously healthy homosexual men: evidence of a new acquired cellular immunodeficiency.* The New England journal of medicine, 1981. **305**(24): p. 1425-31.
6. Pardo, C.A., J.C. McArthur, and J.W. Griffin, *HIV neuropathy: insights in the pathology of HIV peripheral nerve disease.* Journal of the peripheral nervous system : JPNS, 2001. **6**(1): p. 21-7.
7. White, F.A., S.K. Bhangoo, and R.J. Miller, *Chemokines: integrators of pain and inflammation.* Nature reviews. Drug discovery, 2005. **4**(10): p. 834-44.
8. Barre-Sinoussi, F., J.C. Chermann, F. Rey, M.T. Nugeyre, S. Chamaret, J. Gruest, C. Dauguet, C. Axler-Blin, F. Vezinet-Brun, C. Rouzioux, W. Rozenbaum, and L. Montagnier, *Isolation of a T-lymphotropic retrovirus from a patient at risk for acquired immune deficiency syndrome (AIDS).* Science, 1983. **220**(4599): p. 868-71.
9. Levy, J.A., A.D. Hoffman, S.M. Kramer, J.A. Landis, J.M. Shimabukuro, and L.S. Oshiro, *Isolation of lymphocytopathic retroviruses from San Francisco patients with AIDS.* Science, 1984. **225**(4664): p. 840-2.
10. Brown, F., *Human immunodeficiency virus.* Science, 1986. **232**(4757): p. 1486.
11. Fischl, M.A., D.D. Richman, M.H. Grieco, M.S. Gottlieb, P.A. Volberding, O.L. Laskin, J.M. Leedom, J.E. Groopman, D. Mildvan, R.T. Schooley, and et al., *The efficacy of azidothymidine (AZT) in the treatment of patients with AIDS and AIDS-related complex. A double-blind, placebo-controlled trial.* The New England journal of medicine, 1987. **317**(4): p. 185-91.
12. Richman, D.D., M.A. Fischl, M.H. Grieco, M.S. Gottlieb, P.A. Volberding, O.L. Laskin, J.M. Leedom, J.E. Groopman, D. Mildvan, M.S. Hirsch, and et al., *The toxicity of azidothymidine (AZT) in the treatment of patients with AIDS and AIDS-related complex. A double-blind, placebo-controlled trial.* The New England journal of medicine, 1987. **317**(4): p. 192-7.

13. Hammer, S.M., D.A. Katzenstein, M.D. Hughes, H. Gundacker, R.T. Schooley, R.H. Haubrich, W.K. Henry, M.M. Lederman, J.P. Phair, M. Niu, M.S. Hirsch, and T.C. Merigan, *A trial comparing nucleoside monotherapy with combination therapy in HIV-infected adults with CD4 cell counts from 200 to 500 per cubic millimeter. AIDS Clinical Trials Group Study 175 Study Team.* The New England journal of medicine, 1996. **335**(15): p. 1081-90.
14. Jablonowski, H., *Studies of zidovudine in combination with didanosine and zalcitabine.* Journal of acquired immune deficiency syndromes and human retrovirology : official publication of the International Retrovirology Association, 1995. **10 Suppl 1**: p. S52-6.
15. NIH. *HIV Treatment: The Basics*. AIDSinfo 2016 [cited 2016 July 7, 2016]; Available from: https://aidsinfo.nih.gov/education-materials/facts-sheets/.
16. Frankel, A.D. and J.A. Young, *HIV-1: fifteen proteins and an RNA.* Annual review of biochemistry, 1998. **67**: p. 1-25.
17. Zhu, P., J. Liu, J. Bess, Jr., E. Chertova, J.D. Lifson, H. Grise, G.A. Ofek, K.A. Taylor, and K.H. Roux, *Distribution and three-dimensional structure of AIDS virus envelope spikes.* Nature, 2006. **441**(7095): p. 847-52.
18. Kwong, P.D., R. Wyatt, J. Robinson, R.W. Sweet, J. Sodroski, and W.A. Hendrickson, *Structure of an HIV gp120 envelope glycoprotein in complex with the CD4 receptor and a neutralizing human antibody.* Nature, 1998. **393**(6686): p. 648-59.
19. Rizzuto, C.D., R. Wyatt, N. Hernandez-Ramos, Y. Sun, P.D. Kwong, W.A. Hendrickson, and J. Sodroski, *A conserved HIV gp120 glycoprotein structure involved in chemokine receptor binding.* Science, 1998. **280**(5371): p. 1949-53.
20. Buzon, V., G. Natrajan, D. Schibli, F. Campelo, M.M. Kozlov, and W. Weissenhorn, *Crystal structure of HIV-1 gp41 including both fusion peptide and membrane proximal external regions.* PLoS pathogens, 2010. **6**(5): p. e1000880.
21. Briggs, J.A., K. Grunewald, B. Glass, F. Forster, H.G. Krausslich, and S.D. Fuller, *The mechanism of HIV-1 core assembly: insights from three-dimensional reconstructions of authentic virions.* Structure, 2006. **14**(1): p. 15-20.
22. Stremlau, M., M. Perron, M. Lee, Y. Li, B. Song, H. Javanbakht, F. Diaz-Griffero, D.J. Anderson, W.I. Sundquist, and J. Sodroski, *Specific recognition and accelerated uncoating of retroviral capsids by the TRIM5alpha restriction factor.* Proceedings of the National Academy of Sciences of the United States of America, 2006. **103**(14): p. 5514-9.
23. Bishop, K.N., M. Verma, E.Y. Kim, S.M. Wolinsky, and M.H. Malim, *APOBEC3G inhibits elongation of HIV-1 reverse transcripts.* PLoS pathogens, 2008. **4**(12): p. e1000231.
24. Sheehy, A.M., N.C. Gaddis, and M.H. Malim, *The antiretroviral enzyme APOBEC3G is degraded by the proteasome in response to HIV-1 Vif.* Nature medicine, 2003. **9**(11): p. 1404-7.
25. Haffar, O.K., S. Popov, L. Dubrovsky, I. Agostini, H. Tang, T. Pushkarsky, S.G. Nadler, and M. Bukrinsky, *Two nuclear localization signals in the HIV-1 matrix protein regulate nuclear import of the HIV-1 pre-integration complex.* Journal of molecular biology, 2000. **299**(2): p. 359-68.

26. Zhou, M., M.A. Halanski, M.F. Radonovich, F. Kashanchi, J. Peng, D.H. Price, and J.N. Brady, *Tat modifies the activity of CDK9 to phosphorylate serine 5 of the RNA polymerase II carboxyl-terminal domain during human immunodeficiency virus type 1 transcription.* Molecular and cellular biology, 2000. **20**(14): p. 5077-86.
27. Fujinaga, K., T.P. Cujec, J. Peng, J. Garriga, D.H. Price, X. Grana, and B.M. Peterlin, *The ability of positive transcription elongation factor B to transactivate human immunodeficiency virus transcription depends on a functional kinase domain, cyclin T1, and Tat.* Journal of virology, 1998. **72**(9): p. 7154-9.
28. Daugherty, M.D., B. Liu, and A.D. Frankel, *Structural basis for cooperative RNA binding and export complex assembly by HIV Rev.* Nature structural & molecular biology, 2010. **17**(11): p. 1337-42.
29. Daugherty, M.D., D.S. Booth, B. Jayaraman, Y. Cheng, and A.D. Frankel, *HIV Rev response element (RRE) directs assembly of the Rev homooligomer into discrete asymmetric complexes.* Proceedings of the National Academy of Sciences of the United States of America, 2010. **107**(28): p. 12481-6.
30. Gheysen, D., E. Jacobs, F. de Foresta, C. Thiriart, M. Francotte, D. Thines, and M. De Wilde, *Assembly and release of HIV-1 precursor Pr55gag virus-like particles from recombinant baculovirus-infected insect cells.* Cell, 1989. **59**(1): p. 103-12.
31. Hurley, J.H. and P.I. Hanson, *Membrane budding and scission by the ESCRT machinery: it's all in the neck.* Nature reviews. Molecular cell biology, 2010. **11**(8): p. 556-66.
32. Gottlinger, H.G., T. Dorfman, J.G. Sodroski, and W.A. Haseltine, *Effect of mutations affecting the p6 gag protein on human immunodeficiency virus particle release.* Proceedings of the National Academy of Sciences of the United States of America, 1991. **88**(8): p. 3195-9.
33. Pettit, S.C., M.D. Moody, R.S. Wehbie, A.H. Kaplan, P.V. Nantermet, C.A. Klein, and R. Swanstrom, *The p2 domain of human immunodeficiency virus type 1 Gag regulates sequential proteolytic processing and is required to produce fully infectious virions.* Journal of virology, 1994. **68**(12): p. 8017-27.
34. Vidal, N., M. Peeters, C. Mulanga-Kabeya, N. Nzilambi, D. Robertson, W. Ilunga, H. Sema, K. Tshimanga, B. Bongo, and E. Delaporte, *Unprecedented degree of human immunodeficiency virus type 1 (HIV-1) group M genetic diversity in the Democratic Republic of Congo suggests that the HIV-1 pandemic originated in Central Africa.* Journal of virology, 2000. **74**(22): p. 10498-507.
35. Korber, B., M. Muldoon, J. Theiler, F. Gao, R. Gupta, A. Lapedes, B.H. Hahn, S. Wolinsky, and T. Bhattacharya, *Timing the ancestor of the HIV-1 pandemic strains.* Science, 2000. **288**(5472): p. 1789-96.
36. Worobey, M., M. Gemmel, D.E. Teuwen, T. Haselkorn, K. Kunstman, M. Bunce, J.J. Muyembe, J.M. Kabongo, R.M. Kalengayi, E. Van Marck, M.T. Gilbert, and S.M. Wolinsky, *Direct evidence of extensive diversity of HIV-1 in Kinshasa by 1960.* Nature, 2008. **455**(7213): p. 661-4.
37. Hirsch, V.M., R.A. Olmsted, M. Murphey-Corb, R.H. Purcell, and P.R. Johnson, *An African primate lentivirus (SIVsm) closely related to HIV-2.* Nature, 1989. **339**(6223): p. 389-92.

38. Damond, F., M. Worobey, P. Campa, I. Farfara, G. Colin, S. Matheron, F. Brun-Vezinet, D.L. Robertson, and F. Simon, *Identification of a highly divergent HIV type 2 and proposal for a change in HIV type 2 classification.* AIDS research and human retroviruses, 2004. **20**(6): p. 666-72.
39. Peeters, M., C. Honore, T. Huet, L. Bedjabaga, S. Ossari, P. Bussi, R.W. Cooper, and E. Delaporte, *Isolation and partial characterization of an HIV-related virus occurring naturally in chimpanzees in Gabon.* AIDS, 1989. **3**(10): p. 625-30.
40. Huet, T., R. Cheynier, A. Meyerhans, G. Roelants, and S. Wain-Hobson, *Genetic organization of a chimpanzee lentivirus related to HIV-1.* Nature, 1990. **345**(6273): p. 356-9.
41. Sharp, P.M. and B.H. Hahn, *The evolution of HIV-1 and the origin of AIDS.* Philosophical transactions of the Royal Society of London. Series B, Biological sciences, 2010. **365**(1552): p. 2487-94.
42. Beer, B.E., B.T. Foley, C.L. Kuiken, Z. Tooze, R.M. Goeken, C.R. Brown, J. Hu, M. St Claire, B.T. Korber, and V.M. Hirsch, *Characterization of novel simian immunodeficiency viruses from red-capped mangabeys from Nigeria (SIVrcmNG409 and -NG411).* Journal of virology, 2001. **75**(24): p. 12014-27.
43. Courgnaud, V., M. Salemi, X. Pourrut, E. Mpoudi-Ngole, B. Abela, P. Auzel, F. Bibollet-Ruche, B. Hahn, A.M. Vandamme, E. Delaporte, and M. Peeters, *Characterization of a novel simian immunodeficiency virus with a vpu gene from greater spot-nosed monkeys (Cercopithecus nictitans) provides new insights into simian/human immunodeficiency virus phylogeny.* Journal of virology, 2002. **76**(16): p. 8298-309.
44. Pandrea, I., R. Onanga, P. Rouquet, O. Bourry, P. Ngari, E.J. Wickings, P. Roques, and C. Apetrei, *Chronic SIV infection ultimately causes immunodeficiency in African non-human primates.* AIDS, 2001. **15**(18): p. 2461-2.
45. Ling, B., C. Apetrei, I. Pandrea, R.S. Veazey, A.A. Lackner, B. Gormus, and P.A. Marx, *Classic AIDS in a sooty mangabey after an 18-year natural infection.* Journal of virology, 2004. **78**(16): p. 8902-8.
46. Letvin, N.L., M.D. Daniel, P.K. Sehgal, R.C. Desrosiers, R.D. Hunt, L.M. Waldron, J.J. MacKey, D.K. Schmidt, L.V. Chalifoux, and N.W. King, *Induction of AIDS-like disease in macaque monkeys with T-cell tropic retrovirus STLV-III.* Science, 1985. **230**(4721): p. 71-3.
47. Daniel, M.D., N.L. Letvin, N.W. King, M. Kannagi, P.K. Sehgal, R.D. Hunt, P.J. Kanki, M. Essex, and R.C. Desrosiers, *Isolation of T-cell tropic HTLV-III-like retrovirus from macaques.* Science, 1985. **228**(4704): p. 1201-4.
48. Kanki, P.J., M.F. McLane, N.W. King, Jr., N.L. Letvin, R.D. Hunt, P. Sehgal, M.D. Daniel, R.C. Desrosiers, and M. Essex, *Serologic identification and characterization of a macaque T-lymphotropic retrovirus closely related to HTLV-III.* Science, 1985. **228**(4704): p. 1199-201.
49. Apetrei, C., A. Kaur, N.W. Lerche, M. Metzger, I. Pandrea, J. Hardcastle, S. Falkenstein, R. Bohm, J. Koehler, V. Traina-Dorge, T. Williams, S. Staprans, G. Plauche, R.S. Veazey, H. McClure, A.A. Lackner, B. Gormus, D.L. Robertson, and P.A. Marx, *Molecular epidemiology of simian immunodeficiency virus SIVsm*

in U.S. primate centers unravels the origin of SIVmac and SIVstm. Journal of virology, 2005. **79**(14): p. 8991-9005.
50. Apetrei, C., N.W. Lerche, I. Pandrea, B. Gormus, G. Silvestri, A. Kaur, D.L. Robertson, J. Hardcastle, A.A. Lackner, and P.A. Marx, *Kuru experiments triggered the emergence of pathogenic SIVmac.* AIDS, 2006. **20**(3): p. 317-21.
51. Chakrabarti, L., M. Guyader, M. Alizon, M.D. Daniel, R.C. Desrosiers, P. Tiollais, and P. Sonigo, *Sequence of simian immunodeficiency virus from macaque and its relationship to other human and simian retroviruses.* Nature, 1987. **328**(6130): p. 543-7.
52. Hirsch, V.M. and J.D. Lifson, *Simian immunodeficiency virus infection of monkeys as a model system for the study of AIDS pathogenesis, treatment, and prevention.* Advances in pharmacology, 2000. **49**: p. 437-77.
53. Cummins, N.W. and A.D. Badley, *Mechanisms of HIV-associated lymphocyte apoptosis: 2010.* Cell death & disease, 2010. **1**: p. e99.
54. Cummins, N.W. and A.D. Badley, *Making sense of how HIV kills infected CD4 T cells: implications for HIV cure.* Molecular and cellular therapies, 2014. **2**: p. 20.
55. Doitsh, G., N.L. Galloway, X. Geng, Z. Yang, K.M. Monroe, O. Zepeda, P.W. Hunt, H. Hatano, S. Sowinski, I. Munoz-Arias, and W.C. Greene, *Cell death by pyroptosis drives CD4 T-cell depletion in HIV-1 infection.* Nature, 2014. **505**(7484): p. 509-14.
56. Lundgren, J.D., A.G. Babiker, F. Gordin, S. Emery, B. Grund, S. Sharma, A. Avihingsanon, D.A. Cooper, G. Fatkenheuer, J.M. Llibre, J.M. Molina, P. Munderi, M. Schechter, R. Wood, K.L. Klingman, S. Collins, H.C. Lane, A.N. Phillips, and J.D. Neaton, *Initiation of Antiretroviral Therapy in Early Asymptomatic HIV Infection.* The New England journal of medicine, 2015. **373**(9): p. 795-807.
57. De Cock, K.M. and W.M. El-Sadr, *When to start ART in Africa--an urgent research priority.* The New England journal of medicine, 2013. **368**(10): p. 886-9.
58. *Life expectancy of individuals on combination antiretroviral therapy in high-income countries: a collaborative analysis of 14 cohort studies.* Lancet, 2008. **372**(9635): p. 293-9.
59. Effros, R.B., C.V. Fletcher, K. Gebo, J.B. Halter, W.R. Hazzard, F.M. Horne, R.E. Huebner, E.N. Janoff, A.C. Justice, D. Kuritzkes, S.G. Nayfield, S.F. Plaeger, K.E. Schmader, J.R. Ashworth, C. Campanelli, C.P. Clayton, B. Rada, N.F. Woolard, and K.P. High, *Aging and infectious diseases: workshop on HIV infection and aging: what is known and future research directions.* Clinical infectious diseases : an official publication of the Infectious Diseases Society of America, 2008. **47**(4): p. 542-53.
60. Warriner, A.H., G.A. Burkholder, and E.T. Overton, *HIV-related metabolic comorbidities in the current ART era.* Infectious disease clinics of North America, 2014. **28**(3): p. 457-76.
61. Nasi, M., S. De Biasi, L. Gibellini, E. Bianchini, S. Pecorini, V. Bacca, G. Guaraldi, C. Mussini, M. Pinti, and A. Cossarizza, *Aging and inflammation in patients with HIV infection.* Clinical and experimental immunology, 2016.
62. Marin, B., R. Thiebaut, H.C. Bucher, V. Rondeau, D. Costagliola, M. Dorrucci, O. Hamouda, M. Prins, S. Walker, K. Porter, C. Sabin, and G. Chene, *Non-AIDS-*

defining deaths and immunodeficiency in the era of combination antiretroviral therapy. AIDS, 2009. **23**(13): p. 1743-53.
63. Wang, H. and D.P. Kotler, *HIV enteropathy and aging: gastrointestinal immunity, mucosal epithelial barrier, and microbial translocation.* Current opinion in HIV and AIDS, 2014. **9**(4): p. 309-16.
64. Appay, V., J.R. Almeida, D. Sauce, B. Autran, and L. Papagno, *Accelerated immune senescence and HIV-1 infection.* Experimental gerontology, 2007. **42**(5): p. 432-7.
65. Hebbeler, A.M., N. Propp, C. Cairo, H. Li, J.S. Cummings, L.P. Jacobson, J.B. Margolick, and C.D. Pauza, *Failure to restore the Vgamma2-Jgamma1.2 repertoire in HIV-infected men receiving highly active antiretroviral therapy (HAART).* Clinical immunology, 2008. **128**(3): p. 349-57.
66. Kengne, A.P., Z. June-Rose McHiza, A.G. Amoah, and J.C. Mbanya, *Cardiovascular diseases and diabetes as economic and developmental challenges in Africa.* Progress in cardiovascular diseases, 2013. **56**(3): p. 302-13.
67. Kaplan, R.C., D.B. Hanna, and J.R. Kizer, *Recent Insights Into Cardiovascular Disease (CVD) Risk Among HIV-Infected Adults.* Current HIV/AIDS reports, 2016. **13**(1): p. 44-52.
68. Triant, V.A., H. Lee, C. Hadigan, and S.K. Grinspoon, *Increased acute myocardial infarction rates and cardiovascular risk factors among patients with human immunodeficiency virus disease.* The Journal of clinical endocrinology and metabolism, 2007. **92**(7): p. 2506-12.
69. Sandler, N.G., H. Wand, A. Roque, M. Law, M.C. Nason, D.E. Nixon, C. Pedersen, K. Ruxrungtham, S.R. Lewin, S. Emery, J.D. Neaton, J.M. Brenchley, S.G. Deeks, I. Sereti, and D.C. Douek, *Plasma levels of soluble CD14 independently predict mortality in HIV infection.* The Journal of infectious diseases, 2011. **203**(6): p. 780-90.
70. Subramanian, S., A. Tawakol, T.H. Burdo, S. Abbara, J. Wei, J. Vijayakumar, E. Corsini, A. Abdelbaky, M.V. Zanni, U. Hoffmann, K.C. Williams, J. Lo, and S.K. Grinspoon, *Arterial inflammation in patients with HIV.* JAMA : the journal of the American Medical Association, 2012. **308**(4): p. 379-86.
71. Paula, A.A., M.C. Falcao, and A.G. Pacheco, *Metabolic syndrome in HIV-infected individuals: underlying mechanisms and epidemiological aspects.* AIDS research and therapy, 2013. **10**(1): p. 32.
72. Guaraldi, G., C. Stentarelli, S. Zona, and A. Santoro, *HIV-associated lipodystrophy: impact of antiretroviral therapy.* Drugs, 2013. **73**(13): p. 1431-50.
73. Murata, H., P.W. Hruz, and M. Mueckler, *The mechanism of insulin resistance caused by HIV protease inhibitor therapy.* The Journal of biological chemistry, 2000. **275**(27): p. 20251-4.
74. Murata, H., P.W. Hruz, and M. Mueckler, *Indinavir inhibits the glucose transporter isoform Glut4 at physiologic concentrations.* AIDS, 2002. **16**(6): p. 859-63.
75. Pinti, M., P. Salomoni, and A. Cossarizza, *Anti-HIV drugs and the mitochondria.* Biochimica et biophysica acta, 2006. **1757**(5-6): p. 700-7.
76. Erlandson, K.M., G. Guaraldi, and J. Falutz, *More than osteoporosis: age-specific issues in bone health.* Current opinion in HIV and AIDS, 2016. **11**(3): p. 343-50.

77. Collin, F., X. Duval, V. Le Moing, L. Piroth, F. Al Kaied, P. Massip, V. Villes, G. Chene, and F. Raffi, *Ten-year incidence and risk factors of bone fractures in a cohort of treated HIV1-infected adults.* AIDS, 2009. **23**(8): p. 1021-4.
78. Sigel, K., R. Dubrow, M. Silverberg, K. Crothers, S. Braithwaite, and A. Justice, *Cancer screening in patients infected with HIV.* Current HIV/AIDS reports, 2011. **8**(3): p. 142-52.
79. Crum-Cianflone, N., K.H. Hullsiek, V. Marconi, A. Weintrob, A. Ganesan, R.V. Barthel, S. Fraser, B.K. Agan, and S. Wegner, *Trends in the incidence of cancers among HIV-infected persons and the impact of antiretroviral therapy: a 20-year cohort study.* AIDS, 2009. **23**(1): p. 41-50.
80. Shiels, M.S., S.R. Cole, G.D. Kirk, and C. Poole, *A meta-analysis of the incidence of non-AIDS cancers in HIV-infected individuals.* Journal of acquired immune deficiency syndromes, 2009. **52**(5): p. 611-22.
81. Serrano-Villar, S., F. Gutierrez, C. Miralles, J. Berenguer, A. Rivero, E. Martinez, and S. Moreno, *Human Immunodeficiency Virus as a Chronic Disease: Evaluation and Management of Nonacquired Immune Deficiency Syndrome-Defining Conditions.* Open forum infectious diseases, 2016. **3**(2): p. ofw097.
82. Grant, I., R.K. Heaton, J.H. Atkinson, C.A. Wiley, D. Kirson, R. Velin, J. Chandler, and J.A. McCutchan, *HIV-1 associated neurocognitive disorder. The HNRC Group.* Clinical neuropharmacology, 1992. **15 Suppl 1 Pt A**: p. 364A-365A.
83. Elbirt, D., K. Mahlab-Guri, S. Bezalel-Rosenberg, H. Gill, M. Attali, and I. Asher, *HIV-associated neurocognitive disorders (HAND).* The Israel Medical Association journal : IMAJ, 2015. **17**(1): p. 54-9.
84. Burdo, T.H., A. Weiffenbach, S.P. Woods, S. Letendre, R.J. Ellis, and K.C. Williams, *Elevated sCD163 in plasma but not cerebrospinal fluid is a marker of neurocognitive impairment in HIV infection.* AIDS, 2013. **27**(9): p. 1387-95.
85. Fischer-Smith, T., S. Croul, A.E. Sverstiuk, C. Capini, D. L'Heureux, E.G. Regulier, M.W. Richardson, S. Amini, S. Morgello, K. Khalili, and J. Rappaport, *CNS invasion by CD14+/CD16+ peripheral blood-derived monocytes in HIV dementia: perivascular accumulation and reservoir of HIV infection.* Journal of neurovirology, 2001. **7**(6): p. 528-41.
86. Fischer-Smith, T., C. Bell, S. Croul, M. Lewis, and J. Rappaport, *Monocyte/macrophage trafficking in acquired immunodeficiency syndrome encephalitis: lessons from human and nonhuman primate studies.* Journal of neurovirology, 2008. **14**(4): p. 318-26.
87. Burdo, T.H., C. Soulas, K. Orzechowski, J. Button, A. Krishnan, C. Sugimoto, X. Alvarez, M.J. Kuroda, and K.C. Williams, *Increased monocyte turnover from bone marrow correlates with severity of SIV encephalitis and CD163 levels in plasma.* PLoS pathogens, 2010. **6**(4): p. e1000842.
88. Kim, W.K., S. Corey, X. Alvarez, and K. Williams, *Monocyte/macrophage traffic in HIV and SIV encephalitis.* Journal of leukocyte biology, 2003. **74**(5): p. 650-6.
89. Pulliam, L., R. Gascon, M. Stubblebine, D. McGuire, and M.S. McGrath, *Unique monocyte subset in patients with AIDS dementia.* Lancet, 1997. **349**(9053): p. 692-5.

90. Schnell, G., S. Joseph, S. Spudich, R.W. Price, and R. Swanstrom, *HIV-1 replication in the central nervous system occurs in two distinct cell types.* PLoS pathogens, 2011. **7**(10): p. e1002286.
91. Joseph, S.B., K.T. Arrildt, C.B. Sturdevant, and R. Swanstrom, *HIV-1 target cells in the CNS.* Journal of neurovirology, 2015. **21**(3): p. 276-89.
92. Eisfeld, C., D. Reichelt, S. Evers, and I. Husstedt, *CSF penetration by antiretroviral drugs.* CNS drugs, 2013. **27**(1): p. 31-55.
93. Heaton, R.K., D.R. Franklin, R.J. Ellis, J.A. McCutchan, S.L. Letendre, S. Leblanc, S.H. Corkran, N.A. Duarte, D.B. Clifford, S.P. Woods, A.C. Collier, C.M. Marra, S. Morgello, M.R. Mindt, M.J. Taylor, T.D. Marcotte, J.H. Atkinson, T. Wolfson, B.B. Gelman, J.C. McArthur, D.M. Simpson, I. Abramson, A. Gamst, C. Fennema-Notestine, T.L. Jernigan, J. Wong, and I. Grant, *HIV-associated neurocognitive disorders before and during the era of combination antiretroviral therapy: differences in rates, nature, and predictors.* Journal of neurovirology, 2011. **17**(1): p. 3-16.
94. Peluso, M.J., F. Ferretti, J. Peterson, E. Lee, D. Fuchs, A. Boschini, M. Gisslen, N. Angoff, R.W. Price, P. Cinque, and S. Spudich, *Cerebrospinal fluid HIV escape associated with progressive neurologic dysfunction in patients on antiretroviral therapy with well controlled plasma viral load.* AIDS, 2012. **26**(14): p. 1765-74.
95. Treede, R.D., T.S. Jensen, J.N. Campbell, G. Cruccu, J.O. Dostrovsky, J.W. Griffin, P. Hansson, R. Hughes, T. Nurmikko, and J. Serra, *Neuropathic pain: redefinition and a grading system for clinical and research purposes.* Neurology, 2008. **70**(18): p. 1630-5.
96. Osterweis M, K.A., Mechanic D, *Pain and Disability: Clinical, Behavioral, and Public Policy Persepctives*. The Anatomy and Physiology of Pain1987, Washington DC: National Academies Press (US).
97. College, O., *Anatomy and Physiology*, ed. O. CNX.
98. Kaku, M. and D.M. Simpson, *HIV neuropathy.* Current opinion in HIV and AIDS, 2014. **9**(6): p. 521-6.
99. Wulff, E.A., A.K. Wang, and D.M. Simpson, *HIV-associated peripheral neuropathy: epidemiology, pathophysiology and treatment.* Drugs, 2000. **59**(6): p. 1251-60.
100. Verma, S., L. Estanislao, and D. Simpson, *HIV-associated neuropathic pain: epidemiology, pathophysiology and management.* CNS drugs, 2005. **19**(4): p. 325-34.
101. Ellis, R.J., D. Rosario, D.B. Clifford, J.C. McArthur, D. Simpson, T. Alexander, B.B. Gelman, F. Vaida, A. Collier, C.M. Marra, B. Ances, J.H. Atkinson, R.H. Dworkin, S. Morgello, and I. Grant, *Continued high prevalence and adverse clinical impact of human immunodeficiency virus-associated sensory neuropathy in the era of combination antiretroviral therapy: the CHARTER Study.* Archives of neurology, 2010. **67**(5): p. 552-8.
102. Moyle, G., *Clinical manifestations and management of antiretroviral nucleoside analog-related mitochondrial toxicity.* Clinical therapeutics, 2000. **22**(8): p. 911-36; discussion 898.

103. Lewis, W. and M.C. Dalakas, *Mitochondrial toxicity of antiviral drugs.* Nature medicine, 1995. **1**(5): p. 417-22.
104. Schutz, S.G. and J. Robinson-Papp, *HIV-related neuropathy: current perspectives.* HIV/AIDS, 2013. **5**: p. 243-51.
105. Nicholas, P.K., L. Mauceri, A. Slate Ciampa, I.B. Corless, N. Raymond, D.J. Barry, and A. Viamonte Ros, *Distal sensory polyneuropathy in the context of HIV/AIDS.* The Journal of the Association of Nurses in AIDS Care : JANAC, 2007. **18**(4): p. 32-40.
106. Wang, S.X., E.L. Ho, M. Grill, E. Lee, J. Peterson, K. Robertson, D. Fuchs, E. Sinclair, R.W. Price, and S. Spudich, *Peripheral neuropathy in primary HIV infection associates with systemic and central nervous system immune activation.* Journal of acquired immune deficiency syndromes, 2014. **66**(3): p. 303-10.
107. Polydefkis, M., C.T. Yiannoutsos, B.A. Cohen, H. Hollander, G. Schifitto, D.B. Clifford, D.M. Simpson, D. Katzenstein, S. Shriver, P. Hauer, A. Brown, A.B. Haidich, L. Moo, and J.C. McArthur, *Reduced intraepidermal nerve fiber density in HIV-associated sensory neuropathy.* Neurology, 2002. **58**(1): p. 115-9.
108. Shikuma, C.M., K. Bennett, J. Ananworanich, M. Gerschenson, N. Teeratakulpisarn, T. Jadwattanakul, V. DeGruttola, J.C. McArthur, G. Ebenezer, N. Chomchey, P. Praihirunkit, P. Hongchookiat, P. Mathajittiphun, B. Nakamoto, P. Hauer, P. Phanuphak, and N. Phanuphak, *Distal leg epidermal nerve fiber density as a surrogate marker of HIV-associated sensory neuropathy risk: risk factors and change following initial antiretroviral therapy.* Journal of neurovirology, 2015. **21**(5): p. 525-34.
109. Burdo, T.H. and A.D. Miller, *Animal models of HIV peripheral neuropathy.* Future virology, 2014. **9**(5): p. 465-474.
110. Kramer-Hammerle, S., I. Rothenaigner, H. Wolff, J.E. Bell, and R. Brack-Werner, *Cells of the central nervous system as targets and reservoirs of the human immunodeficiency virus.* Virus research, 2005. **111**(2): p. 194-213.
111. Keswani, S.C., M. Polley, C.A. Pardo, J.W. Griffin, J.C. McArthur, and A. Hoke, *Schwann cell chemokine receptors mediate HIV-1 gp120 toxicity to sensory neurons.* Annals of neurology, 2003. **54**(3): p. 287-96.
112. Nath, A., K. Psooy, C. Martin, B. Knudsen, D.S. Magnuson, N. Haughey, and J.D. Geiger, *Identification of a human immunodeficiency virus type 1 Tat epitope that is neuroexcitatory and neurotoxic.* Journal of virology, 1996. **70**(3): p. 1475-80.
113. Patel, C.A., M. Mukhtar, and R.J. Pomerantz, *Human immunodeficiency virus type 1 Vpr induces apoptosis in human neuronal cells.* Journal of virology, 2000. **74**(20): p. 9717-26.
114. Rao, V.R., A.P. Ruiz, and V.R. Prasad, *Viral and cellular factors underlying neuropathogenesis in HIV associated neurocognitive disorders (HAND).* AIDS research and therapy, 2014. **11**: p. 13.
115. Younas, M., C. Psomas, J. Reynes, and P. Corbeau, *Immune activation in the course of HIV-1 infection: Causes, phenotypes and persistence under therapy.* HIV medicine, 2015.

116. Mehla, R., S. Bivalkar-Mehla, M. Nagarkatti, and A. Chauhan, *Programming of neurotoxic cofactor CXCL-10 in HIV-1-associated dementia: abrogation of CXCL-10-induced neuro-glial toxicity in vitro by PKC activator.* Journal of neuroinflammation, 2012. **9**: p. 239.
117. Sui, Y., L. Stehno-Bittel, S. Li, R. Loganathan, N.K. Dhillon, D. Pinson, A. Nath, D. Kolson, O. Narayan, and S. Buch, *CXCL10-induced cell death in neurons: role of calcium dysregulation.* The European journal of neuroscience, 2006. **23**(4): p. 957-64.
118. Shi, C. and E.G. Pamer, *Monocyte recruitment during infection and inflammation.* Nature reviews. Immunology, 2011. **11**(11): p. 762-74.
119. Ingersoll, M.A., A.M. Platt, S. Potteaux, and G.J. Randolph, *Monocyte trafficking in acute and chronic inflammation.* Trends in immunology, 2011. **32**(10): p. 470-7.
120. Faissner, S., B. Ambrosius, K. Schanzmann, B. Grewe, A. Potthoff, J. Munch, U. Sure, T. Gramberg, S. Wittmann, N. Brockmeyer, K. Uberla, R. Gold, T. Grunwald, and A. Chan, *Cytoplasmic HIV-RNA in monocytes determines microglial activation and neuronal cell death in HIV-associated neurodegeneration.* Experimental neurology, 2014. **261**: p. 685-97.
121. Dorsey, J.L., L.M. Mangus, P. Hauer, G.J. Ebenezer, S.E. Queen, V.A. Laast, R.J. Adams, and J.L. Mankowski, *Persistent Peripheral Nervous System Damage in Simian Immunodeficiency Virus-Infected Macaques Receiving Antiretroviral Therapy.* Journal of neuropathology and experimental neurology, 2015. **74**(11): p. 1053-60.
122. Laast, V.A., C.A. Pardo, P.M. Tarwater, S.E. Queen, T.A. Reinhart, M. Ghosh, R.J. Adams, M.C. Zink, and J.L. Mankowski, *Pathogenesis of simian immunodeficiency virus-induced alterations in macaque trigeminal ganglia.* Journal of neuropathology and experimental neurology, 2007. **66**(1): p. 26-34.
123. Toggas, S.M., E. Masliah, E.M. Rockenstein, G.F. Rall, C.R. Abraham, and L. Mucke, *Central nervous system damage produced by expression of the HIV-1 coat protein gp120 in transgenic mice.* Nature, 1994. **367**(6459): p. 188-93.
124. Keswani, S.C., C. Jack, C. Zhou, and A. Hoke, *Establishment of a rodent model of HIV-associated sensory neuropathy.* The Journal of neuroscience : the official journal of the Society for Neuroscience, 2006. **26**(40): p. 10299-304.
125. Laast, V.A., B. Shim, L.M. Johanek, J.L. Dorsey, P.E. Hauer, P.M. Tarwater, R.J. Adams, C.A. Pardo, J.C. McArthur, M. Ringkamp, and J.L. Mankowski, *Macrophage-mediated dorsal root ganglion damage precedes altered nerve conduction in SIV-infected macaques.* The American journal of pathology, 2011. **179**(5): p. 2337-45.
126. Westmoreland, S.V., E. Halpern, and A.A. Lackner, *Simian immunodeficiency virus encephalitis in rhesus macaques is associated with rapid disease progression.* Journal of neurovirology, 1998. **4**(3): p. 260-8.
127. Williams, K. and T.H. Burdo, *Monocyte mobilization, activation markers, and unique macrophage populations in the brain: observations from SIV infected monkeys are informative with regard to pathogenic mechanisms of HIV infection in humans.* Journal of neuroimmune pharmacology : the official journal of the Society on NeuroImmune Pharmacology, 2012. **7**(2): p. 363-71.

128. Burdo, T.H., K. Orzechowski, H.L. Knight, A.D. Miller, and K. Williams, *Dorsal root ganglia damage in SIV-infected rhesus macaques: an animal model of HIV-induced sensory neuropathy.* The American journal of pathology, 2012. **180**(4): p. 1362-9.
129. Austin, P.J. and G. Moalem-Taylor, *The neuro-immune balance in neuropathic pain: involvement of inflammatory immune cells, immune-like glial cells and cytokines.* Journal of neuroimmunology, 2010. **229**(1-2): p. 26-50.
130. Thacker, M.A., A.K. Clark, T. Bishop, J. Grist, P.K. Yip, L.D. Moon, S.W. Thompson, F. Marchand, and S.B. McMahon, *CCL2 is a key mediator of microglia activation in neuropathic pain states.* European journal of pain, 2009. **13**(3): p. 263-72.
131. Hahn, K., B. Robinson, C. Anderson, W. Li, C.A. Pardo, S. Morgello, D. Simpson, and A. Nath, *Differential effects of HIV infected macrophages on dorsal root ganglia neurons and axons.* Experimental neurology, 2008. **210**(1): p. 30-40.
132. Biber, K. and E. Boddeke, *Neuronal CC chemokines: the distinct roles of CCL21 and CCL2 in neuropathic pain.* Frontiers in cellular neuroscience, 2014. **8**: p. 210.
133. Miller, R.J., H. Jung, S.K. Bhangoo, and F.A. White, *Cytokine and chemokine regulation of sensory neuron function.* Handbook of experimental pharmacology, 2009(194): p. 417-49.
134. Perkins, N.M. and D.J. Tracey, *Hyperalgesia due to nerve injury: role of neutrophils.* Neuroscience, 2000. **101**(3): p. 745-57.
135. Mueller, M., K. Wacker, E.B. Ringelstein, W.F. Hickey, Y. Imai, and R. Kiefer, *Rapid response of identified resident endoneurial macrophages to nerve injury.* The American journal of pathology, 2001. **159**(6): p. 2187-97.
136. Perrin, F.E., S. Lacroix, M. Aviles-Trigueros, and S. David, *Involvement of monocyte chemoattractant protein-1, macrophage inflammatory protein-1alpha and interleukin-1beta in Wallerian degeneration.* Brain : a journal of neurology, 2005. **128**(Pt 4): p. 854-66.
137. Shubayev, V.I., M. Angert, J. Dolkas, W.M. Campana, K. Palenscar, and R.R. Myers, *TNFalpha-induced MMP-9 promotes macrophage recruitment into injured peripheral nerve.* Molecular and cellular neurosciences, 2006. **31**(3): p. 407-15.
138. Richardson, J.D. and M.R. Vasko, *Cellular mechanisms of neurogenic inflammation.* The Journal of pharmacology and experimental therapeutics, 2002. **302**(3): p. 839-45.
139. Zhuang, Z.Y., Y. Kawasaki, P.H. Tan, Y.R. Wen, J. Huang, and R.R. Ji, *Role of the CX3CR1/p38 MAPK pathway in spinal microglia for the development of neuropathic pain following nerve injury-induced cleavage of fractalkine.* Brain, behavior, and immunity, 2007. **21**(5): p. 642-51.
140. White, F.A., J. Sun, S.M. Waters, C. Ma, D. Ren, M. Ripsch, J. Steflik, D.N. Cortright, R.H. Lamotte, and R.J. Miller, *Excitatory monocyte chemoattractant protein-1 signaling is up-regulated in sensory neurons after chronic compression of the dorsal root ganglion.* Proceedings of the National Academy of Sciences of the United States of America, 2005. **102**(39): p. 14092-7.
141. Scholz, J. and C.J. Woolf, *The neuropathic pain triad: neurons, immune cells and glia.* Nature neuroscience, 2007. **10**(11): p. 1361-8.

142. Zhang, N., S. Inan, A. Cowan, R. Sun, J.M. Wang, T.J. Rogers, M. Caterina, and J.J. Oppenheim, *A proinflammatory chemokine, CCL3, sensitizes the heat- and capsaicin-gated ion channel TRPV1.* Proceedings of the National Academy of Sciences of the United States of America, 2005. **102**(12): p. 4536-41.
143. Oh, S.B., P.B. Tran, S.E. Gillard, R.W. Hurley, D.L. Hammond, and R.J. Miller, *Chemokines and glycoprotein120 produce pain hypersensitivity by directly exciting primary nociceptive neurons.* The Journal of neuroscience : the official journal of the Society for Neuroscience, 2001. **21**(14): p. 5027-35.
144. Cunha, T.M., W.A. Verri, Jr., J.S. Silva, S. Poole, F.Q. Cunha, and S.H. Ferreira, *A cascade of cytokines mediates mechanical inflammatory hypernociception in mice.* Proceedings of the National Academy of Sciences of the United States of America, 2005. **102**(5): p. 1755-60.
145. Schafers, M., D.H. Lee, D. Brors, T.L. Yaksh, and L.S. Sorkin, *Increased sensitivity of injured and adjacent uninjured rat primary sensory neurons to exogenous tumor necrosis factor-alpha after spinal nerve ligation.* The Journal of neuroscience : the official journal of the Society for Neuroscience, 2003. **23**(7): p. 3028-38.
146. Kiguchi, N., Y. Kobayashi, and S. Kishioka, *Chemokines and cytokines in neuroinflammation leading to neuropathic pain.* Current opinion in pharmacology, 2012. **12**(1): p. 55-61.
147. Abbadie, C., *Chemokines, chemokine receptors and pain.* Trends in immunology, 2005. **26**(10): p. 529-34.
148. Gilliatt, R.W. and R.J. Hjorth, *Nerve conduction during Wallerian degeneration in the baloon.* Journal of neurology, neurosurgery, and psychiatry, 1972. **35**(3): p. 335-41.
149. Chaudhry, V. and D.R. Cornblath, *Wallerian degeneration in human nerves: serial electrophysiological studies.* Muscle & nerve, 1992. **15**(6): p. 687-93.
150. Lubinska, L., *Early course of Wallerian degeneration in myelinated fibres of the rat phrenic nerve.* Brain research, 1977. **130**(1): p. 47-63.
151. George, E.B., J.D. Glass, and J.W. Griffin, *Axotomy-induced axonal degeneration is mediated by calcium influx through ion-specific channels.* The Journal of neuroscience : the official journal of the Society for Neuroscience, 1995. **15**(10): p. 6445-52.
152. Kerschensteiner, M., M.E. Schwab, J.W. Lichtman, and T. Misgeld, *In vivo imaging of axonal degeneration and regeneration in the injured spinal cord.* Nature medicine, 2005. **11**(5): p. 572-7.
153. Gray, M., W. Palispis, P.G. Popovich, N. van Rooijen, and R. Gupta, *Macrophage depletion alters the blood-nerve barrier without affecting Schwann cell function after neural injury.* Journal of neuroscience research, 2007. **85**(4): p. 766-77.
154. Campana, W.M., *Schwann cells: activated peripheral glia and their role in neuropathic pain.* Brain, behavior, and immunity, 2007. **21**(5): p. 522-7.
155. Griffin, J.W. and W.J. Thompson, *Biology and pathology of nonmyelinating Schwann cells.* Glia, 2008. **56**(14): p. 1518-31.

156. Stoll, G., J.W. Griffin, C.Y. Li, and B.D. Trapp, *Wallerian degeneration in the peripheral nervous system: participation of both Schwann cells and macrophages in myelin degradation.* Journal of neurocytology, 1989. **18**(5): p. 671-83.
157. Perry, V.H., J.W. Tsao, S. Fearn, and M.C. Brown, *Radiation-induced reductions in macrophage recruitment have only slight effects on myelin degeneration in sectioned peripheral nerves of mice.* The European journal of neuroscience, 1995. **7**(2): p. 271-80.
158. Chen, Z.L., W.M. Yu, and S. Strickland, *Peripheral regeneration.* Annual review of neuroscience, 2007. **30**: p. 209-33.
159. Sulaiman, O.A. and T. Gordon, *Effects of short- and long-term Schwann cell denervation on peripheral nerve regeneration, myelination, and size.* Glia, 2000. **32**(3): p. 234-46.
160. Tofaris, G.K., P.H. Patterson, K.R. Jessen, and R. Mirsky, *Denervated Schwann cells attract macrophages by secretion of leukemia inhibitory factor (LIF) and monocyte chemoattractant protein-1 in a process regulated by interleukin-6 and LIF.* The Journal of neuroscience : the official journal of the Society for Neuroscience, 2002. **22**(15): p. 6696-703.
161. Siebert, H., A. Sachse, W.A. Kuziel, N. Maeda, and W. Bruck, *The chemokine receptor CCR2 is involved in macrophage recruitment to the injured peripheral nervous system.* Journal of neuroimmunology, 2000. **110**(1-2): p. 177-85.
162. Beuche, W. and R.L. Friede, *The role of non-resident cells in Wallerian degeneration.* Journal of neurocytology, 1984. **13**(5): p. 767-96.
163. Bruck, W., I. Huitinga, and C.D. Dijkstra, *Liposome-mediated monocyte depletion during wallerian degeneration defines the role of hematogenous phagocytes in myelin removal.* Journal of neuroscience research, 1996. **46**(4): p. 477-84.
164. Hikawa, N. and T. Takenaka, *Myelin-stimulated macrophages release neurotrophic factors for adult dorsal root ganglion neurons in culture.* Cellular and molecular neurobiology, 1996. **16**(4): p. 517-28.
165. Gitik, M., S. Liraz-Zaltsman, P.A. Oldenborg, F. Reichert, and S. Rotshenker, *Myelin down-regulates myelin phagocytosis by microglia and macrophages through interactions between CD47 on myelin and SIRPalpha (signal regulatory protein-alpha) on phagocytes.* Journal of neuroinflammation, 2011. **8**: p. 24.
166. Fry, E.J., C. Ho, and S. David, *A role for Nogo receptor in macrophage clearance from injured peripheral nerve.* Neuron, 2007. **53**(5): p. 649-62.
167. Jacque, J.M. and M. Stevenson, *The inner-nuclear-envelope protein emerin regulates HIV-1 infectivity.* Nature, 2006. **441**(7093): p. 641-5.
168. Alkhatib, G. and E.A. Berger, *HIV coreceptors: from discovery and designation to new paradigms and promise.* European journal of medical research, 2007. **12**(9): p. 375-84.
169. Verani, A., G. Gras, and G. Pancino, *Macrophages and HIV-1: dangerous liaisons.* Molecular immunology, 2005. **42**(2): p. 195-212.
170. Gavegnano, C., E.M. Kennedy, B. Kim, and R.F. Schinazi, *The Impact of Macrophage Nucleotide Pools on HIV-1 Reverse Transcription, Viral Replication, and the Development of Novel Antiviral Agents.* Molecular biology international, 2012. **2012**: p. 625983.

171. Lahouassa, H., W. Daddacha, H. Hofmann, D. Ayinde, E.C. Logue, L. Dragin, N. Bloch, C. Maudet, M. Bertrand, T. Gramberg, G. Pancino, S. Priet, B. Canard, N. Laguette, M. Benkirane, C. Transy, N.R. Landau, B. Kim, and F. Margottin-Goguet, *SAMHD1 restricts the replication of human immunodeficiency virus type 1 by depleting the intracellular pool of deoxynucleoside triphosphates.* Nature immunology, 2012. **13**(3): p. 223-8.
172. Hrecka, K., C. Hao, M. Gierszewska, S.K. Swanson, M. Kesik-Brodacka, S. Srivastava, L. Florens, M.P. Washburn, and J. Skowronski, *Vpx relieves inhibition of HIV-1 infection of macrophages mediated by the SAMHD1 protein.* Nature, 2011. **474**(7353): p. 658-61.
173. Bukrinsky, M.I., N. Sharova, M.P. Dempsey, T.L. Stanwick, A.G. Bukrinskaya, S. Haggerty, and M. Stevenson, *Active nuclear import of human immunodeficiency virus type 1 preintegration complexes.* Proceedings of the National Academy of Sciences of the United States of America, 1992. **89**(14): p. 6580-4.
174. Frank, I., H. Stoiber, S. Godar, H. Stockinger, F. Steindl, H.W. Katinger, and M.P. Dierich, *Acquisition of host cell-surface-derived molecules by HIV-1.* AIDS, 1996. **10**(14): p. 1611-20.
175. Tan, J. and Q.J. Sattentau, *The HIV-1-containing macrophage compartment: a perfect cellular niche?* Trends in microbiology, 2013. **21**(8): p. 405-12.
176. Herbein, G. and A. Varin, *The macrophage in HIV-1 infection: from activation to deactivation?* Retrovirology, 2010. **7**: p. 33.
177. Campbell, J.H., A.C. Hearps, G.E. Martin, K.C. Williams, and S.M. Crowe, *The importance of monocytes and macrophages in HIV pathogenesis, treatment, and cure.* AIDS, 2014. **28**(15): p. 2175-87.
178. Walker, J.A., M.L. Sulciner, K.D. Nowicki, A.D. Miller, T.H. Burdo, and K.C. Williams, *Elevated numbers of CD163+ macrophages in hearts of simian immunodeficiency virus-infected monkeys correlate with cardiac pathology and fibrosis.* AIDS research and human retroviruses, 2014. **30**(7): p. 685-94.
179. Anzinger, J.J., T.R. Butterfield, T.A. Angelovich, S.M. Crowe, and C.S. Palmer, *Monocytes as regulators of inflammation and HIV-related comorbidities during cART.* Journal of immunology research, 2014. **2014**: p. 569819.
180. Brenchley, J.M., D.A. Price, T.W. Schacker, T.E. Asher, G. Silvestri, S. Rao, Z. Kazzaz, E. Bornstein, O. Lambotte, D. Altmann, B.R. Blazar, B. Rodriguez, L. Teixeira-Johnson, A. Landay, J.N. Martin, F.M. Hecht, L.J. Picker, M.M. Lederman, S.G. Deeks, and D.C. Douek, *Microbial translocation is a cause of systemic immune activation in chronic HIV infection.* Nature medicine, 2006. **12**(12): p. 1365-71.
181. Chen, M.F., A.J. Gill, and D.L. Kolson, *Neuropathogenesis of HIV-associated neurocognitive disorders: roles for immune activation, HIV blipping and viral tropism.* Current opinion in HIV and AIDS, 2014. **9**(6): p. 559-64.
182. El-Sadr, W.M., J. Lundgren, J.D. Neaton, F. Gordin, D. Abrams, R.C. Arduino, A. Babiker, W. Burman, N. Clumeck, C.J. Cohen, D. Cohn, D. Cooper, J. Darbyshire, S. Emery, G. Fatkenheuer, B. Gazzard, B. Grund, J. Hoy, K. Klingman, M. Losso, N. Markowitz, J. Neuhaus, A. Phillips, and C. Rappoport, *CD4+ count-guided interruption of antiretroviral treatment.* The New England journal of medicine, 2006. **355**(22): p. 2283-96.

183. Yurochko, A.D. and E.S. Huang, *Human cytomegalovirus binding to human monocytes induces immunoregulatory gene expression.* Journal of immunology, 1999. **162**(8): p. 4806-16.
184. Martinez, F.O. and S. Gordon, *The M1 and M2 paradigm of macrophage activation: time for reassessment.* F1000prime reports, 2014. **6**: p. 13.
185. Li, Y., W. Ling, H. Xu, M. Wang, and C. Wu, *The activation and dynamics of cytokine expression by CD4+ T cells and AIDS progression in HIV-1-infected Chinese individuals.* Microbial pathogenesis, 2012. **53**(5-6): p. 189-97.

CHAPTER II

Title: Pathology of the peripheral nervous system associated with SIV infection.

Adapted from:

"Monocyte traffic, dorsal root ganglion histopathology, and loss of intraepidermal nerve fiber density (IENFD) in SIV peripheral neuropathy"

by Jessica R. Lakritz, Ayman Bodair, Neal Shah, Ryan O'Donnell, Michael J Polydefkis, Andrew D. Miller, and Tricia H. Burdo

American Journal of Pathology. 2015. Jul;185(7):1912-23.

Reprinted with permission from Elsevier.

and

"Loss of intraepidermal nerve fiber density during SIV peripheral neuropathy is mediated by monocyte activation and elevated monocyte chemotactic proteins"

by Jessica R. Lakritz, Jake A. Robinson, Michael J. Polydefkis, Andrew D. Miller, and Tricia H, Burdo

Journal of Neuroinflammation. 2015 Dec 18; 12:237.

Author contributions:

JRL and THB conceived and designed the experiments. JRL, AB, NS, RO'D, ADM, JAR performed the experiments. JRL, THB, ADM, and MJP analyzed the data. JRL and THB wrote the paper. All authors carried out paper revisions.

ABSTRACT

SIV-infected, CD8-depleted rhesus macaques rapidly progress to AIDS and develop pathologies that are seen in HIV-infected humans with peripheral neuropathy. Here, we describe histopathological changes in the dorsal root ganglia (DRG) including satellitosis, neuronophagia, and Nageotte nodules. Severity of DRG pathology was correlated to a greater loss of intraepidermal nerve fiber density (IENFD) at necropsy. IENFD decreased during early SIV-infection (<21 days post-infection) and failed to recover over the course of progression to AIDS. DRG pathology did not develop until late infection. We found a late decline at necropsy in tropomyosin receptor kinase A (TRKA)+ peptidergic DRG neurons and isolectin B4 (IB4)+ non-peptidergic DRG neurons (occurring between 55 and 168 dpi). Neurofilament 200 (NF200)+ myelinated, large-diameter neurons were not affected by SIV infection. Thus, SIV-infected, CD8-depleted rhesus macaques develop a loss of IENFD that precedes damage, consisting of loss of small-diameter neurons, to the DRG.

INTRODUCTION

Peripheral neuropathy (PN) is the most common neurologic complication of HIV infection and continues to negatively affect patient quality of life [1, 2]. Distal sensory polyneuropathy (DSP) is a common type of HIV-PN that persists despite the decreased use neurotoxic antiretroviral drugs [1-4]. HIV-DSP is identical to antiretroviral neurotoxicity (ATN) clinically; both result in pain, numbness, and hypersensitivity in the lower legs and feet, as well as sometimes in the hands [1, 4]. Despite the clinical similarities, the underlying pathophysiological mechanism of HIV-DSP and ATN are unique.

The study of the pathology of peripheral neuropathy in HIV-infected human subjects is confounded by the use of antiretroviral drugs, including nucleotide reverse transcriptase inhibitors (NRTIs) and protease inhibitors (PI), which may cause ATN. HIV-PN pathology can be confounded by increased alcohol consumption [5] and vitamin B12 deficiency [6]. Diagnosis of PN in humans relies on a combination of autonomic testing, nerve biopsies, and skin biopsies [7]. However, examining intraepidermal nerve fiber density (IENFD) via skin biopsies is an objective pathological measure of PN pathogenesis.

Animal models lend themselves to the study of viral pathogenesis and immune response (as reviewed in Burdo TH and Miller AD [8]). Transgenic mice expressing gp120 have failed to develop peripheral neuropathy after two months [9]. However, in a murine immunodeficiency virus model [10] and after perineural application of gp120 to the sciatic nerve in rats [11] peripheral nerve damage has been shown. Feline immunodeficiency virus (FIV) recapitulates PN damage with HIV infection, but the virus

uses a different co-receptor (CD134) [12, 13]. SIV is particularly attractive given the similarities between humans and nonhuman primates with simian immunodeficiency virus (SIV) being closely related to HIV genomically, structurally, and clinically [8, 13]. Both viruses target the CD4+ lymphocytes, monocytes, and macrophages through CD4 and CCR5, resulting in immune suppression and neuropathology that includes a decline in IENF densities and similar pathology in the DRG [8].

Using a neurovirulent clone and immunosuppressive SIV swarm in pigtailed macaques, Mankowski et. al. demonstrated that the SIV+ cells in the DRG were CD68+ macrophages and that damage to the DRG precedes nerve fiber functional loss [14-16]. We have previously demonstrated that CD8+ lymphocyte depleted SIV-infected rhesus macaques rapidly develop AIDS and histopathology that reproduces the hallmarks of human HIV infection pre-ART including SIVE encephalitis (SIVE), lymph node damage, the depletion of gut T cells, and peripheral neuropathy [17-19].

Here, we sought to characterize the pathology of the peripheral nervous system (PNS) in SIV+ CD8-depleted macaques. Pathology in human patients with HIV consists of a reduction of IENFD [20, 21] and neuronal loss in the DRG [22, 23], even in the cART era and in patients with no history of neurotoxic d-drugs [1, 23]. In this study, we sought to further investigate the neuronal loss in the DRG. There are several classes of DRG neurons, which perform different functions. Historically, DRG neurons have been classified as “small” and “large” diameter neurons, but this method of neuron classification is unreliable in that neuron diameter size is continuous and thus it is difficult to create a threshold for one size versus the other. Additionally, it has recently been shown by transcription analysis that there are three large clusters of DRG neurons

that can be identified by immunohistochemistry markers [24]. The neurofilament (NF) containing cluster can be identified by its expression of the NF heavy chain (NF200). NF200+ neurons are large diameter, myelinated neurons that are responsible for mechanoreceptive and proprioceptive signals that are transmitted through Aβ fibers. The second cluster of neurons is the peptidergic nociceptors group, which can be identified by expression of tropomyosin receptor kinase A (TRKA). TRKA+ neurons are peptidergic nociceptors. Finally, the third group is non-peptidergic nociceptors and express isolectin B4 glycoprotein (IB4). Both IB4+ neurons and TRKA+ neurons are small diameter neurons that give rise to C-fibers and Aδ fibers that transmit nociceptive, thermal, and mechanoreceptive signals. These three clusters consist of different subclasses of neurons that have been the focus of recent debate [24-26]. We chose to simplify our studies and focus on NF, peptidergic, and non-peptidergic neurons to gain insight into what classes of neurons are being lost during SIV infection.

MATIERIALS and METHODS

Ethical Statement

All animals used in this study were handled in strict accordance with American Association for Accreditation of Laboratory Animal Care with the approval of the Institutional Animal Care and Use Committee of Harvard University and the Institutional Animal Care and Use Committee of Tulane University.

Animals, viral infection, and CD8 lymphocyte depletion

Seventeen rhesus macaques (*Macaca mulatta*) were used in this study. Four animals were uninfected control animals. Thirteen macaques were inoculated intravenously with SIVmac251 (a generous gift from Dr. Ronald Desrosiers, University of Miami). All infected animals were administered 10 mg/kg of anti-CD8 antibody subcutaneously at day 6 after infection and 5 mg/kg intravenously at days 8 and 12 after infection in order to achieve rapid progression to AIDS. The human anti-CD8 antibody was provided by the NIH Non-human Primate Reagent Resource (RR016001, AI040101). 3/13 SIV-infected animals were timed sacrificed at 21 dpi. 10/13 SIV-infected animals were sacrificed at the onset of terminal AIDS. The development of simian AIDS was determined post-mortem by the presence of: *Pneumocystis carinii*-associated interstitial pneumonia, *Mycobacterium avium*-associated granulomatous enteritis, hepatitis, lymphadenitis and/or adenovirus infection of surface enterocytes in both small and large intestines. Animals were housed at either the New England Primate Research Center (NEPRC; Southborough, MA) or Tulane University's National Primate Research Center (TNPRC; Covington, LA) in strict accordance with standards of the American Association for Accreditation of Laboratory Animal Care.

Necropsy and Histopathology

Animals were necropsied immediately following death and representative sections of all major organs were collected, fixed in 10% neutral buffered formalin (NBF), embedded in paraffin and sectioned at 5μm. After deparaffinization in xylene, the tissues were hydrated in graded alcohols, counterstained with Harris Hematoxylin

Solution (Sigma-Aldrich) for two minutes and rinsed with running water. The slides were then dipped sequentially in acid alcohol (90% methanol, 5% sulfuric acid, 5% acetic acid; Sigma-Aldrich) and ammonia water (15-20 drops ammonium hydroxide in 250 ml water; Sigma-Aldrich), rinsing with running water after each, followed by 80% alcohol for two minutes and eosin (Sigma-Aldrich) for two minutes. Tissue sections were then rinsed in graded alcohols and dehydrated with xylene and mounted with VectaMount (Vector).

Histopathologic analysis of DRG morphology

Hematoxylin (H) and eosin (E) stained sections of DRG were evaluated blindly for histopathologic lesions by a board-certified veterinary anatomic pathologist and scored based on the presence and severity of infiltrating mononuclear cells, neuronophagia and Nageotte nodules as previously described [17, 27]. Overall pathology was scored on a previously validated [27] scale of 0-3 at increments of 0.5 via the following criteria: (0) No significant findings; (1) Mild: scattered infiltrating mononuclear cells with rare evidence of neuronophagia and/or neuronal loss; (2) Moderate: Increased numbers of infiltrating mononuclear cells with occasional neuronophagia and/or neuronal loss; and (3) Severe: Abundant infiltrating mononuclear cells, frequent neuronophagia and neuronal loss were all present [16, 17, 27].

Skin Punch and IENFD Measurement

Skin punch biopsy specimens with IENF were performed in SIV+ animals that were sacrificed with AIDS. Skin punches (3 mm) were taken serially near the sural innervation site just distal to the lateral malleolus. Biopsy specimens were taken for each animal at pre-infection, several time points during infection, and at necropsy. Biopsy specimens were fixed in Zamboni's fixative and processed for dividing into sections. Sections (50μm thick) of serial punch skin biopsy specimens were stained with anti-PGP 9.5, a panaxonal marker (1:10,000 dilution; ABD Serotec). Nerve fiber length/volume of epidermis (IENFD) was quantified using computer software (Space balls program; Microbrightfield Bioscience) as previously described [27, 28].

Immunohistochemistry and quantification

DRG sections were deparaffinized with xylene and hydrated in a series of graded alcohols and stained for neuronal markers. Slides were stained with either anti-NF200 (1:800, EMD Millipore), anti-TRKA (1:2000, Abcam), or biotinylated Lectin I Isolectin B4 (1:50, Vector Laboratories). Sections were counterstained with hematoxylin, dehydrated, and mounted using VectaMount permanent mounting medium (Vector), visualized and photographs were taken using a Zeiss Axio Imager M1 microscope (Carl Zeiss MicroImaging, Inc.) using Plan-Apochromat x20/0.8 Korr objectives.

Neurons were identified based on morphology. The average diameter of each type of neuronal cell body was determined using Image J software (NIH). 100 neuronal cell bodies were measured in the same uninfected animal for each neuronal marker.

The number of positive and negative neuronal cell bodies was counted on eight non-overlapping fields of view at 200x magnification. The percentage of positive neurons of all neurons in the DRG was calculated by dividing the number of positive neurons by the number of positive plus negative neurons and multiplying by 100.

Statistical methods

Prism version 5.0f (GraphPad Software, Inc., San Diego, CA) software was used for statistical analyses. Spearman correlation was used for all correlations. A Wilcoxon matched-pairs rank test was used to determine loss when the loss of IENFD occurred. Non-parametric ANOVA was used to detect difference in the number of neurons between different groups of animals, followed by a Dunn's post-test. A p value less than 0.05 was considered significant.

RESULTS

Animals used in this study

Thirteen rhesus macaques were infected intravenously with SIVmac251 and were administered a CD8-depletion antibody on days 6, 8, and 12 post-infection (DPI). 3/13 infected animals were sacrificed at 21 DPI. 10/13 infected animals were sacrificed at the development of terminal AIDS with an average survival of 106.2 ± 11.8 DPI (Table 2.1)

Intraepidermal nerve fiber densities decreased with SIV infection

Serial skin biopsies of the central footpad were obtained in the ten (animals A01-A10) SIV-infected rhesus macaques used in this study at pre-infection and days 8 (animals A01-A03 only), 21, 42, 63 post-infection, and at necropsy. The pre-infection biopsies had several long contiguous fibers terminating in the basement layer of the stratum corneum (Figure 2.1A, arrows), whereas the biopsies taken at necropsy had very few segmented fibers (Figure 2.1B, arrows). IENFD decreased after SIV infection in all animals (Figure 2.1C). These data were standardized where the percent change in fiber density from pre-infection was compared between the animals over time (Figure 2.1D). IENFD decreased by an average of 45.6% (S.E.M. of 7.3%) from pre-infection to the time of necropsy with AIDS (range of 13.0 to 82.5%) (Figure 2.1D). A significant loss of IENFD occurred during early infection by 21 dpi ($p<0.01$; Figure 2.1C-D).

Dorsal root ganglia pathology

DRG pathology was evaluated based on the presence and severity of satellitosis, neuronophagia, and Nageotte nodules. Satellitosis refers to an increase in the number of satellite cells. In normal DRG tissue, there is a thin layer of satellite cells, which surround the neuronal cell bodies. These satellite cells consist of Schwann cells, macrophages, T cells, and other types of immune cells. During SIV infection, we have observed that there is an increase in the number of satellite cells (satellitosis). We have noted varying degrees of satellitosis ranging from mild to severe (Figure 2.2A-B). Neuronophagia refers to the phagocytosis of dying neurons by satellite cells (Figure 2.2C). Neuronophagia is the precursor lesion to a Nageotte nodule. A Nageotte nodule

is the most severe type of lesion in the DRG. A Nageotte nodule forms when satellite cells have completely overtaken the foci of what was once a neuronal cell body (Figure 2.2D). DRG pathology was ranked on a scale of zero to three at increments of 0.5. A score of zero indicated no pathology (normal findings). A score of 1, 2, or 3 referred to mild, moderate, or severe pathology, respectively.

DRG tissue was examined from lumbar (LDRG), sacral (SDRG), and thoracic (TDRG) regions. Cervical (CDRG) regions were not consistently obtained from all animals, and thus were excluded from future studies. LDRG, SDRG, and TDRG had varying degrees of pathology both within the same animal and between animals. LDRG was consistently the most severe region and thus was evaluated for neuronal loss. Additionally, a greater percent loss of IENFD from pre-infection to necropsy was associated with a higher DRG pathology score (Figure 2.3; $p<0.05$). These data show that pathology of DRG and loss of IENFD are linked in severity.

Differential loss of neurons with SIV infection.

A loss of neuronal density in the DRG during HIV and SIV infection has been previously reported [4, 14, 29]. DRG neurons are heterogeneous. We used common neuronal markers (NF200, TRKA, and IB4) to identify different populations of neurons (Figure 2.4A-C). All three markers labeled neurons of different sizes ($p<0.0001$; Figure 2.4D). NF200+ neurons were the largest, with an average diameter 58.2μm (SEM of 1.1). IB4 and TRKA labeled small diameter neurons, although IB4+ neurons were slightly larger. IB4+ neurons had an average diameter of 42.9μm (SEM of 0.82) and TRKA+ neurons had a diameter of 37.6μm (SEM of 0.9).

Next, we examined the density of the three types of neurons in LDRG tissue from uninfected animals and infected animals that were sacrificed at 21 dpi or with terminal AIDS. The absolute densities of neurons per total area of DRG tissue and the percents of total DRG neurons were calculated. We found that there were no differences in the absolute numbers of NF200+ large diameter neurons per mm^2 of tissue (223.6±19.3 versus 176.5±8.7 cells/mm^2; p=0.10; Figure 2.5A) or in the percentages of NF200+ neurons of all neurons (60.6±4.1 versus 53.5±2.6 %; p=0.24; Figure 2.5B) between uninfected and infected animals. There was a significant reduction in the absolute number of TRKA+ small diameter neurons (133.2±6.2 versus 96.6±4.7 cells/mm^2; $p<0.05$; Figure 2.5C) and the percentage of TRKA+ neurons (42.5±3.9 versus 29.6±1.4 %; $p<0.01$; Figure 2.5D). There was no significant difference in the absolute number of IB4+ neurons (206.8±31.0 versus 184.7±22.4 cells/mm^2; p=0.43; Figure 2.5E), but the percentage of IB4+ neurons was reduced in SIV-infected animals that progressed to AIDS (62.5±3.6 versus 48.1±2.9 %; $p<0.05$; Figure 2.5F). There was no significant difference between uninfected and DPI 21 animals in absolute number or percent of subpopulations of neurons, suggesting that the differential loss of small-diameter neurons occurs during late infection.

DISCUSSION

In this study, we characterized the pathology associated with SIV-PN. We found the presence of satellitosis, neuronophagia, and Nageotte nodules in multiple DRG regions in infected animals, as well as a loss of IENFD; similar to what has been

observed during HIV infection in humans [4]. There was a link between the severity of DRG pathology and a greater loss of small nerve fiber density in the footpad. This association between pathology at different regions of the PNS, suggests a relay of signals from one region to the other, or perhaps systemic neuroinflammatory/neurotoxic proteins that facilitate damage to both regions simultaneously. Here, we observed a significant early loss of IENFD at 21 DPI and no loss of DRG neurons in animals sacrificed at 21 DPI, suggesting that damage to peripheral nerves precedes damage to the DRG. In fact, loss of IENFD may occur even before 21 DPI. Three animals in this study received skin biopsies at 8 DPI and all three animals had a decrease in IENFD compared to pre-infection. However, this observation was not statistically significant likely due to a low sample size.

Our finding that damage to the nerve fibers in the skin occurs before damage to the DRG supports the findings from another study that found an early loss of IENFD, followed by DRG neuronal loss, and finally reduced nerve fiber conduction velocity [14]. This study found that IENFD and conduction velocity of C-fibers were not correlated, probably due to sampling locations. The data presented by Laast, et al [14] and in this study support the fact that long C-fibers are the most sensitive to viral or cytokine toxicity during SIV infection and that there is an associated loss of DRG neurons. Measuring nerve fiber conduction velocity and IENFD are both valid techniques to diagnose PNs, although recently, clinicians have favored IENFD measure because it is minimally invasive, easy, and strongly correlates with clinical symptoms [7].

Skin biopsies are a valuable tool for clinical diagnosis of small fiber neuropathies and have largely replaced sural nerve biopsies for assessment of unmyelinated nerve

fibers in conditions such as diabetic neuropathy and HIV-associated sensory neuropathy. A recent report indicates that rhesus macaques (inoculated with both the neurovirulent molecular SIV clone SIV/17E-Fr and the immunosuppressive strain SIV/DeltaB670) do not develop a significant decline in IENFD [30]. In contrast, here we show that SIVmac251 infected, CD8 depleted rhesus macaques show a significant decrease in IENFD and that this decrease occurs early after infection. These differences may be due to the different viral swarms used in the models. The early loss of IENFD demonstrates that the animals developed signs of SIV-PN, early in infection, before AIDS-induced diarrhea could have caused a nutritional deficiency, resulting in metabolic neuropathy prior to sacrifice. Loss of sensory fibers and pathology of the sensory nerve cell bodies that reside in the DRG are hallmarks of HIV/SIV pathogenesis. It is interesting to note that we do not see robust evidence of axonal degeneration along the course of the nerve, but there is subtle damage to the IENF in the skin, possibly because not enough time may have passed to develop prominent lesions within the course of the nerve.

We also found that small-diameter neurons were differentially lost during late SIV infection. Both IB4+ and TRKA+ neurons give rise to unmyelinated C-fibers. C-fibers are responsible for the “second pain” sensation in response to strong stimuli that results in a deeper and slower pain sensation. Damage to C-fibers or hyperexcitability of C-fibers results in neuropathic pain. We found that both peptidergic and non-peptidergic neurons are lost during SIV-infection. Peptidergic neurons respond to substance P (SP) and calcitonin gene-related peptide (CGRP) [24]. These neuropeptides are heavily involved in neuropathic pain sensation and transmission. SP has also been implicated in HIV

pathogenesis and inflammatory pathways [31-34]. While there have been reports of all different types of afferent nerve fibers being affected by HIV and SIV infection, C-fibers are damaged the most robustly and cause neuropathic pain [4, 14, 27].

Table 2.1: SIV+ animals used in this study.

Treatment Group	Animal ID	Survival (days)	Satellitosis in LDRG	Neuronophagia in LDRG	Nageotte nodules in LDRG
SIV+, CD8-depleted (AIDS)	A01	146	Severe	Moderate	Moderate
	A02	55	Moderate	Mild	Rare
	A03	174	Severe	Mild	Mild
	A04	168	Mild	None	None
	A05	77	Moderate	Moderate	Rare
	A06	97	Mild	None	None
	A07	77	Severe	Mod-Severe	Extensive
	A08	84	Severe	Moderate	Moderate
	A09	106	Moderate	Mild	Mild
	A10	96	Mild	None	None
SIV+, CD8-depleted (DPI 21)	B01	21	Moderate	Moderate	Rare
	B02	21	Moderate	Moderate	Rare
	B03	21	Mild	Mild	None

Figure 2.1

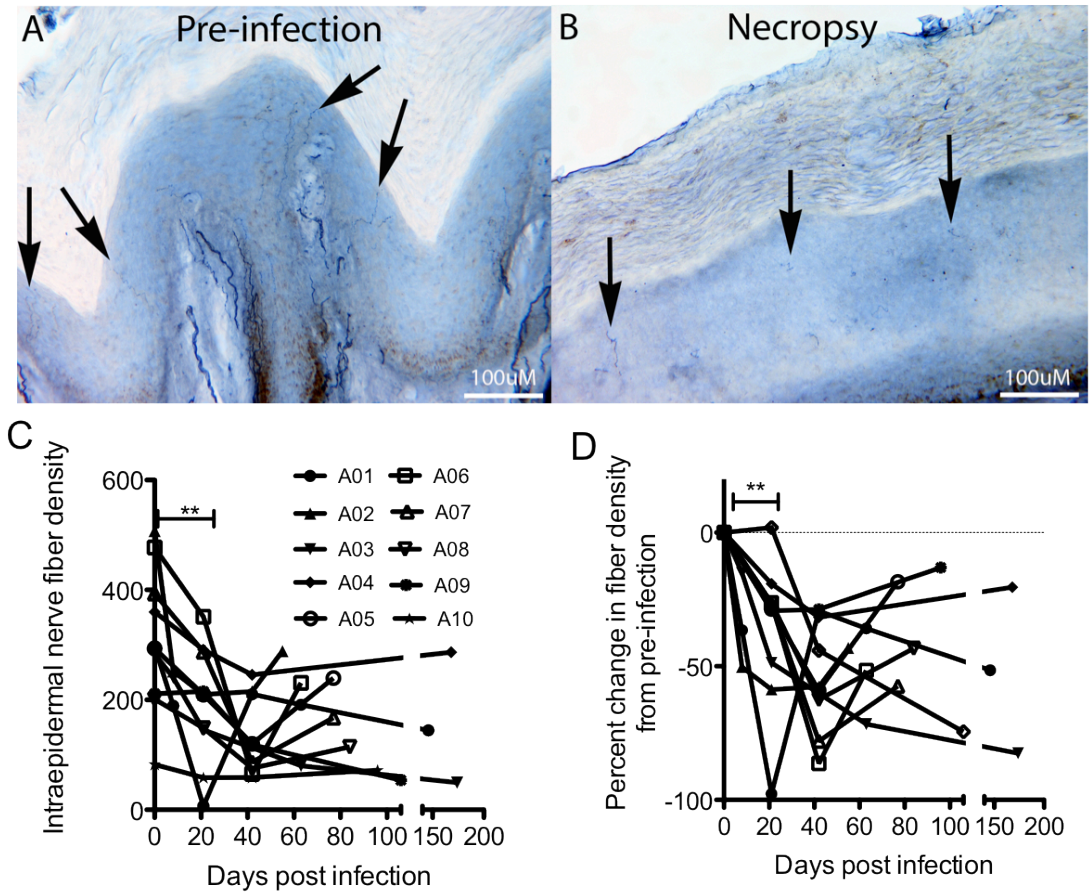
A
Pre-infection
100uM
B
Necropsy
100uM
C
Intraepidermal nerve fiber density
600
400
200
0
**
A01
A02
A03
A04
A05
A06
A07
A08
A09
A10
0 20 40 60 80 100 150 200
Days post infection
D
Percent change in fiber density from pre-infection
0
-50
-100
**
0 20 40 60 80 100 150 200
Days post infection

Figure 2.1: Intraepidermal nerve fiber (IENF) density decreased post-infection.

Pre-infection biopsy of animal A07 had several long contiguous IENFs terminating in the basement layer of the stratum corneum (A, arrows). Biopsy of Animal A07 taken at necropsy upon AIDS had very few segmented IENFs (B, arrows). (C) IENF density (IENFD) was serially measured. (D) Percent lost over time was calculated. Difference between pre-infection and 21 DPI was calculated using a Wilcoxon matching-pairs rank test. **$p<0.01$

Figure 2.2

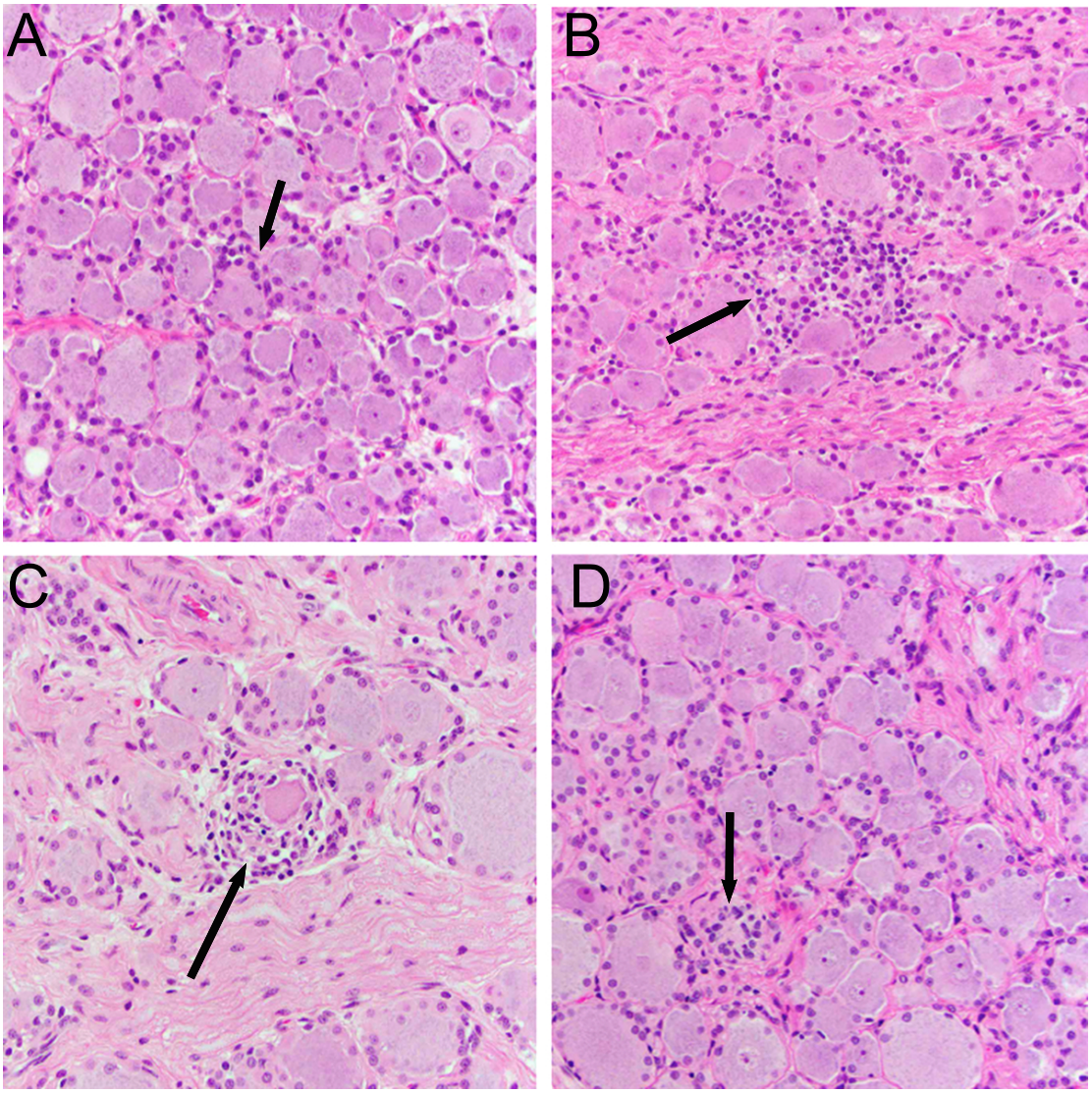

Figure 2.2: Dorsal root ganglia pathology.

(A) DRG with mild focal satellitosis, which is defined as increased numbers of cells around a neuronal cell body (arrow). (B) DRG with moderate inflammation that has replaced a few ganglion cells (arrow) with an increase in satellite cells (C) DRG with inflammation associated with a degenerate ganglion cell (arrow). Note the cells encroaching around the outside of the ganglion indicative of neuronophagia, a precursor lesion to the development of a Nageotte nodule. (D) DRG with a Nageotte nodule, focal proliferation of satellite cells that completely replace foci of neuronal cell loss (arrow). Images were captured at 200x magnification.

Figure 2.3

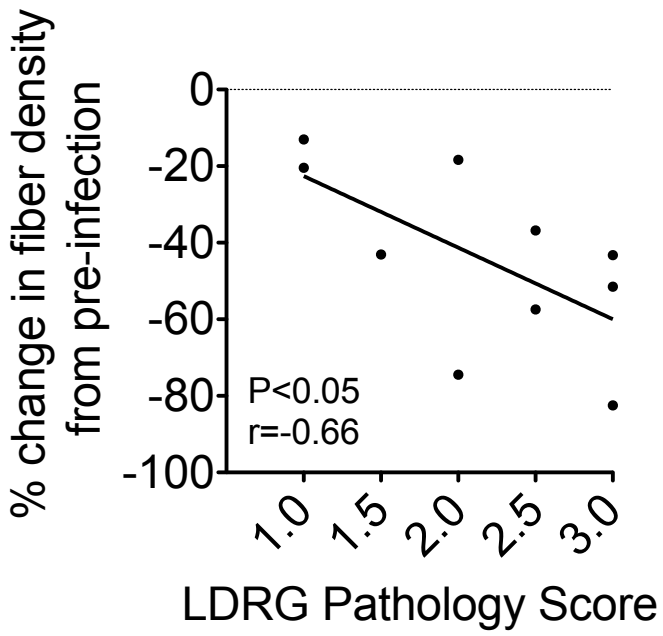
% change in fiber density from pre-infection
0
-20
-40
-60
-80
-100
P<0.05
r=-0.66
1.0
1.5
2.0
2.5
3.0
LDRG Pathology Score

Figure 2.3: Severe DRG pathology is correlated to a greater loss of IENFD.

Lumbar DRG (LDRG) pathology was scored on a scale of 1.0 (mild) to 3.0 (severe). IENFD was measured at pre-infection and necropsy and the percent change was calculated by dividing the difference in IENFD from pre-infection to necropsy by the pre-infection value and multiplying by 100. Percent change of IENFD was correlated to LDRG pathology using a Spearman correlation test. $P < 0.05$, $r = -0.66$.

Figure 2.4

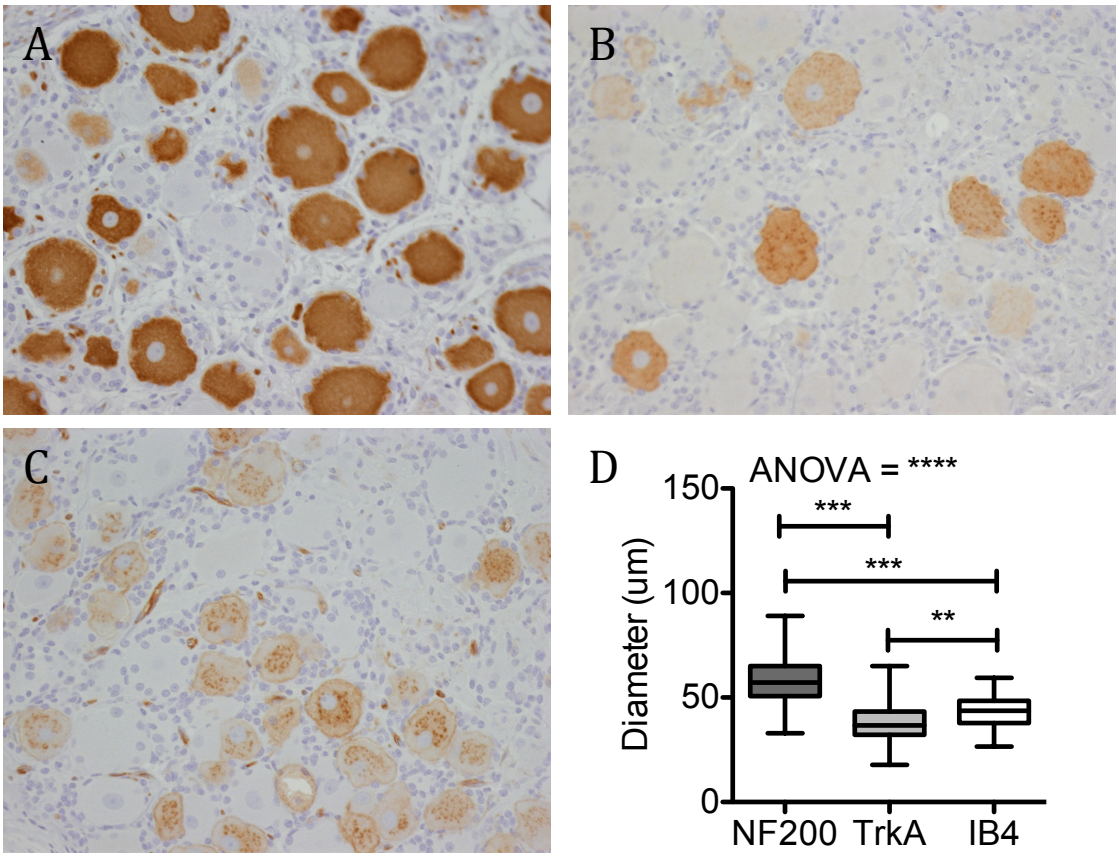

Figure 2.4: Classification of types of DRG neurons.

Lumbar DRG was stained for A) NF200, B) TRKA, and C) IB4. D) Each of these markers labeled neurons with different diameters. Images were captured at 200x magnification. A Kruskal-Wallis test, followed by a Dunn's post-test was used to determine significant differences between the average diameters of each class of neurons. **, $p<0.01$; ***, $p<0.001$; ****, $p<0.0001$.

Figure 2.5

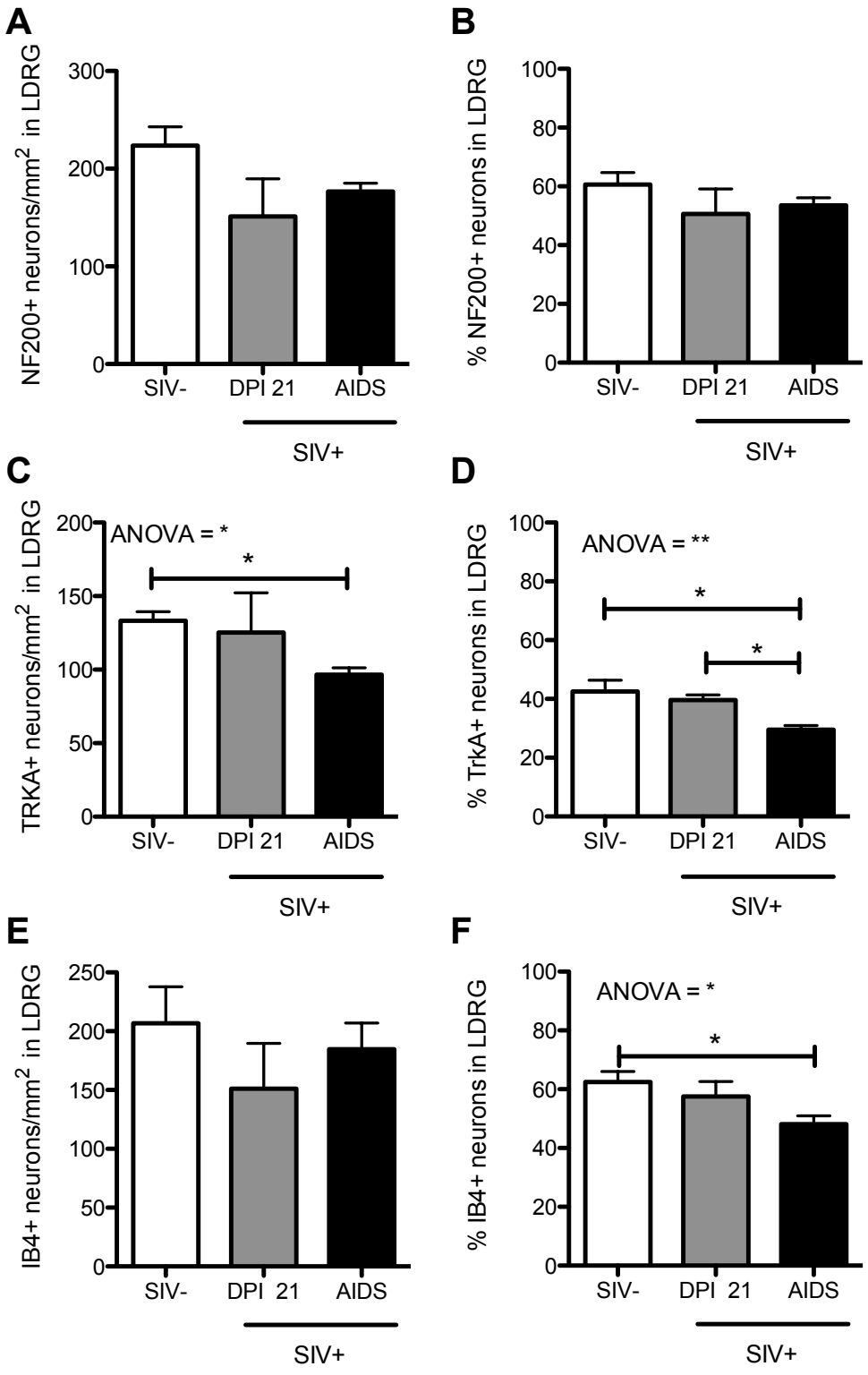
A
NF200+ neurons/mm2 in LDRG
300
200
100
0
SIV-
DPI 21
AIDS
SIV+
B
% NF200+ neurons in LDRG
100
80
60
40
20
0
SIV-
DPI 21
AIDS
SIV+
C
TRKA+ neurons/mm2 in LDRG
ANOVA = *
*
200
150
100
50
0
SIV-
DPI 21
AIDS
SIV+
D
% TrkA+ neurons in LDRG
ANOVA = **
*
*
100
80
60
40
20
0
SIV-
DPI 21
AIDS
SIV+
E
IB4+ neurons/mm2 in LDRG
250
200
150
100
50
0
SIV-
DPI 21
AIDS
SIV+
F
% IB4+ neurons in LDRG
ANOVA = *
*
100
80
60
40
20
0
SIV-
DPI 21
AIDS
SIV+

Figure 2.5: SIV-infection results in a differential loss of small-diameter neurons that occurs during late infection.

Lumbar DRG from 4 uninfected and 13 SIV-infected animals used to detect early or late loss of DRG neurons. 3/13 SIV-infected animals were sacrificed at 21 dpi. The remained SIV-infected animals (10/13) were sacrificed with AIDS. Tissues were stained for A-B) NF200, C-D) TrkA, or E-F) IB4. The absolute density (A, C, and E) of neurons (number of positive neurons per mm^2 of DRG tissue) and the percentage of positive neurons per total DRG (B, D, and F) were calculated. Differences between the three groups (uninfected, DPI 21, and AIDS) were detected with a Kruskal-Wallis test, followed by a Dunn's post-test. *, $p<0.05$; ** $p<0.01$.

REFERENCES

1. Ellis, R.J., D. Rosario, D.B. Clifford, J.C. McArthur, D. Simpson, T. Alexander, B.B. Gelman, F. Vaida, A. Collier, C.M. Marra, B. Ances, J.H. Atkinson, R.H. Dworkin, S. Morgello, and I. Grant, *Continued high prevalence and adverse clinical impact of human immunodeficiency virus-associated sensory neuropathy in the era of combination antiretroviral therapy: the CHARTER Study.* Archives of neurology, 2010. **67**(5): p. 552-8.
2. Nicholas, P.K., L. Mauceri, A. Slate Ciampa, I.B. Corless, N. Raymond, D.J. Barry, and A. Viamonte Ros, *Distal sensory polyneuropathy in the context of HIV/AIDS.* The Journal of the Association of Nurses in AIDS Care : JANAC, 2007. **18**(4): p. 32-40.
3. Verma, S., L. Estanislao, and D. Simpson, *HIV-associated neuropathic pain: epidemiology, pathophysiology and management.* CNS drugs, 2005. **19**(4): p. 325-34.
4. Pardo, C.A., J.C. McArthur, and J.W. Griffin, *HIV neuropathy: insights in the pathology of HIV peripheral nerve disease.* Journal of the peripheral nervous system : JPNS, 2001. **6**(1): p. 21-7.
5. Mellion, M.L., E. Silbermann, J.M. Gilchrist, J.T. Machan, L. Leggio, and S. de la Monte, *Small-fiber degeneration in alcohol-related peripheral neuropathy.* Alcoholism, clinical and experimental research, 2014. **38**(7): p. 1965-72.
6. Kalita, J., S. Chandra, S.K. Bhoi, R. Agarwal, U.K. Misra, S.K. Shankar, and A. Mahadevan, *Clinical, nerve conduction and nerve biopsy study in vitamin B12 deficiency neurological syndrome with a short-term follow-up.* Nutritional neuroscience, 2014. **17**(4): p. 156-63.
7. England, J.D., G.S. Gronseth, G. Franklin, G.T. Carter, L.J. Kinsella, J.A. Cohen, A.K. Asbury, K. Szigeti, J.R. Lupski, N. Latov, R.A. Lewis, P.A. Low, M.A. Fisher, D. Herrmann, J.F. Howard, G. Lauria, R.G. Miller, M. Polydefkis, and A.J. Sumner, *Practice parameter: the evaluation of distal symmetric polyneuropathy: the role of autonomic testing, nerve biopsy, and skin biopsy (an evidence-based review). Report of the American Academy of Neurology, the American Association of Neuromuscular and Electrodiagnostic Medicine, and the American Academy of Physical Medicine and Rehabilitation.* PM & R : the journal of injury, function, and rehabilitation, 2009. **1**(1): p. 14-22.
8. Burdo, T.H. and A.D. Miller, *Animal models of HIV peripheral neuropathy.* Future virology, 2014. **9**(5): p. 465-474.
9. Keswani, S.C., C. Jack, C. Zhou, and A. Hoke, *Establishment of a rodent model of HIV-associated sensory neuropathy.* The Journal of neuroscience : the official journal of the Society for Neuroscience, 2006. **26**(40): p. 10299-304.
10. Cao, L., M.B. Butler, L. Tan, K.S. Draleau, and W.Y. Koh, *Murine immunodeficiency virus-induced peripheral neuropathy and the associated cytokine responses.* Journal of immunology, 2012. **189**(7): p. 3724-33.
11. Wallace, V.C., J. Blackbeard, T. Pheby, A.R. Segerdahl, M. Davies, F. Hasnie, S. Hall, S.B. McMahon, and A.S. Rice, *Pharmacological, behavioural and*

mechanistic analysis of HIV-1 gp120 induced painful neuropathy. Pain, 2007. **133**(1-3): p. 47-63.
12. Shimojima, M., T. Miyazawa, Y. Ikeda, E.L. McMonagle, H. Haining, H. Akashi, Y. Takeuchi, M.J. Hosie, and B.J. Willett, *Use of CD134 as a primary receptor by the feline immunodeficiency virus.* Science, 2004. **303**(5661): p. 1192-5.
13. Lackner, A.A., S. Dandekar, and M.B. Gardner, *Neurobiology of simian and feline immunodeficiency virus infections.* Brain pathology, 1991. **1**(3): p. 201-12.
14. Laast, V.A., B. Shim, L.M. Johanek, J.L. Dorsey, P.E. Hauer, P.M. Tarwater, R.J. Adams, C.A. Pardo, J.C. McArthur, M. Ringkamp, and J.L. Mankowski, *Macrophage-mediated dorsal root ganglion damage precedes altered nerve conduction in SIV-infected macaques.* The American journal of pathology, 2011. **179**(5): p. 2337-45.
15. Dorsey, J.L., L.M. Mangus, J.D. Oakley, S.E. Beck, K.M. Kelly, S.E. Queen, K.A. Metcalf Pate, R.J. Adams, C.F. Marfurt, and J.L. Mankowski, *Loss of Corneal Sensory Nerve Fibers in SIV-Infected Macaques: An Alternate Approach to Investigate HIV-Induced PNS Damage.* The American journal of pathology, 2014. **184**(6): p. 1652-9.
16. Laast, V.A., C.A. Pardo, P.M. Tarwater, S.E. Queen, T.A. Reinhart, M. Ghosh, R.J. Adams, M.C. Zink, and J.L. Mankowski, *Pathogenesis of simian immunodeficiency virus-induced alterations in macaque trigeminal ganglia.* Journal of neuropathology and experimental neurology, 2007. **66**(1): p. 26-34.
17. Burdo, T.H., K. Orzechowski, H.L. Knight, A.D. Miller, and K. Williams, *Dorsal root ganglia damage in SIV-infected rhesus macaques: an animal model of HIV-induced sensory neuropathy.* The American journal of pathology, 2012. **180**(4): p. 1362-9.
18. Burdo, T.H., C. Soulas, K. Orzechowski, J. Button, A. Krishnan, C. Sugimoto, X. Alvarez, M.J. Kuroda, and K.C. Williams, *Increased monocyte turnover from bone marrow correlates with severity of SIV encephalitis and CD163 levels in plasma.* PLoS pathogens, 2010. **6**(4): p. e1000842.
19. Williams, K. and T.H. Burdo, *Monocyte mobilization, activation markers, and unique macrophage populations in the brain: observations from SIV infected monkeys are informative with regard to pathogenic mechanisms of HIV infection in humans.* Journal of neuroimmune pharmacology : the official journal of the Society on NeuroImmune Pharmacology, 2012. **7**(2): p. 363-71.
20. Polydefkis, M., C.T. Yiannoutsos, B.A. Cohen, H. Hollander, G. Schifitto, D.B. Clifford, D.M. Simpson, D. Katzenstein, S. Shriver, P. Hauer, A. Brown, A.B. Haidich, L. Moo, and J.C. McArthur, *Reduced intraepidermal nerve fiber density in HIV-associated sensory neuropathy.* Neurology, 2002. **58**(1): p. 115-9.
21. Polydefkis, M., *Skin biopsy findings predict development of symptomatic neuropathy in patients with HIV.* Nature clinical practice. Neurology, 2006. **2**(12): p. 650-1.
22. Authier, F.J. and R.K. Gheradi, *Peripheral neuropathies in HIV-infected patients in the era of HAART.* Brain pathology, 2003. **13**(2): p. 223-8.
23. Kaku, M. and D.M. Simpson, *HIV neuropathy.* Current opinion in HIV and AIDS, 2014. **9**(6): p. 521-6.

24. Usoskin, D., A. Furlan, S. Islam, H. Abdo, P. Lonnerberg, D. Lou, J. Hjerling-Leffler, J. Haeggstrom, O. Kharchenko, P.V. Kharchenko, S. Linnarsson, and P. Ernfors, *Unbiased classification of sensory neuron types by large-scale single-cell RNA sequencing.* Nature neuroscience, 2015. **18**(1): p. 145-53.
25. Li, C.L., K.C. Li, D. Wu, Y. Chen, H. Luo, J.R. Zhao, S.S. Wang, M.M. Sun, Y.J. Lu, Y.Q. Zhong, X.Y. Hu, R. Hou, B.B. Zhou, L. Bao, H.S. Xiao, and X. Zhang, *Somatosensory neuron types identified by high-coverage single-cell RNA-sequencing and functional heterogeneity.* Cell research, 2016. **26**(1): p. 83-102.
26. Chiu, I.M., L.B. Barrett, E.K. Williams, D.E. Strochlic, S. Lee, A.D. Weyer, S. Lou, G.S. Bryman, D.P. Roberson, N. Ghasemlou, C. Piccoli, E. Ahat, V. Wang, E.J. Cobos, C.L. Stucky, Q. Ma, S.D. Liberles, and C.J. Woolf, *Transcriptional profiling at whole population and single cell levels reveals somatosensory neuron molecular diversity.* eLife, 2014. **3**.
27. Lakritz, J.R., A. Bodair, N. Shah, R. O'Donnell, M.J. Polydefkis, A.D. Miller, and T.H. Burdo, *Monocyte Traffic, Dorsal Root Ganglion Histopathology, and Loss of Intraepidermal Nerve Fiber Density in SIV Peripheral Neuropathy.* The American journal of pathology, 2015. **185**(7): p. 1912-23.
28. Liu, Y., J. Billiet, G.J. Ebenezer, B. Pan, P. Hauer, J. Wei, and M. Polydefkis, *Factors influencing sweat gland innervation in diabetes.* Neurology, 2015. **84**(16): p. 1652-9.
29. Bradley, W.G., P. Shapshak, S. Delgado, I. Nagano, R. Stewart, and B. Rocha, *Morphometric analysis of the peripheral neuropathy of AIDS.* Muscle & nerve, 1998. **21**(9): p. 1188-95.
30. Mangus, L.M., J.L. Dorsey, V.A. Laast, M. Ringkamp, G.J. Ebenezer, P. Hauer, and J.L. Mankowski, *Unraveling the Pathogenesis of HIV Peripheral Neuropathy: Insights from a Simian Immunodeficiency Virus Macaque Model.* ILAR journal / National Research Council, Institute of Laboratory Animal Resources, 2014. **54**(3): p. 296-303.
31. Munoz, M. and R. Covenas, *Involvement of substance P and the NK-1 receptor in human pathology.* Amino acids, 2014. **46**(7): p. 1727-50.
32. Chernova, I., J.P. Lai, H. Li, L. Schwartz, F. Tuluc, H.M. Korchak, S.D. Douglas, and L.E. Kilpatrick, *Substance P (SP) enhances CCL5-induced chemotaxis and intracellular signaling in human monocytes, which express the truncated neurokinin-1 receptor (NK1R).* Journal of leukocyte biology, 2009. **85**(1): p. 154-64.
33. Douglas, S.D., J.P. Lai, F. Tuluc, L. Schwartz, and L.E. Kilpatrick, *Neurokinin-1 receptor expression and function in human macrophages and brain: perspective on the role in HIV neuropathogenesis.* Annals of the New York Academy of Sciences, 2008. **1144**: p. 90-6.
34. Jiang, M.H., E. Chung, G.F. Chi, W. Ahn, J.E. Lim, H.S. Hong, D.W. Kim, H. Choi, J. Kim, and Y. Son, *Substance P induces M2-type macrophages after spinal cord injury.* Neuroreport, 2012. **23**(13): p. 786-92.

CHAPTER III

Title: Monocyte traffic and accumulation of macrophages in the dorsal root ganglia during SIV peripheral neuropathy

Adapted from:
"Monocyte traffic, dorsal root ganglion histopathology, and loss of intraepidermal nerve fiber density (IENFD) in SIV peripheral neuropathy"

by Jessica R. Lakritz, Ayman Bodair, Neal Shah, Ryan O'Donnell, Michael J Polydefkis, Andrew D. Miller, and Tricia H. Burdo

American Journal of Pathology. 2015. Jul;185(7):1912-23.

Author contributions:

JRL and THB conceived and designed the experiments. JRL, AB, NS, RO'D, and ADM performed the experiments. JRL, MJP, ADM, and THB analyzed the data. JRL and THB wrote the paper. All authors carried paper revisions.

ABSTRACT

Human immunodeficiency virus-associated peripheral neuropathy (HIV-PN) remains the most common neurologic complication of HIV infection. HIV-PN is characterized by dorsal root ganglia (DRG) inflammation and intraepidermal nerve fiber density (IENFD) loss. Chronic peripheral immune cell activation and accumulation may cause damage to the DRG, but has not been fully investigated to date. Using a simian immunodeficiency virus (SIV)-infected CD8-lymphocyte depleted rhesus macaque model, we sought to define immune cells surrounding DRG neurons and their role in DRG pathology and to measure cell traffic from the bone marrow to the DRGs using bromodeoxyuridine (BrdU) pulse. We found an increase in CD68+ and CD163+ macrophages in DRGs of SIV-infected animals. MAC387+ recently recruited monocyte/macrophages were increased along with BrdU+ cells in the DRGs of SIV-infected macaques. We demonstrated 83.5% of all BrdU+ cells in DRGs were also MAC387+. The number of BrdU+ monocytes correlated with severe DRG histopathology, which included neuronophagia, neuronal loss, and Nageotte nodules. These data demonstrate that newly recruited MAC387+BrdU+ macrophages may play a significant role in DRG pathogenesis. Infected animals also had an early decline in IENFD, which was associated with elevated BrdU+ cells in the DRG. These data suggest that increased recruitment of macrophages to DRG is associated with severe DRG histopathology and IENFD loss.

INTRODUCTION

HIV-distal sensory polyneuropathy (DSP) consists of sensory nerve fiber axonal degeneration in the extremities [1]. It is unclear if this axonal degeneration is a result of HIV's direct damage to nerve fibers or indirect damage by activated macrophages and glial cells in the dorsal root ganglia (DRG) [2]. Histopathology of the DRG during HIV infection consists of an increased number of macrophages, decreased lymphocytes, fewer neurons, and increased presence of Nageotte nodules [1].

Because HIV and simian immunodeficiency virus (SIV) are unable to productively infect neurons, damage at the DRG is thought to be due to infected and activated macrophages and glial cells, which can secrete neurotoxic products [3]. Whether inflammation or recruited monocyte/macrophages play a role in damage has yet to be defined in an experimental SIV model. Factors involved in immune cell trafficking to the DRG during HIV/SIV infection are poorly understood. Previous studies have used CD68 or Iba-1 as monocyte/macrophage markers in the DRG [4-6]. However, these markers do not differentiate between circulating and infiltrating monocyte/macrophages and resident macrophages. It is likely that resident macrophages (CD68+ and CD163+) and infiltrating macrophages (MAC387+) play different roles during HIV-associated DRG damage [7] as do M1 versus M2 cells in the DRG.

MATERIALS and METHODS

Ethical Statement

All animals used in this study were handled in strict accordance with American Association for Accreditation of Laboratory Animal Care, the Harvard University's Institutional Animal Care and Use Committee (protocol #04785) or Tulane University's Institutional Animal Care and Use Committee (protocols #P0066 and #P0263), and these committees approved all animal work. This work was also approved by Boston College's Institutional Animal Care and Use Committee (protocol #2013-002). All possible measures are taken to minimize discomfort of the animals. All procedures were performed using chemical restraint to ensure the safety of both staff and animals and the choice of anesthetic includes ketamine (10-20 mg/kg, IM), telazol (4-10 mg/kg, IM), and/or dexdomitor (7.5-15 μg/kg, IM), depending on the procedure.

BrdU administration

A 30 mg/ml stock of solution was prepared by adding 5-bromo-2-deoxyuridine (BrdU) (Sigma-Aldrich, USA) to 1× PBS (without Ca^{2+} and Mg^{2+}) and heated to 60°C in water bath as previously described [8]. BrdU was administered as a slow bolus intravenous injection at a dose of 60 mg BrdU/kg body weight. BrdU was administered at days 8, 21, 42, 62 post-infection and 24 hours prior to necropsy in animals A05-A12 and days 42, 62 post-infection and 24 hours prior to necropsy in animals A13-A16.

Necropsy and Histopathology

Tissue collection, preparation for immunohistochemistry, H&E staining, and histopathologic analysis of DRG morophology were performed as described in Chapter 2 [4, 9].

Immunohistochemistry (IHC)

DRG sections were deparaffinized with xylene and hydrated in a series of graded alcohols and stained with either anti-SIV protein p28 (Fitzgerald), the pan-macrophage marker anti-CD68 (Clone KP1, Dako, Carpinteria, CA), the scavenger receptor anti-CD163 (Clone MCA1853, Serotec, Raleigh, NC), the early inflammatory marker anti-MAC387 (Clone M0747, Dako, Carpinteria, CA), anti-BrdU (Clone M0744, Dako, Carpinteria, CA) or the T lymphocyte marker anti-CD3 (Clone A0452, Dako, Carpinteria, CA). Sections were counterstained with hematoxylin, dehydrated, and mounted using VectaMount permanent mounting medium (Vector), visualized and photographs taken using a Zeiss Axio Imager M1 microscope (Carl Zeiss MicroImaging, Inc., Thornwood, NY) using Plan-Apochromat x20/0.8 and x40/0.95 Korr objectives.

Quantitation of monocyte/macrophages in DRGs

For quantitation of monocyte/macrophage populations by immunohistochemical analyses, eight non-overlapping fields at 200x magnification were quantitated per DRG tissue. Data were expressed as mean ± standard error of the mean (SEM). The percentage of immune positive cells was calculated as the number of positively stained cells (DAB+ brown cells) divided by the total number of satellite cells (total hematoxylin (blue nuclei)-positive cells) surrounding the DRGs, multiplied by 100. The absolute

number of cells was calculated by dividing the number of positively stained cells (DAB+ brown cells) by the area of tissue examined (cells/mm^2). Each non-overlapping field at 200x magnification was 0.147 mm^2.

Immunofluorescence

Dual immunofluorescence staining was performed on paraffinized DRG tissue sections as previously described [7]. DRG slides were stained with anti-BrdU (Clone M0744, Dako, Carpineria, CA), and anti-MAC387 (Clone MCA874G, Serotec, Raleigh, NC), or anti-CD68 (Clone KP1, Thermo Fisher Scientific, Waltham, MA). MAC387 and CD68 antibodies were biotinylated with DSB-X Biotin Protein Labeling Kit (Life Technologies, Carlsbad, CA) according to the manufacturer's instructions. Endogenous biotin was blocked using Avidin/Biotin Blocking Kit (Vector Labs, Burlingame, CA) according to the manufacturer's instructions. The secondary antibodies used were goat anti-mouse IgG1- AlexaFluor488 (Molecular Probes, Eugene, OR) and Streptavidin - AlexaFluor568 (Molecular Probes, Eugene, OR), both at a 1:500 dilution. After immunofluorescence labeling, tissue sections were treated with 50 mmol/L Cu_3SO_4 ammonium buffer for 15 minutes at room temperature to quench autofluorescence. Single color controls and double negative control slides were used to determine potential spectral overlap of fluorophores. Slides were mounted with Vectashield mounting media containing DAPI (Vector Labs, Burlingame, CA) and visualized under a microscrope (Zeiss Axio Imager.M1, Carl Zeiss Microimaging, Thornwood, NY). Blue, Red, and Green color channels were collected simultaneously and analyzed using computer software (AxioVision, version 4.6.3).

Quantitation of doubled labeled BrdU+MAC387+ and BrdU+CD68+ cells

For quantitation of double labeled BrdU+MAC387+ or BrdU+CD68+ cells eight non-overlapping fields at 200x magnification were examined per DRG tissue. Alexa568+ or Alexa488+ cells only and overlapping Alexa568+ and Alexa488+ cells were quantified. Percent of double positive cells was calculated by dividing the number of double positive cells by the number of total positive cells (total of single and double positive), multiplied by 100. Data were expressed as mean ± standard error of the mean (SEM).

In situ hybridization

In situ hybridization for SIV RNA was performed using digoxigenin-labeled antisense riboprobes (Lofstrand Labs, Gaithersburg, MD), as previously described [10] [11, 12]. The probes were synthesized from five DNA templates that spanned 90% of the SIV genome.

Skin punch and intraepidermal nerve fiber density measurement

Skin punch biopsies with IENF were performed in 8 of the 12 SIV-infected animals (A09-A16). 3mm skin punches were taken serially near the sural innervation site just distal to the lateral malleolus. Biopsies were taken for each animal at pre-infection and every 2 weeks starting at 8 days post-infection to necropsy, 24 hours after BrdU injection. Measurement of IENFD was performed as described in Chapter 2 [6, 13, 14].

Statistical methods

Prism version 5.0f (GraphPad Software, Inc., San Diego, CA) software was used for statistical analyses. Student t tests were used to detect variation cells number between uninfected and infected rhesus macaques. ANOVA was used to measure variation among cell populations in animals with different degrees of DRG pathology. A P value less than 0.05 was considered significant. If the ANOVA was significant, then post-hoc t-tests were performed. Non-parametric Spearman correlation was used, where a P value < 0.05 was considered significant.

RESULTS

DRG pathology

All twelve SIV-infected CD8 depleted animals had some degree of DRG pathology (mild to severe). In 8 of the 12 animals multiple levels of DRGs were examined including DRGs from the thoracic, lumbar, and sacral regions. DRGs from mixed unspecified regions were examined in the remaining four infected animals. In these animals, we consistently detected more severe pathology in the lumbar and sacral DRGs compared to thoracic DRGs (Table 3.1). DRGs from all four uninfected animals had normal histology. Animals that had severe DRG pathology in their lumbar DRGs had a greater loss of intraepidermal nerve fiber density (IENFD), as previously reported (Chapter 2). These data point to a potential association between IENFD loss and severe DRG pathology.

Active viral replication in DRG satellite cells

Viral infection in macrophages in the dorsal nerve root (Figure 3.1A) and the DRG (Figure 3.1B, 3.1C) was seen in SIV-infected CD8 depleted macaques. Multinucleated giant cells (MNGCs) were seen in DRGs of two CD8 depleted SIV infected animals. The percent and absolute number of SIV virally infected cells in the DRG ranged from zero to 317 infected cells/mm^2 and zero to 8.2% of the total cells surrounding the DRG neurons were productively infected. Even in DRGs with low levels of productive viral infection, there was still notable pathology including infiltrating mononuclear cells, neuronophagia, and neuronal loss. Therefore, active viral infection is not necessary for DRG damage and loss of neurons. Plasma viral load from all animals peaked early and remained elevated throughout the study. There was no significant difference between plasma viral loads between animals (data not shown).

Resident cell activation in the DRG with SIV infection

Consistent with data previously reported [4], the percent and absolute number of CD68+ cells surrounding DRG neurons was significantly increased in SIV-infected animals compared to uninfected controls ($P< 0.01$; mean of 13.3 (SEM of 0.8) vs. 26.7 (SEM of 1.9)% and $P< 0.001$; mean of 531.1 (SEM of 55.5) vs 1228.0 (SEM of 72.0) cells/mm^2, respectively)(Figure 3.2A-C). DRGs were then divided into groups based on the severity of pathology: mild, moderate and severe (as described in Materials and Methods section). There was a statistically significant difference in the amount of CD68+ macrophages/mm^2 of DRGs among the three groups ($P< 0.01$; Figure 3.2D).

There were greater numbers of activated resident CD68+ macrophages in the DRGs with severe pathology compared to both those with mild ($P < 0.05$) and moderate ($P < 0.05$) pathology (Figure 3.2D).

In order to further phenotype the cells surrounding the DRG neurons, we examined the percentage of CD163+ M2-like macrophages and the absolute number of these cells in DRGs. The CD163+ macrophages made up an average of 5.8% (SEM of 2.1) (range 2.4 to 11.7%) of all cells surrounding normal uninfected DRG. This percentage was increased to an average of 27.4% (SEM of 1.8) (range 4.5 to 45.5%) in all DRGs from infected animals. The absolute number of CD163+ cells surrounding the DRG neurons was significantly increased in SIV-infected animals compared to uninfected controls ($P < 0.01$; mean of 262.3 (SEM of 106.7) vs 1200.0 (SEM of 105.1) cells/mm^2)(Figure 3.3A-C). There was no significant difference in the amount of CD163+ cells in the DRGs with mild, moderate or severe pathology (Figure 3.3D).

We have previously shown that the absolute number of CD3+ and CD8+ cells was not different between SIV-infected and uninfected DRGs [4]. CD4 IHC is not reliable in rhesus paraffin embedded tissue sections because of low antigenicity. In order to confirm the extent of T lymphocytes in DRG tissues, we used the pan T cell marker CD3 to quantitate percent and absolute number of T cells in the DRG. The mean absolute number of CD3+ T lymphocytes in DRG tissue was not significantly different between uninfected and SIV-infected animals (mean of 232.8 (SEM of 54.3) vs 249.5 (SEM of 43.3) cells/mm^2.

Immune cell traffic to the DRG

To identify monocytes that recently emigrated from bone marrow, we used BrdU labeling in SIV-infected CD8+ T lymphocyte depleted macaques. Newly migrated monocyte/macrophages were identified within the DRG using both anti-BrdU and anti-MAC387 antibodies. BrdU+ cells in DRGs were quantified in uninfected compared to SIV-infected macaques (Figure 3.4A-C). Less than 1% of cells were BrdU+ in the DRGs of uninfected animals representing a basal level of cell turnover in the DRG. The absolute number of BrdU+ cells trafficking to the DRG tissue trended toward an increase with SIV infection (mean of 40.0 (SEM of 0.5) vs. 148.5 (SEM of 26.6) cells/mm^2) (Figure 3.4C). When DRGs were divided by severity of pathology, BrdU+ cells were significantly different among groups (ANOVA $P< 0.01$)(Figure 3.4D). BrdU+ cells were significantly elevated in the severe group compared to mild ($P< 0.05$) and the moderate ($P< 0.05$) groups (Figure 3.4D). Thus, trafficking of BrdU+ cells from the bone marrow to the DRG correlates with severity of DRG pathology. We also found that the average number of BrdU+ cells in the DRG positively and significantly correlated with the percent loss of IENFD at necropsy ($P< 0.05$, $r= 0.64$) (Figure 3.4E). The number of CD68+ and CD163+ macrophages, MAC387+ recently recruited cells and CD3+ T cells in the DRG did not correlate with IENFD loss (data not shown). These data suggest an association between monocyte recruitment from the bone marrow to DRG histopathology and IENFD loss.

MAC387+ cells are early inflammatory cells that represent recent recruits to tissues upon inflammation and are considered to have an M1-like phenotype [7, 15, 16]. We found few MAC387+ cells in uninflammed tissues and in the uninfected DRGs accounted for an average of 1.5% (SEM of 0.6) (range 0.7 to 3.1%) of cells surrounding

DRG neurons. The percentage of MAC387+ cells surrounding the DRG neurons in SIV-infected animals was increased to an average of 4.3% (SEM of 0.5). The absolute number of MAC387+ cells in the DRG tissue was significantly increased in SIV-infected animals compared to uninfected controls ($P< 0.05$; mean of 60.4 (SEM of 29.1) vs 187.7 (SEM of 20.4) cells/mm^2) (Figure 3.5A-C). When animals were separated by severity of DRG pathology (mild, moderate and severe), the absolute numbers of MAC387+ cells were different among groups (ANOVA $P< 0.01$)(Figure 3.5D). MAC387+ cells were most abundant in the severe group compared to mild ($P< 0.01$) and the moderate group ($P< 0.01$) (Figure 3.5D). Thus, the accumulation of MAC387+ cells correlated with severity of DRG pathology.

In order to further characterize the BrdU+ cells that have recently emigrated to the tissue, we performed double immunofluorescence staining on DRG tissues for BrdU and MAC387 or CD68. We found that an average of 83.5% (SEM of 7.5%) (range 57.4-96.5%) of total BrdU+ cells were also MAC387+, while only an average of 7.4% (SEM of 1.4) (range of 3.9-12.2%) of all BrdU+ cells were also CD68+ (Table 3.2). This corroborates with our previously published data examining cell traffic to the brain where we demonstrated that 90% of all BrdU+ cells in SIV encephalitic lesions were also MAC387+ [7,8]. These data demonstrate that the majority of the BrdU+ cells are also MAC387+ and these cells are the main cell population trafficking to the DRG during SIV infection.

DISCUSSION

HIV-DSP continues to negatively affect patient quality of life. Treatment for HIV-DSP currently focuses on treating the symptomatic pain because the underlying cause is poorly understood [17]. Thus, there exists a need to understand the pathophysiological mechanisms of HIV-DSP. Here, we sought to characterize the immune response in the DRGs and correlate it with histopathology and IENFD loss in the peripheral nerves. The DRG has long been implicated in pathogenesis of HIV-DSP, but the mechanism(s) have not yet been fully characterized [1]. Previous research suggested that macrophages may traffic to the DRG and inflict damage during HIV and SIV infection [4-6], but this has not been investigated systematically within an appropriate animal model.

This study was the first to investigate cell trafficking from the bone marrow to the DRG during SIV infection. Dividing cells were labeled using intravenous BrdU pulse [8]. BrdU is a thymidine analog that incorporates into all newly synthesized DNA. Monocytes undergo their last cell division in the bone marrow; therefore BrdU labels while they are in the bone marrow [18]. We found an increased number of BrdU+ macrophages in the DRGs with SIV infection. The amount of BrdU+ cells was increased with more severe DRG histopathology suggesting a potential role in DRG pathology. Our previous data demonstrated that 90% of BrdU+ macrophages in the SIV encephalitic lesions were also MAC387+ (a marker of recently recruited monocytes, M1-type macrophage), but few were CD68+ or CD163+ [7]. Here, we have demonstrated that the majority (83.5%) of the BrdU+ cells in DRGs were also MAC387+ and few (7.4%) were CD68+. Although there have been recent papers suggesting that macrophages undergo division in situ [19, 20], we believe that these BrdU+MAC387+

cells represent cells coming from the bone marrow, supported by the fact that BrdU is incorporated in monocytes in the bone marrow and that blood monocytes are MAC387+ cells. In addition, MAC387 is a marker of monocytes that have recently infiltrated tissues and is perhaps the earliest marker expressed on such cells as they enter tissues [7]. We found significantly increased numbers of MAC387+ macrophages in DRGs of SIV-infected animals compared to uninfected controls and as expected, increased numbers of MAC387+ cells also correlated with severity of DRG pathology. These data together suggest that newly recruited BrdU+MAC387+ monocytes may play significant roles in severity of DRG pathogenesis during SIV infection. Our findings regarding cell traffic and the correlation to DRG pathology are consistent with previously published data that demonstrated a correlation between monocyte traffic and severity of SIV encephalitic brain lesions in the same model system [8].

Previous studies of SIV-peripheral neuropathy (PN) examined CD68+ or Iba-1 macrophages in the DRG [4, 6, 9]. Here, CD68 was used as a marker for resident macrophages and CD163+ cells represent M2-like perivascular macrophages. CD163 is a scavenger receptor expressed on activated mononuclear cells and is shed in its soluble form (sCD163) [21-23]. Elevated sCD163 in plasma has been shown to be a biomarker of SIV and HIV infection and correlates with severity of neurologic disease associated with HIV [8, 22, 24, 25]. It should be noted that these two markers are not expressed on exclusive cell populations. A majority of the CD163+ cells co-express CD68 (data not shown) [7]. Both absolute numbers of CD68+ and CD163+ macrophages were increased with SIV infection. Interestingly, only greater numbers of

CD68+, but not CD163+ macrophages correlated with severity of DRG pathology. It is possible that CD163+ macrophages may be exerting a protective M2-like effect.

Macrophages are often classified as being either M1 or M2 polarized. However, M1 and M2 classifications are not rigid in that macrophages can switch phenotypes. HIV-1 proteins cause a phenotypic switch from M2 to M1 by preferentially activating M2 macrophages [26]. CD163+ cells are typically considered to be M2 polarized macrophages that are associated with tissue repair, tumor progression, and production of anti-inflammatory cytokines [27, 28]. In contrast, MAC387+ macrophages are thought to be M1 polarized which produce pro-inflammatory cytokines and contribute to host protection from pathogens [27, 28].

We have previously shown that the absolute number of CD3+ and CD8+ T lymphocytes was not different between SIV-infected and uninfected DRGs and have confirmed that data here [4]. Together, these data suggest that macrophages, but not T cells, are either inflicting or exacerbating damage in the DRG.

ACKNOWLEDGEMENTS

This worked was supported by NIH/NINDS R01 NS082116 (awarded to TB) and a Tulane National Primate Research Center (TNPRC) pilot grant (awarded to TB) and TNPRC's base grant (NIH P51 RR00164). The *in vivo* CD8 T lymphocyte depletion antibodies used in these studies were provided by the NIH Nonhuman Primate Reagent Resource (RR016001, AI040101). We thank the veterinary staff at the NEPRC and

TNRPC for animal care, pathology residents, and staff for assisting with necropsies and tissue collection.

Table 3.1: Animals used in the study.

Animal groups	Animal ID	Primate center	Survival (days)	Terminal plasma viral load (log 10)	Brain Pathology	DRG Pathology*
Uninfected	A01	NEPRC	N/A	N/A	normal	normal
	A02	NEPRC	N/A	N/A	normal	normal
	A03	TNPRC	N/A	N/A	normal	normal
	A04	TNPRC	N/A	N/A	normal	normal
SIV-infected CD8 lymphocyte depleted	A05	NEPRC	77	8.69	SIVE	severe
	A06	NEPRC	131	8.15	SIVE	mod-severe
	A07	TNPRC	91	7.04	SIVE	mod-severe
	A08	NEPRC	56	7.86	SIVE	moderate
	A09	TNPRC	89	7.71	SIVE	mild (T), mod-severe (L, S)
	A10	TNPRC	55	7.83	SIVE	mild (T), mild-mod (L, S)
	A11	TNPRC	174	7.28	AIDS no E	severe (T, L, S)
	A12	TNPRC	146	7.67	AIDS no E	moderate (T), severe (L, S)
	A13	NEPRC	77	8.54	SIVE	moderate (T), mod-severe (L, S)
	A14	NEPRC	77	7.23	SIVE	moderate (T, L, S)
	A15	NEPRC	168	6.79	AIDS no E	mild (L, S)
	A16	NEPRC	97	7.79	SIVE	mild (L, S)

TNPRC= Tulane National Primate Research Center; NEPRC; New England Primate Center; SIVE= SIV encephalitis; AIDS no E= AIDS without SIVE; T= thoracic DRG; L= lumbar DRG; S= sacral DRG; mod= moderate pathology

* Sections of DRGs from animals A01 through A08 contained multiple DRGs per block but specific anatomical location was not specified so they may have included thoracic, lumbar, and/or sacral DRGs.

Table 3.2: The majority of the BrdU+ cells surrounding the DRG neurons are MAC387+.

	A05	A10	A11	A12	A14	Average
BrdU+Mac387+ cells vs. all BrdU+ cells *	57.4 ± 10.9	92.1 ± 3.9	96.5 ± 1.1	95.7 ± 1.7	76.0 ± 5.7	83.5 ± 7.5
BrdU+CD68+ cells vs. all BrdU+ cells †	8.9 ± 3.0	12.2 ± 2.8	3.9 ± 2.0	5.9 ± 1.2	6.2 ± 2.4	7.4 ± 1.4
BrdU+Mac387+ cells vs. all Mac387+ cells ‡	31.7 ± 8.7	77.2 ± 3.7	84.9 ± 2.6	90.3 ± 2.8	81.7 ± 3.0	73.2 ± 10.6
BrdU+CD68+ cells vs. all CD68+ cells §	1.7 ± 1.4	2.4 ± 0.8	2.5 ± 0.9	1.3 ± 0.5	2.2 ± 1.3	2.0 ± 0.2

*Mean ± SEM of the percentage of BrdU+ cells expressing Mac387 surrounding DRG neurons was calculated as followed; (number of BrdU+Mac387+ cells/total number of BrdU+ cells) x 100.

†Mean ± SEM of the percentage of BrdU+ cells expressing CD68 calculated as followed; (number of BrdU+CD68+ cells/total number of BrdU+ cells) x 100.

‡Mean ± SEM of the percentage of Mac387+ cells expressing BrdU calculated as followed; (number of BrdU+Mac387+ cells/total number of Mac387+ cells) x 100.

§Mean ± SEM of the percentage of CD68+ cells expressing BrdU calculated as followed; (number of BrdU+CD68+ cells/total number of CD68+ cells) x 100.

The average of the rows was the calculated by averaging the 5 average values and the standard error of the mean of the 5 values is shown.

Figure 3.1

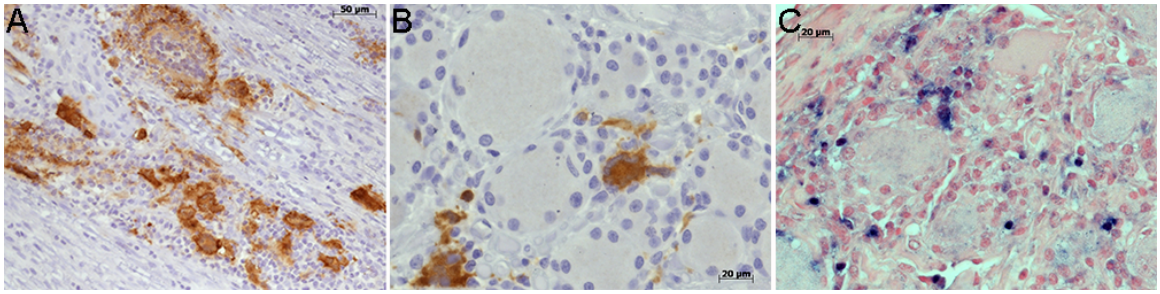

Figure 3.1: Productive viral replication in the macrophage in the dorsal nerve root and DRG of SIV-infected macaques.

(A) Dorsal nerve root of animal A11 with abundant SIVp28 (brown) immunoreactivity and multinucleated giant cells (MNGCs) in SIV-infected rhesus macaque. (B) Dorsal root ganglia of animal A06 with abundant SIVp28 (brown) immunoreactivity and a MNGC. (C) Dorsal root ganglia of animal A05 with in situ hybridization identifying SIV RNA+ cells (blue).

Figure 3.2:

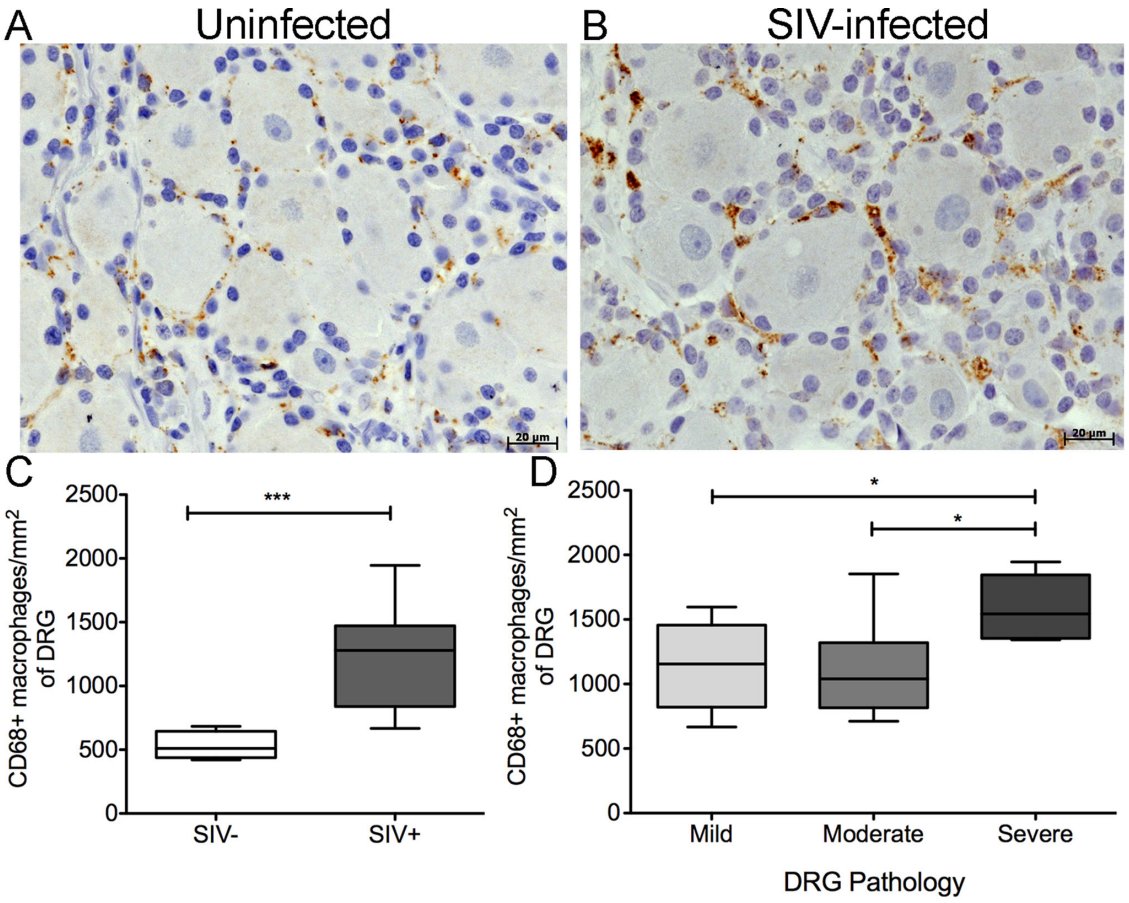
A
Uninfected
B
SIV-infected
20 µm
20 µm
C
CD68+ macrophages/mm2 of DRG
2500
2000
1500
1000
500
0
***
SIV-
SIV+
D
CD68+ macrophages/mm2 of DRG
2500
2000
1500
1000
500
0
*
*
Mild
Moderate
Severe
DRG Pathology

Figure 3.2: Elevated numbers of CD68+ macrophages are associated with SIV infection and severity of DRG pathology.

(A) Dorsal root ganglia of uninfected animal A01 with scant CD68 immunoreactivity (brown). (B) Dorsal root ganglia of animal A08 a SIV-infected rhesus macaque with marked increase in CD68 immunoreactivity (brown). (C) The box plot shows the mean +/- the standard error of the mean of the absolute number of CD68+ cells per mm^2 in SIV- (n=4 DRGSs) and SIV+ (n=26 DRGs) DRGs. The absolute number of CD68+ cells per mm^2 was significantly increased in the SIV-infected DRGs. (D) The box plot shows the mean +/- the standard error of the mean of the absolute number of CD68+ cells per mm^2 in mild (n=8 DRGSs), moderate (n=12 DRGs) and severe (n=6 DRGs) DRGs. Elevated numbers of CD68+ macrophages were associated with severity of DRG pathology. ANOVA ($P< 0.01$) was performed followed by post-hoc t tests. *$P < 0.05$, ***$P < 0.001$.

Figure 3.3:

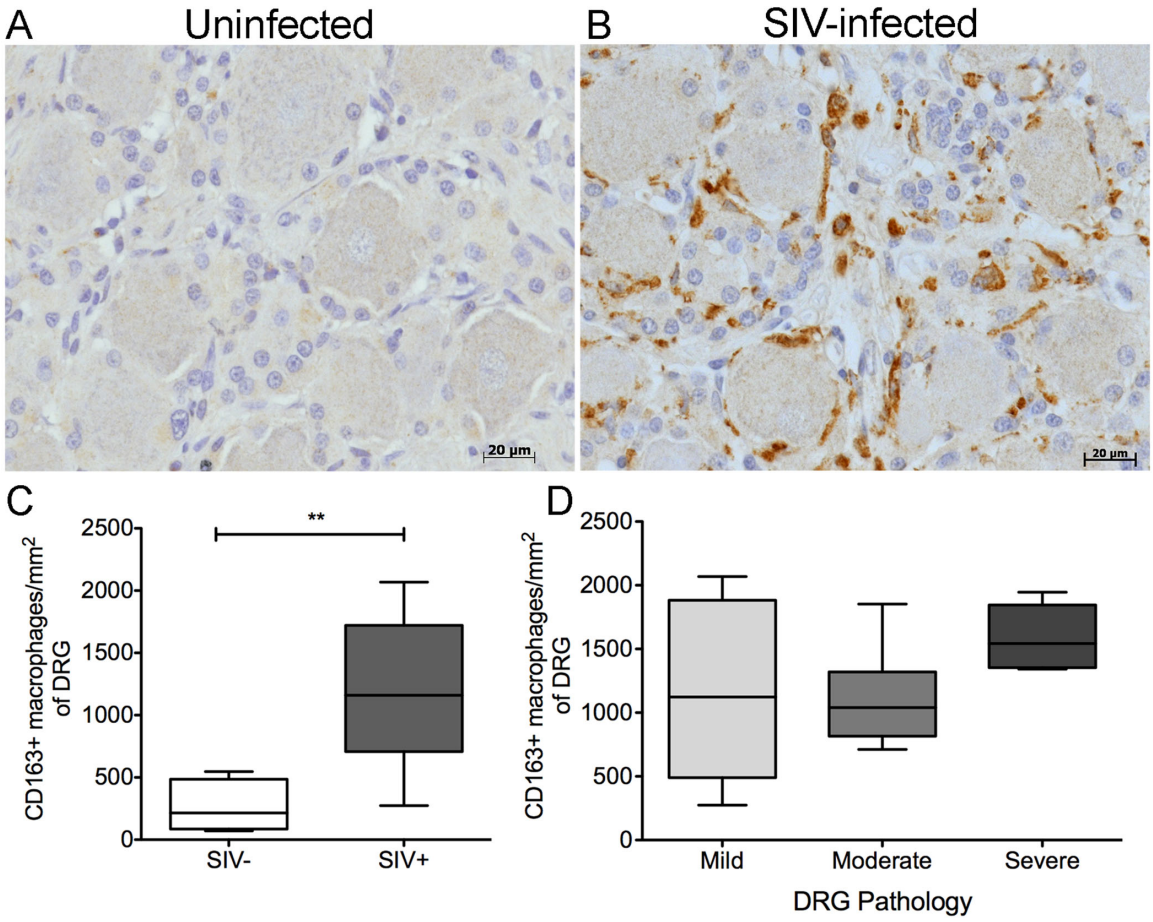
A
Uninfected
B
SIV-infected
20 µm
20 µm
C
CD163+ macrophages/mm2 of DRG
2500
2000
1500
1000
500
0
**
SIV-
SIV+
D
CD163+ macrophages/mm2 of DRG
2500
2000
1500
1000
500
0
Mild
Moderate
Severe
DRG Pathology

Figure 3.3: Elevated numbers of CD163+ macrophages are associated with SIV infection.

(A) Dorsal root ganglia of uninfected animal A02 with scant CD163 immunoreactivity (brown). (B) Dorsal root ganglia of SIV-infected animal A05 with marked increase in CD163 immunoreactivity (brown). (C) The box plot shows the mean +/- the standard error of the mean of the absolute number of CD163+ cells per mm^2 in SIV- (n=4 DRGSs) and SIV+ (n=26 DRGs) DRGs. The absolute number of CD163+ cells per mm^2 was significantly increased in the SIV-infected group. (D) The box plot shows the mean +/- the standard error of the mean of the absolute number of CD163+ cells per mm^2 in mild (n=8 DRGSs), moderate (n=12 DRGs) and severe (n=6 DRGs) DRGs. Elevated numbers of CD163+ macrophages were not associated with severity of DRG pathology. **P < 0.01.

Figure 3.4

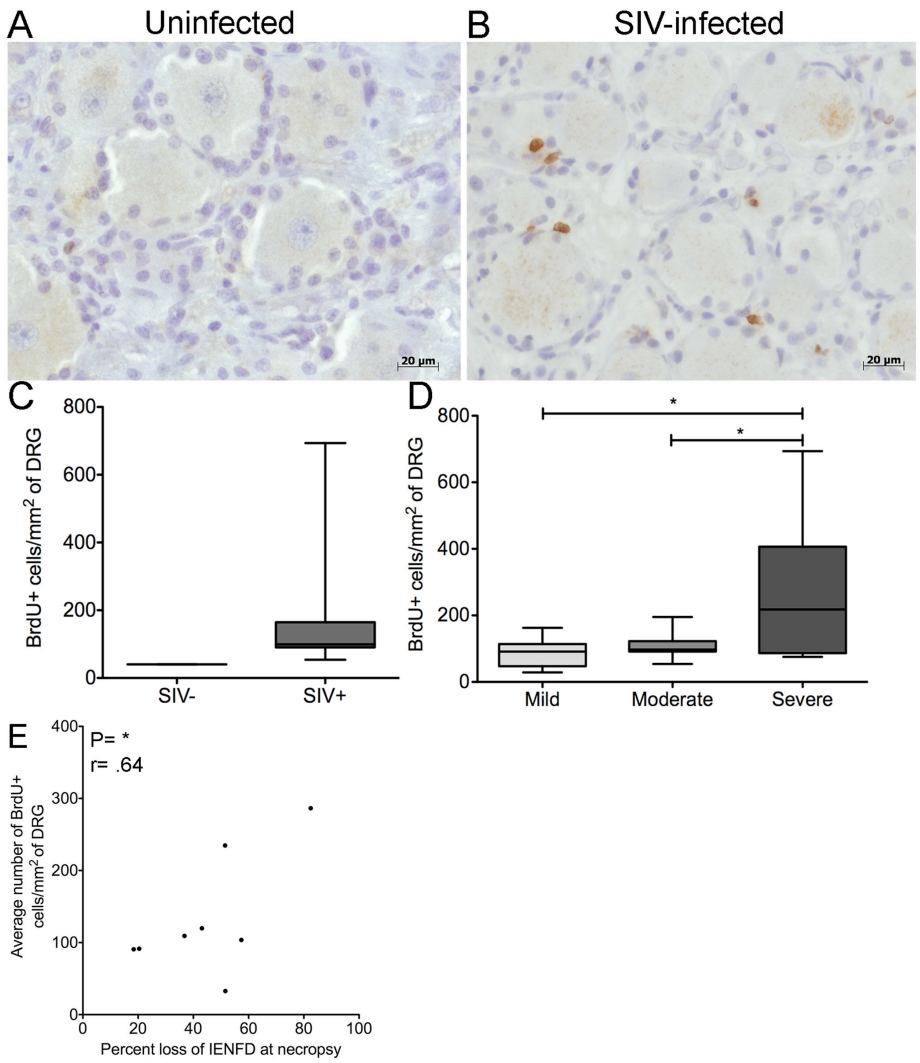
A
Uninfected
B
SIV-infected
20 µm
20 µm
C
BrdU+ cells/mm2 of DRG
800
600
400
200
0
SIV-
SIV+
D
BrdU+ cells/mm2 of DRG
*
*
800
600
400
200
0
Mild
Moderate
Severe
E
P= *
r= .64
Average number of BrdU+ cells/mm2 of DRG
400
300
200
100
0
0
20
40
60
80
100
Percent loss of IENFD at necropsy

Figure 3.4: Cell traffic from the bone marrow to the DRG measured by increased BrdU+ cells with SIV infection.

Animals were serially injected with BrdU to label recently divided monocytes in the bone marrow and then traffic to DRG. (A) Dorsal root ganglia of uninfected animal A02 with scant BrdU immunoreactivity (brown). (B) Dorsal root ganglia of SIV-infected animal A06 with marked increase in BrdU immunoreactivity (brown). (C) The box plot shows the mean +/- the standard error of the mean of the absolute number of BrdU+ cells per mm^2 in SIV- (n=4 DRGSs) and SIV+ (n=26 DRGs) DRGs. The absolute number of BrdU+ cells per mm^2 of DRG tissue was calculated. (D) The box plot shows the mean +/- the standard error of the mean of the absolute number of BrdU+ cells per mm^2 in mild (n=8 DRGSs), moderate (n=12 DRGs) and severe (n=6 DRGs) DRGs. Higher numbers of BrdU+ cells correlated with the severity of DRG pathology. ANOVA ($P< 0.01$) was performed followed by post-hoc t tests. (E) The average number of BrdU+ cells in the DRGs per animal was calculated. Increased numbers of BrdU+ cells in the DRG correlates with percent loss of IENFD at necropsy Spearman correlation was used and *$P < 0.05$, $r=0.64$. *$P < 0.05$.

Figure 3.5

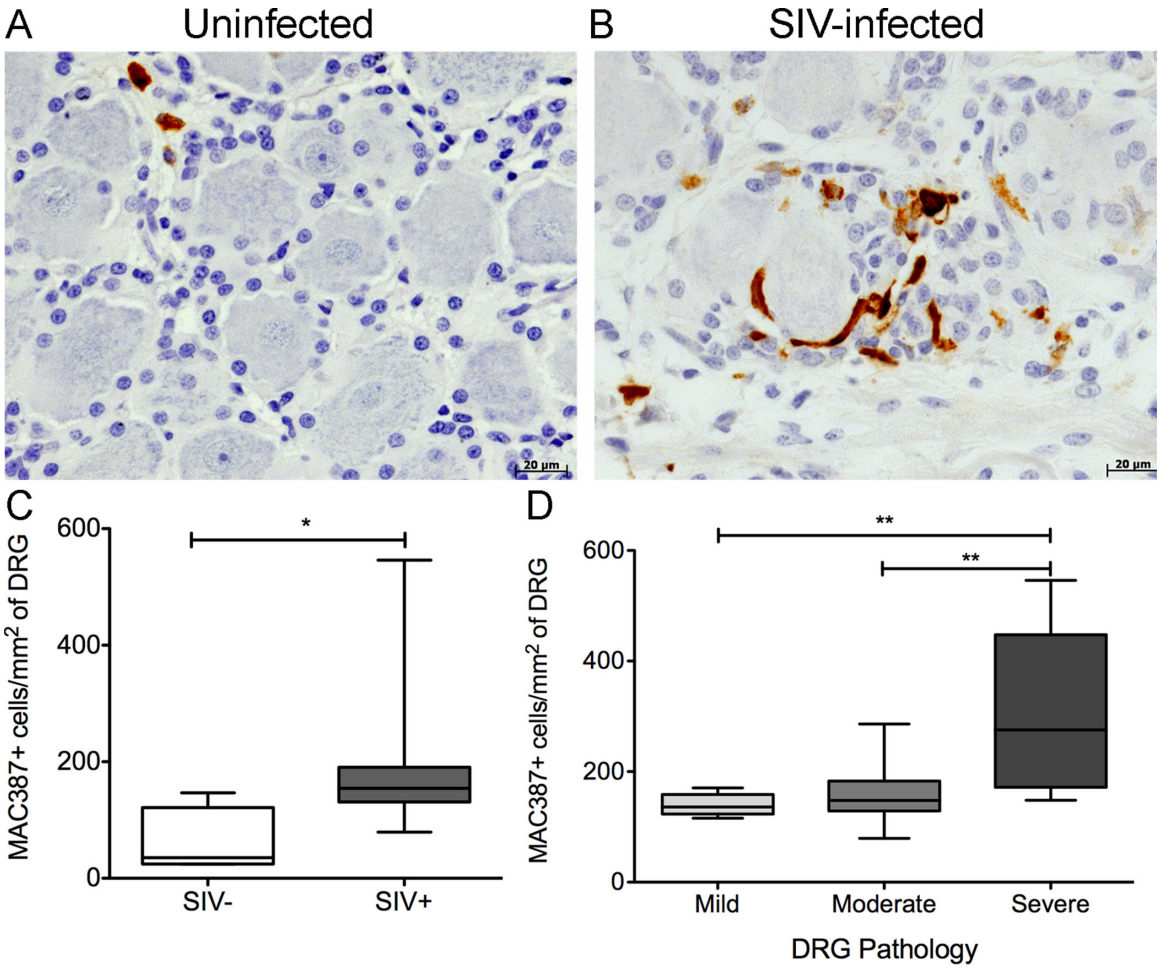
A
Uninfected
B
SIV-infected
20 µm
20 µm
C
MAC387+ cells/mm2 of DRG
600
400
200
0
*
SIV-
SIV+
D
MAC387+ cells/mm2 of DRG
600
400
200
0
**
**
Mild
Moderate
Severe
DRG Pathology

Figure 3.5: Elevated numbers of MAC387+ macrophages are associated with SIV infection and severity of DRG pathology.

(A) Dorsal root ganglia of uninfected animal A01 with scant MAC387 immunoreactivity (brown). (B) Dorsal root ganglia of SIV-infected animal A05 with marked increase in MAC387 immunoreactivity (brown). (C) The box plot shows the mean +/- the standard error of the mean of the absolute number of MAC387+ cells per mm^2 in SIV- (n=4 DRGSs) and SIV+ (n=26 DRGs) DRGs. The absolute number of MAC387+ cells per mm^2 was significantly increased in the SIV infected group. (D) The box plot shows the mean +/- the standard error of the mean of the absolute number of MAC387+ cells per mm^2 in mild (n=8 DRGSs), moderate (n=12 DRGs) and severe (n=6 DRGs) DRGs. Elevated number of MAC387+ macrophages was associated with severity of DRG pathology. ANOVA ($P< 0.01$) was performed followed by post-hoc t tests. *$P < 0.05$, **$P < 0.01$.

REFERENCES:

1. Pardo, C.A., J.C. McArthur, and J.W. Griffin, *HIV neuropathy: insights in the pathology of HIV peripheral nerve disease.* J Peripher Nerv Syst, 2001. **6**(1): p. 21-7.
2. Mangus, L.M., J.L. Dorsey, V.A. Laast, M. Ringkamp, G.J. Ebenezer, P. Hauer, and J.L. Mankowski, *Unraveling the Pathogenesis of HIV Peripheral Neuropathy: Insights from a Simian Immunodeficiency Virus Macaque Model.* ILAR J, 2014. **54**(3): p. 296-303.
3. Rao, V.R., A.P. Ruiz, and V.R. Prasad, *Viral and cellular factors underlying neuropathogenesis in HIV associated neurocognitive disorders (HAND).* AIDS Res Ther, 2014. **11**: p. 13.
4. Burdo, T.H., K. Orzechowski, H.L. Knight, A.D. Miller, and K. Williams, *Dorsal root ganglia damage in SIV-infected rhesus macaques: an animal model of HIV-induced sensory neuropathy.* Am J Pathol, 2012. **180**(4): p. 1362-9.
5. Hahn, K., B. Robinson, C. Anderson, W. Li, C.A. Pardo, S. Morgello, D. Simpson, and A. Nath, *Differential effects of HIV infected macrophages on dorsal root ganglia neurons and axons.* Exp Neurol, 2008. **210**(1): p. 30-40.
6. Laast, V.A., B. Shim, L.M. Johanek, J.L. Dorsey, P.E. Hauer, P.M. Tarwater, R.J. Adams, C.A. Pardo, J.C. McArthur, M. Ringkamp, and J.L. Mankowski, *Macrophage-mediated dorsal root ganglion damage precedes altered nerve conduction in SIV-infected macaques.* Am J Pathol, 2011. **179**(5): p. 2337-45.
7. Soulas, C., C. Conerly, W.K. Kim, T.H. Burdo, X. Alvarez, A.A. Lackner, and K.C. Williams, *Recently infiltrating MAC387(+) monocytes/macrophages a third macrophage population involved in SIV and HIV encephalitic lesion formation.* Am J Pathol, 2011. **178**(5): p. 2121-35.
8. Burdo, T.H., C. Soulas, K. Orzechowski, J. Button, A. Krishnan, C. Sugimoto, X. Alvarez, M.J. Kuroda, and K.C. Williams, *Increased Monocyte Turnover from Bone Marrow Correlates with Severity of SIV Encephalitis and CD163 Levels in Plasma.* PLoS Pathog, 2010. **6**(4): p. e1000842.
9. Laast, V.A., C.A. Pardo, P.M. Tarwater, S.E. Queen, T.A. Reinhart, M. Ghosh, R.J. Adams, M.C. Zink, and J.L. Mankowski, *Pathogenesis of simian immunodeficiency virus-induced alterations in macaque trigeminal ganglia.* J Neuropathol Exp Neurol, 2007. **66**(1): p. 26-34.
10. Williams, K., A. Schwartz, S. Corey, M. Orandle, W. Kennedy, B. Thompson, X. Alvarez, C. Brown, S. Gartner, and A. Lackner, *Proliferating cellular nuclear antigen expression as a marker of perivascular macrophages in simian immunodeficiency virus encephalitis.* Am J Pathol, 2002. **161**(2): p. 575-85.

11. Kim, W.K., X. Alvarez, J. Fisher, B. Bronfin, S. Westmoreland, J. McLaurin, and K. Williams, *CD163 identifies perivascular macrophages in normal and viral encephalitic brains and potential precursors to perivascular macrophages in blood.* Am J Pathol, 2006. **168**(3): p. 822-34.
12. Fox, C.H. and M. Cottler-Fox, *In situ hybridization for detection of HIV RNA.* Curr Protoc Immunol, 2001. **Chapter 12**: p. Unit 12 8.
13. Mangus, L.M., J.L. Dorsey, V.A. Laast, P. Hauer, S.E. Queen, R.J. Adams, J.C. McArthur, and J. Mankowski, *Neuroinflammation and virus replication in the spinal cord of simian immunodeficiency virus-infected macaques.* J Neuropathol Exp Neurol., 2015. **74**(1): p. 38-47.
14. Ebenezer, G.J., V.A. Laast, B. Dearman, P. Hauer, P.M. Tarwater, R.J. Adams, M.C. Zink, J.C. McArthur, and J.L. Mankowski, *Altered cutaneous nerve regeneration in a simian immunodeficiency virus / macaque intracutaneous axotomy model.* J Comp Neurol, 2009. **514**(3): p. 272-83.
15. Esiri, M.M. and C.S. Morris, *Immunocytochemical study of macrophages and microglial cells and extracellular matrix components in human CNS disease. 2. Non-neoplastic diseases.* J Neurol Sci, 1991. **101**(1): p. 59-72.
16. Otani, I., K. Mori, T. Sata, K. Terao, K. Doi, H. Akari, and Y. Yoshikawa, *Accumulation of MAC387+ macrophages in paracortical areas of lymph nodes in rhesus monkeys acutely infected with simian immunodeficiency virus.* Microbes Infect, 1999. **1**(12): p. 977-85.
17. Nicholas, P.K., L. Mauceri, A. Slate Ciampa, I.B. Corless, N. Raymond, D.J. Barry, and A. Viamonte Ros, *Distal sensory polyneuropathy in the context of HIV/AIDS.* J Assoc Nurses AIDS Care, 2007. **18**(4): p. 32-40.
18. Hasegawa, A., H. Liu, B. Ling, J.T. Borda, X. Alvarez, C. Sugimoto, H. Vinet-Oliphant, W.K. Kim, K.C. Williams, R.M. Ribeiro, A.A. Lackner, R.S. Veazey, and M.J. Kuroda, *The level of monocyte turnover predicts disease progression in the macaque model of AIDS.* Blood, 2009. **114**(14): p. 2917-25.
19. Robbins, C.S., I. Hilgendorf, G.F. Weber, I. Theurl, Y. Iwamoto, J.L. Figueiredo, R. Gorbatov, G.K. Sukhova, L.M. Gerhardt, D. Smyth, C.C. Zavitz, E.A. Shikatani, M. Parsons, N. van Rooijen, H.Y. Lin, M. Husain, P. Libby, M. Nahrendorf, R. Weissleder, and F.K. Swirski, *Local proliferation dominates lesional macrophage accumulation in atherosclerosis.* Nat Med, 2013. **19**(9): p. 1166-72.
20. Amano, S.U., J.L. Cohen, P. Vangala, M. Tencerova, S.M. Nicoloro, J.C. Yawe, Y. Shen, M.P. Czech, and M. Aouadi, *Local proliferation of macrophages contributes to obesity-associated adipose tissue inflammation.* Cell Metab, 2014. **19**(1): p. 162-71.
21. Weaver, L.K., K.A. Hintz-Goldstein, P.A. Pioli, K. Wardwell, N. Qureshi, S.N. Vogel, and P.M. Guyre, *Pivotal advance: activation of cell surface Toll-like receptors causes shedding of the hemoglobin scavenger receptor CD163.* J Leukoc Biol, 2006. **80**(1): p. 26-35.
22. Burdo, T.H., M.R. Lentz, P. Autissier, A. Krishnan, E. Halpern, S. Letendre, E.S. Rosenberg, R.J. Ellis, and K.C. Williams, *Soluble CD163 Made by Monocyte/Macrophages Is a Novel Marker of HIV Activity in*

Early and Chronic Infection Prior to and After Anti-retroviral Therapy. J Infect Dis, 2011. **204**(1): p. 154-63.
23. Davis, B.H. and P.V. Zarev, *Human monocyte CD163 expression inversely correlates with soluble CD163 plasma levels.* Cytometry B Clin Cytom, 2005. **63**(1): p. 16-22.
24. Burdo, T.H., J. Lo, S. Abbara, J. Wei, M.E. DeLelys, F. Preffer, E.S. Rosenberg, K.C. Williams, and S. Grinspoon, *Soluble CD163, a novel marker of activated macrophages, is elevated and associated with noncalcified coronary plaque in HIV-infected patients.* J Infect Dis, 2011. **204**(8): p. 1227-36.
25. Burdo, T.H., A. Weiffenbach, S.P. Woods, S. Letendre, R.J. Ellis, and K.C. Williams, *Elevated sCD163 in plasma but not cerebrospinal fluid is a marker of neurocognitive impairment in HIV infection.* AIDS, 2013. **27**(9): p. 1387-95.
26. Chihara, T., M. Hashimoto, A. Osman, Y. Hiyoshi-Yoshidomi, I. Suzu, N. Chutiwitoonchai, M. Hiyoshi, S. Okada, and S. Suzu, *HIV-1 proteins preferentially activate anti-inflammatory M2-type macrophages.* J Immunol, 2012. **188**(8): p. 3620-7.
27. Davies, L.C., S.J. Jenkins, J.E. Allen, and P.R. Taylor, *Tissue-resident macrophages.* Nat Immunol, 2013. **14**(10): p. 986-95.
28. Liu, Y.C., X.B. Zou, Y.F. Chai, and Y.M. Yao, *Macrophage Polarization in Inflammatory Diseases.* Int J Biol Sci, 2014. **10**(5): p. 520-529.

CHAPTER IV

Title: a4-integrin antibody treatment blocks monocyte/macrophage traffic to, VCAM-1 expression in and pathology of the dorsal root ganglia in a SIV macaque model of HIV-peripheral neuropathy

Adapted from:
"a4-integrin antibody treatment blocks monocyte/macrophage traffic to, VCAM-1 expression in and pathology of the dorsal root ganglia in a SIV macaque model of HIV-peripheral neuropathy"

by Jessica R. Lakritz, Derek M. Thibault, Jake A. Robinson, Jennifer H. Campbell, Andrew D. Miller, Kenneth C. Williams, and Tricia H. Burdo

American Journal of Pathology. 2016. Jul;186(7):1754-61

Author contributions:

JRL, JHC, KCW, and THB conceived and designed the experiments. JRL, DMT, JAR, and ADM performed the experiments. JRL and THB analyzed the data. JRL and THB wrote the paper. All authors carried out paper revisions.

ABSTRACT

Traffic of activated monocytes into the dorsal root ganglia (DRG) is critical for pathology in HIV peripheral neuropathy. We have shown that accumulation of recently recruited (BrdU+MAC387+) monocytes is associated with severe DRG pathology and loss of intraepidermal nerve fibers in SIV-infected macaques (Chapters 2 and 3). Here, we blocked leukocyte traffic by treating animals with natalizumab, which binds to α4-integrins. SIV-infected CD8-depleted macaques treated with natalizumab either early (the day of infection) or late (28 days post infection (DPI)) were compared to untreated SIV-infected animals sacrificed at similar times. Histopathology showed diminished DRG pathology with natalizumab treatment including decreased inflammation, neuronophagia, and Nageotte nodules. Natalizumab treatment resulted in a decrease in the number of BrdU+ (early), MAC387+ (late), CD68+ (early and late) and SIVp28+ (late) macrophages in DRG tissues. The number of CD3+ T lymphocytes in DRGs was not affected by natalizumab treatment. Vascular cell adhesion molecule 1 (VCAM-1), an adhesion molecule that mediates leukocyte traffic, was diminished in DRGs of all natalizumab-treated animals. These data show that blocking monocyte, but not T lymphocyte, traffic to the DRG results in decreased inflammation and pathology supporting a role for monocyte traffic and activation in HIV peripheral neuropathy.

INTRODUCTION

Primary mechanisms of the human immunodeficiency virus (HIV) peripheral neuropathy include immune damage secondary to viral infection and mitochondrial toxicity from antiretrovirals. Since HIV and simian immunodeficiency (SIV) do not productively infect neurons or Schwann cells, damage to the dorsal root ganglia (DRG) in peripheral neuropathy is believed to be due, in part, to infected and activated macrophages. In vitro and in vivo studies suggest that both viral proteins and systemic inflammation secondary to the viral infection may damage neurons and axons (reviewed in [1]). Using a CD8-depleted SIV-infected rhesus macaque model of peripheral neuropathy, we have shown that accumulation of recruited (BrdU+MAC387+) monocyte/macrophages was associated with severe DRG pathology (Chapter 3) [2]. The number of bromodeoxyuridine (BrdU)+ monocytes correlated with DRG histopathology, which included neuronophagia, satellitosis, and Nageotte nodules (Chapter 3) [2]. Our data demonstrate that newly recruited MAC387+BrdU+ macrophages play a significant role in DRG pathogenesis.

Natalizumab was approved for the treatment of relapsing-remitting Multiple Sclerosis and Crohn's disease [3]. Natalizumab blocks traffic of leukocytes (monocyte/macrophages, T cells, and B cells) to the CNS of patients with relapsing-remitting Multiple Sclerosis [3] and to the gut of patients with Crohn's disease [4]. We have shown that natalizumab treatment of SIV-infected rhesus macaques resulted in stabilization of ongoing neuronal injury (NAA/Cr by

1H MRS), and decreased numbers of monocytes/macrophages and productive SIV infection in the brain and gut [5]. We found similar numbers of CD68+ and MAC387+ monocyte/macrophages in lymph nodes of untreated and treated SIV-infected animals suggesting that natalizumab did not significantly affect traffic to lymph nodes as previously described [5]. In a more recent study, we have also shown that natalizumab treatment of SIV-infected rhesus macaques blocks monocyte traffic to the heart resulting in decreased cardiac pathology, cardiovascular disease and fibrosis [6]. Here, we extend these studies to determine whether ongoing monocyte/macrophage traffic is required for SIV-associated DRG damage. We found that natalizumab treatment decreased inflammation, monocyte traffic, SIV infection and pathology of DRGs.

MATERIALS and METHODS

Ethical Statement

All animals used in this study were handled in strict accordance with American Association for Accreditation of Laboratory Animal Care with the approval of the Massachusetts General Hospital Subcommittee on Research and Animal Care, the Institutional Animal Care and Use Committee of Harvard University and Tulane University.

Animals, viral infection, and CD8 lymphocyte depletion

Sixteen adult male rhesus macaques (Macaca mulatta) were utilized in this study. Animals were inoculated intravenously with SIVmac251 (5ng SIV p27) (a generous gift from Dr. Ronald Desrosiers, University of Miami) and were administered an anti-CD8 antibody subcutaneously at day 6 after infection (10 mg/kg), and intravenously at days 8 and 12 after infection (5 mg/kg) in order to achieve rapid AIDS. The human anti-CD8 antibody was provided by the NIH Non-human Primate Reagent Resource (RR016001, AI040101) [7-12]. Eight macaques (n=4 late natalizumab treated, n=4 late untreated) were sacrificed between 49 to 77 day post infection (DPI) and eight animals (n=5 early natalizumab treated, n=3 early untreated) were sacrificed at 21 or 22 DPI [5]. All animals were anesthetized with ketamine-HCl and euthanized by an intravenous pentobarbital overdose and exsanguinated. Both early and late natalizumab treated groups and the early untreated group were timed sacrificed (days 21, 49 and 22 post infection, respectively) (Table 4.1). Late untreated animals were sacrificed based on the guidelines for euthanasia of SIV-infected rhesus macaques. All animals were still fully CD8 depleted at the time of necropsy.

Anti-α4 integrin (natalizumab) administration

The recombinant humanized IgG4 monoclonal anti-α4 integrin mAb (natalizumab) was kindly provided by Biogen Idec (Cambridge, MA). The antibody was administered once weekly (30 mg/kg) for three weeks beginning on the day of infection (early, 0 DPI, n = 5) or 28 days after infection (late, 28 DPI, n = 4) in a slow bolus. A high dose of natalizumab was given three times with one-

week intervals between each treatment to avoid hypersensitivity responses [5]. This regimen maintains high serum levels of natalizumab [13].

BrdU administration

BrdU was administered as a slow bolus intravenous injection at a dose of 60 mg BrdU/kg body weight as previously described (Chapter 3) [14]. To monitor levels of monocyte/macrophage trafficking out of the bone marrow, in blood, and into the DRG, BrdU was administered prior to infection (−9 DPI), 26 DPI, and 24 hours prior to necropsy in two macaques given natalizumab beginning on 28 DPI. In the other natalizumab treated animals, BrdU was administered once natalizumab treatment was initiated, on days 33 and 47 post infection (n = 2 late natalizumab) or days 6 and 20 post infection (n = 5 early natalizumab). For the early, untreated animals, BrdU was also given at days 6 and 20 post-infection (n=3 early untreated). For the late untreated animals, BrdU was administered prior to infection (−9 DPI), at peak infection (7 and 20 or 26 DPI), day 41 post infection and 24 hours prior to necropsy in two macaques and days 41, 62 and 24 hours prior to necropsy in the other two macaques (Table 4.1).

Necropsy and Histopathology

Animals were necropsied immediately following death and representative sections of all major organs were collected, fixed in 10% neutral buffered formalin (NBF), embedded in paraffin, and sectioned at 5μm. Sections were stained with hematoxylin and eosin as previously described (Chapter 2) [2, 15].

Histopathologic analysis of DRG morphology was analyzed and ranked on a scale of 0 to 3 as previously described (Chapter 2) [2, 15, 16].

Immunohistochemistry

DRG sections were stained with either anti-SIV protein p28 (Fitzgerald), the pan-macrophage marker anti-CD68 (Clone KP1, Dako, Carpinteria, CA), the scavenger receptor anti-CD163 (Clone MCA1853, Serotec, Raleigh, NC), the early inflammatory marker anti-MAC387 (Clone M0747, Dako, Carpinteria, CA), anti-BrdU (Clone M0744, Dako, Carpinteria, CA), the T lymphocyte marker anti-CD3 (Clone A0452, Dako, Carpinteria, CA), or anti-VCAM-1 (4E8 Clone, Antibodies-Online) as previously described (Chapter 3) [17].

Immunohistochemistry quantification

For quantitation of monocyte/macrophage and T cell populations by immunohistochemical analyses, at least eight non-overlapping fields at 200x magnification were quantitated per DRG tissue as previously described (Chapter 3) [17]. Data were expressed as mean ± standard error of the mean (SEM). For animals that had more than one region of DRG, the means were averaged.

DRG tissue was stained for vascular cell adhesion protein 1 (VCAM-1) as described above. Eight random, non-overlapping fields at 200x magnification were imaged and the percent of VCAM-1+ area of total DRG tissue area was calculated. The area of VCAM-1+ tissue was quantified using ImageJ analysis software (v1.45s, National Institutes of Health). Images underwent color

deconvolution to separate histological dyes into DAB (brown) and hematoxylin (purple) channels. The color threshold on the DAB channel was adjusted uniformly on all images to measure DAB+ area. The percent of VCAM-1+ area of total tissue was calculated by dividing the total DAB+ area by the total area of tissue and multiplying by 100. For animals that had more than one region DRG, the percentages of each region were averaged.

Statistical methods

Prism version 5.0f (GraphPad Software, Inc., San Diego, CA) software was used for statistical analyses. Student t tests were used to detect variation in cell numbers between untreated and natalizumab treated rhesus macaques. A P value of <0.05 was considered significant.

RESULTS

Histopathologic analysis show diminished DRG pathology with natalizumab treatment

Sixteen SIV-infected CD8-depleted rhesus macaques were included in this study (Table 4.1). Eight animals were sacrificed at 21 or 22 DPI. Five of these animals received natalizumab treatment beginning on the day of infection (0 DPI) and 3 animals were untreated controls. An additional eight macaques were sacrificed at similar time points (49 to 77 DPI). Four of these animals received natalizumab treatment at day 28 and 4 animals were untreated controls.

In two out of three early sacrificed, untreated animals there was moderate DRG pathology characterized by increased numbers of satellite cells and lymphocytic and histiocytic infiltration into the ganglia. This was associated with a moderate degree of neuronophagia. Nageotte nodules were either rare or absent in this group of animals (Figure 4.1A). In the early natalizumab treated animals, DRG pathology ranged from mild to moderate. In these animals, neuronophagia was mild and no Nageotte nodules were noted (Figure 4.1B).

Late untreated animals had moderate to severe inflammation, satellite cell proliferation, and neuronophagia. Nageotte nodules were rare in three of the four animals and one animal had extensive Nageotte nodules (Figure 4.1C). In the late natalizumab treated animals, the dorsal root ganglia had a moderate degree of inflammation and satellite cell proliferation, milder degrees of neuronophagia, and no or rare Nageotte nodules (Figure 4.1D). Thus, overall there was diminished DRG pathology with natalizumab treatment, which included less inflammation, neuronophagia, neuronal loss/degeneration, and Nageotte nodules.

Natalizumab blocks traffic of monocytes into DRGs

To identify monocyte traffic to the DRGs, we counted the number of recently recruited MAC387+ monocytes and used BrdU pulse to label monocytes that divide in and egress from bone marrow into the circulation and traffic to tissues. The antibody MAC387 antibody recognizes the myeloid-related protein 14 (MRP14) [18-20], which is expressed on recently infiltrating

monocytes/macrophages during early acute inflammation [21]. In the early, untreated animals there were 225.6 MAC387+cells/mm^2 in the DRG, which decreased by 2.9 fold in the natalizumab-treated animals (Figure 4.2A). In the late untreated animals, there were 144.3 MAC387+ monocytes/mm^2 in the DRG. The number of MAC387+ monocytes was significantly decreased by 9.1 fold to 15.88 MAC387+ monocytes/mm^2 in DRGs of natalizumab-treated animals (Figure 4.2A, $P< 0.0001$). In early, untreated animals, there were 94.40 BrdU+ cells/mm^2, which significantly decreased by 3.5 fold to 26.93 BrdU+ cells/mm^2 of DRG tissue in early natalizumab-treated animals (Figure 4.2B, $P< 0.01$). In late animals, there was a 1.6 fold decrease, although not statistically significant, in the number of BrdU+ cells with natalizumab treatment (Figure 4.2B). Overall, these data suggest that treatment with natalizumab decreases monocyte traffic into the DRG during SIV infection.

Natalizumab treatment significantly decreases the number of CD68+ macrophages, but not CD163+ macrophages nor CD3+ T lymphocytes in DRGs

In early, untreated animals, there were 1101 CD68+ macrophages/mm^2, which significantly decreased by 17.6 fold to 62.73 CD68+ macrophages/mm^2 of DRG tissue in early natalizumab-treated animals (Figure 4.2C, $P< 0.01$). In late untreated animals, there were 1016 CD68+ macrophages/mm^2, which significantly decreased by 9.4 fold to 107.8 CD68+ macrophages/mm^2 of DRG tissue in late natalizumab-treated animals (Figure 4.2C, $P< 0.01$). Although not significant, there was a trend towards a decrease in number of CD163+

macrophages in both early and late natalizumab-treated animals compared to untreated animals (Figure 4.2D). These data show that natalizumab significantly decreased the number of CD68+ macrophages in DRG tissues. Interestingly, there were no significant differences in number of CD3+ T lymphocytes between untreated and either early or late natalizumab-treated animals (Figure 4.2E). Since animals were CD8 depleted, these CD3+ T lymphocytes were most likely CD4+ T cells.

Natalizumab treatment significantly decreases SIV infection in DRGs

In early, untreated animals, there were 84.22 SIVp28+ cells/mm^2, which decreased 3.2 fold to 25.92 SIVp28+ cells/mm^2 of DRG tissue in early natalizumab-treated animals (Figure 4.2F). In late animals, there were 39.55 SIVp28+ cells/mm^2, which significantly decreased by 10.9 fold to only 3.63 SIVp28+ cells/$mm^2$of DRG tissue in late natalizumab-treated animals (Figure 4.2F, $P< 0.05$). These data show that natalizumab significantly decreased SIV-infected cells in DRG tissues.

Natalizumab treatment decreases VCAM-1 expression on the surface of DRG blood vessels

Because natalizumab blocks α4-integrin binding to VCAM-1, an adhesion molecule involved in mediating leukocyte traffic, DRG tissues were examined for VCAM-1 expression. VCAM-1 expression was detected on blood vessels in DRGs of early and late untreated animals, but was diminished in DRGs from

natalizumab-treated animals (Figure 4.3A-D). This reduction was quantitated and VCAM-1 expression was significantly decreased in both early and late natalizumab treatment compared to untreated control animals (Figure 4.3E; $P < 0.05$). Thus, reducing expression of VCAM-1 on blood vessels in DRGs by natalizumab may be one mechanism of inhibiting monocyte recruitment to DRGs during SIV infection or less cell traffic due to natalizumab treatment may have caused decreased VCAM-1 expression.

DISCUSSION

Natalizumab is a monoclonal antibody against human α4-integrin indicated for treatment of Multiple Sclerosis [3] and Crohn's disease [4] that blocks the extravasation of leukocytes into tissues and thus, reduces inflammation. Since α4-integrins and their receptors are involved in immune cell trafficking, natalizumab interferes with these processes [22]. We have previously shown that monocyte traffic to the DRG is associated with severe DRG pathology, as well as a loss of intraepidermal nerve fiber density (IENFD) (Chapter 3) [2]. In this current study, we used natalizumab to determine the effect of blocking leukocyte traffic on DRG pathology. This is the first study that blocked monocyte traffic to the DRG, which resulted in diminished macrophage inflammation and reduced DRG pathology. In natalizumab-treated animals there was less severe DRG pathology that included decreased inflammation, mild neuronophagia and none-to-rare Nageotte nodules. All of these changes are associated with damage to

the structure of the ganglion and in turn will lead to functional deficits. One manifestation of this is the loss of IENFD, which we have shown is correlated with damage to the DRG (Chapter 2) [23], while others have shown it is correlated with pain [24].

Natalizumab treatment resulted in decreased numbers of recently recruited M1-like MAC387+BrdU+ monocytes, decreased CD68+ macrophages and reduced the number of productively SIV-infected macrophages in DRGs suggesting that these all relate to DRG pathology. These results demonstrate that by blocking α4-integrins and thus traffic of monocytes to DRGs, subsequent histopathology is diminished and suggests that monocyte traffic, viral replication and macrophage activation have causative roles in perpetuating neuronal damage, and are not simply correlative. Thus, drugs that directly target monocyte traffic may prevent or reduce severity of HIV peripheral neuropathy.

This study examined if stopping leukocyte traffic prevents DRG pathology either during early or late infection. In the late treated animals, natalizumab was not administered until 28 DPI, and thus damage may have already been initiated during early infection. However, by stopping late leukocyte traffic, animals did not develop severe DRG pathology as seen in untreated animals sacrificed at similar time points [2]. Unlike in the central nervous system (CNS), peripheral nervous system (PNS) neurons can regenerate over time, and thus even late treatment may allow for the PNS to recover fully over a longer period of time.

The induction of integrin receptors is the limiting event in initiating monocyte recruitment and extravasation during inflammation. VCAM-1 is

expressed on vasculature and is known to mediate adhesion of mononuclear cells to endothelial cells via binding of very late antigen-4 (VLA-4), which is essential for transmigration across the endothelium. A recent study has demonstrated macrophage infiltration into the DRG was related to upregulation of VCAM-1 using an experimental model of early stage lumbar disc herniation [25]. It was also shown that systemic administration of a tumor necrosis factor (TNF)-α inhibitor prevented macrophage infiltration and upregulation of VCAM-1 [25]. Another study has demonstrated that administration of a TNF-α inhibitor, given after the onset of inflammation, prevented both macrophage invasion and VCAM-1 upregulation in the DRG in a rat model of arthritis [26]. TNF-α and IL-1β are secreted by activated resident macrophages during inflammatory events and induce expression of VCAM-1 and other adhesion molecules on the local vasculature. In this study, by blocking VLA-4 (the ligand for VCAM-1), we prevented additional monocytes from entering the tissue, as indicated by the reduced number of MAC387+ and BrdU+ cells. We showed a significant reduction in VCAM-1 expression in DRG tissues with natalizumab treatment.

We examined if decreased expression of VCAM-1 was due to enhanced shedding of VCAM-1 and thus elevated plasma soluble (s)VCAM-1 or decreased TNF-α, since TNF-α induces VCAM-1 expression. We found low to undetectable levels of TNF-α in all untreated and treated animals (data not shown). sVCAM-1 was not significantly increased in any of the treatment groups from pre-infection to necropsy (data not shown). sVCAM-1 in serum has been used as a surrogate marker of VCAM-1 endothelial expression and studies in MS patients show that

sVCAM-1 is decreased with natalizumab . Here, sVCAM-1 in plasma collected at necropsy positively correlated to VCAM-1 expression in DRG tissue suggesting that reduced tissue expression is not due to increased shedding (data not shown). Thus, we hypothesize that the reduced VCAM-1 expression is due to a feedback mechanism where VCAM-1 is downregulated in natalizumab-treated animals due to the absence of its ligand.

There is overlap between CD68 and CD163 cell populations, although CD68+CD163- and CD68-CD163+ cells have been detected both in the brain [27] and in the DRG (unpublished data). Here, we found that natalizumab treatment significantly reduced the number of CD68+ macrophages in both early and late groups and a trend in a reduction of CD163+ macrophage numbers, although not significant. There is a reduction of CD68+ antigen expression with decreased activation. The kinetics and turnover of CD68+ and CD163+ macrophage with natalizumab are unknown but our data suggests differences in the populations.

We have recently shown that natalizumab treatment in SIV+ macaques decreased traffic of CD3+ T cells in the brain and the gut [5], but not cardiac tissues [6]. In this study, we showed that CD3+ T lymphocytes numbers in DRGs were not decreased with natalizumab treatment. This suggests that CD3+ T lymphocytes may use different integrins to traffic to the DRG and cardiac tissue than to the brain or gut. Alternatively, we have previously shown no difference in CD3+ T cells in the DRG in infected and uninfected animals (Chapter 3) [2, 15], suggesting that T cells do not home to the DRG during SIV-induced

inflammation. Thus, blocking all leukocyte traffic will not modulate these numbers since few CD3+ T cells traffic to the DRG in untreated, SIV-infected animals.

Other drug studies regarding the role of monocytes in HIV infection have focused either on reducing the infectivity of monocytes/macrophages or suppressing inflammation [28, 29]. For example, maraviroc, a CCR5 inhibitor, reduced the size of the viral reservoir in monocytes and macrophages and may also reduce inflammation [30]. Statins have also been under investigation for their anti-inflammatory properties. Rosuvastatin reduced sCD14 and tissue factor expression on monocytes in HIV+ patients [31]. However, natalizumab is the only drug known to block leukocyte traffic and reduce inflammation.

We have recently shown that natalizumab treatment in SIV+ macaques reduces cell traffic to the brain and heart, thus reducing the incidence of encephalitis and fibrosis [5, 6]. Here, we have demonstrated that blocking leukocyte traffic reduced the severity of DRG pathology. Long-term natalizumab treatment (greater than 1 year) in HIV+ patients is not recommended due to risk of developing progressive multifocal leukoencephalopathy (PML) [32]. However, our data suggests it may be beneficial for patients to receive natalizumab for short periods of time to slow progression of DRG tissue damage due to continuous leukocyte traffic. Regardless of natalizumab's benefit or risk in a clinical setting, this study has demonstrated, in a proof-of-concept manner, that stopping leukocyte traffic by blocking VLA-4 and down-regulation of VCAM-1 results in less severe DRG pathology during SIV infection.

ACKNOWLEDGEMENTS

This worked was supported by NIH/NINDS R01 NS082116 (awarded to THB) and NIH/NINDS R01 NS40327 (awarded to KW). The in vivo CD8 T lymphocyte depletion antibodies used in these studies were provided by the NIH Nonhuman Primate Reagent Resource (RR016001, AI040101). We thank the veterinary staff at the NEPRC and TNRPC for animal care, pathology residents, and staff for assisting with necropsies and tissue collection. Natalizumab was kindly provided by Biogen Idec (Cambridge, MA). THB is the guarantor of this work and, as such, had full access to all of the data in the study and takes responsibility for the integrity of the data and the accuracy of the data analysis.

Table 4.1: SIV-infected CD8-depleted rhesus macaques used in this study and brain and DRG pathology.

Animal groups	ID	DRGs examined *	BrdU admin. (dpi)	Survival (days)	Plasma viral load at necropsy (log10)	Brain Pathology	Overall DRG Pathology	Inflammation/ satellite cell proliferation	Neuronophagia	Nageotte nodules
Early untreated N=3	A01	M	6, 20	22	6.87	PV cuffs	moderate	moderate	Moderate	rare
	A02	M	6, 20	22	7.15	PV cuffs	moderate	moderate	Moderate	rare
	A03	M	20	22	6.84	Normal	mild	mild	Mild	no
Early natalizumab N=5	A04	L, S	6, 20	21	7.54	Normal	mild-mod	moderate	Mild	no
	A05	L	6, 20	21	7.3	Normal	mild	mild	No	no
	A06	M	6, 20	21	7.64	Normal	mild-mod	moderate	Mild	no
	A07	C	6, 20	21	7.43	Normal	mild-mod	moderate	Mild	no
	A08	M	6, 20	21	7.54	Normal	mild	mild	No	no
Late untreated N=4	A09	M	pre, 7, 26, 55	56	7.86	mild-SIVE	moderate	moderate	Moderate	rare
	A10	T, L, S	pre, 7, 20, 41, 54	55	7.83	SIVE	mild-mod	moderate	Mild	rare
	A11	T, L, S	41, 62, 76	77	7.23	SIVE	mod-severe	severe	mod-severe	extensive
	A12	T, L, S	41, 62, 76	77	8.54	SIVE	moderate	moderate	Moderate	rare
Late natalizumab N=4	A13	M	pre, 26, 47	49	7.95	Satellitosis	mild-mod	moderate	Mild	no
	A14	M	pre, 26, 47	49	7.71	mild-SIVE	moderate	moderate	Mild	rare
	A15	T, S	33, 47	49	7.56	Normal	moderate	moderate	Mild	rare
	A16	S	33, 47	49	7.91	Normal	moderate	moderate	Mild	rare

pre= prior to infection, dpi= days post-infection, SIVE= SIV encephalitis; AIDS no E= AIDS without SIVE; *DRGs examined where from mixed DRGs i.e. may contain thoracic, lumbar, sacral, and/or cervical DRGs; M= mixed DRG; T= thoracic DRG; L= lumbar DRG; S= sacral DRG; C= cervical; mod= moderate pathology; Satellitosis= rare neuronal satellitosis in frontal cortex; Normal= no significant pathology

Figure 4.1

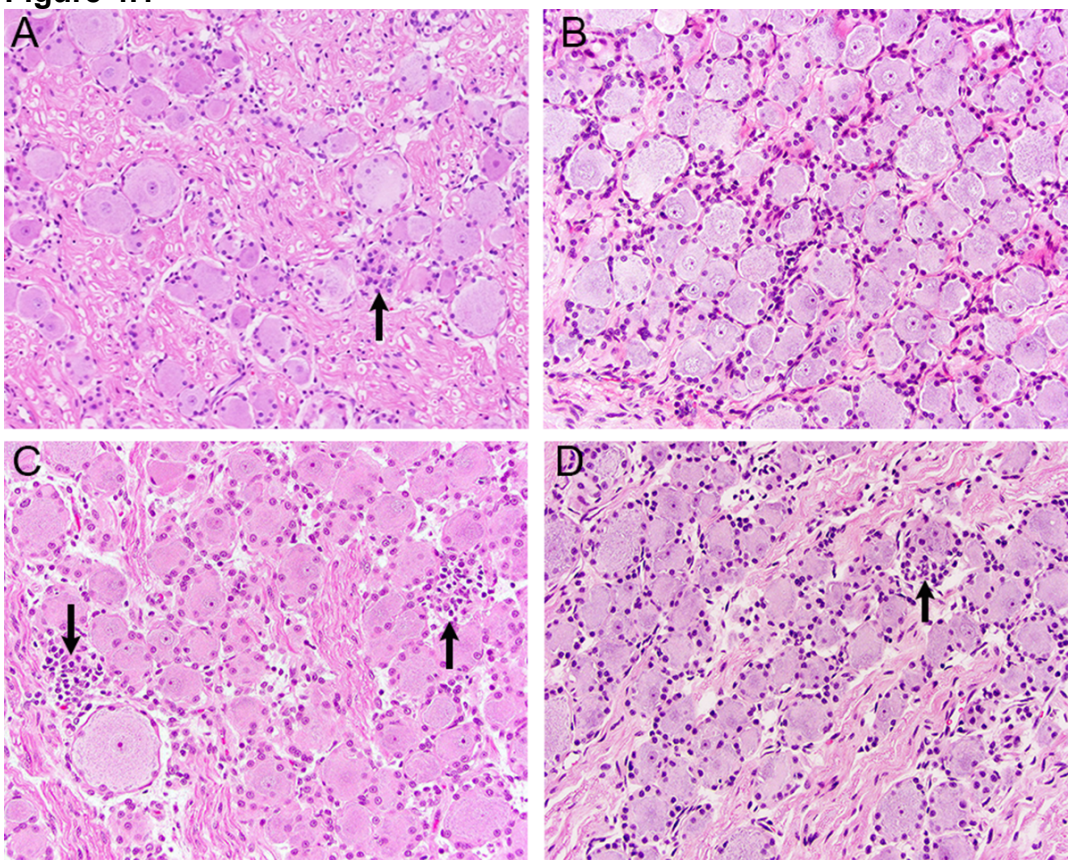

Figure 4.1: Decreased DRG pathology with Natalizumab treatment.

During histologic examination, the following terminology was used. Satellitosis is defined as increased numbers of cells around a neuronal cell body. A Nageotte nodule is defined as focal proliferations of satellite cells that partially to completely replace foci of neuronal cell loss. Neuronophagia is defined as increased numbers of satellite cells phagocytosing a neuronal cell body. Neuronophagia is a precursor lesion to the development of a Nageotte nodule. Cells were identified by morphology and the pattern of tissue reaction detailed above. Neurons were not counted, but loss was examined by the presence of Nageotte nodule and neuronophagia, which are satellite cells that replace foci of neuronal cell loss. (A) A representative image of a DRG from an early untreated with a mild increase in satellite cells with a Nageotte nodule (arrow). (B) A representative image of a DRG from an early natalizumab-treated animal with mild increase in satellite cells with no evidence of neuronophagia or Nageotte nodules. (C) A representative image of a DRG from a late untreated animal with multifocal foci of inflammation with neuronophagia (arrows). (D) A representative image of a DRG from a late natalizumab-treated SIV-infected CD8-depleted rhesus macaques with moderate increase in satellite cells with rare neuronophagia (arrow). HE, 200x.

Figure 4.2

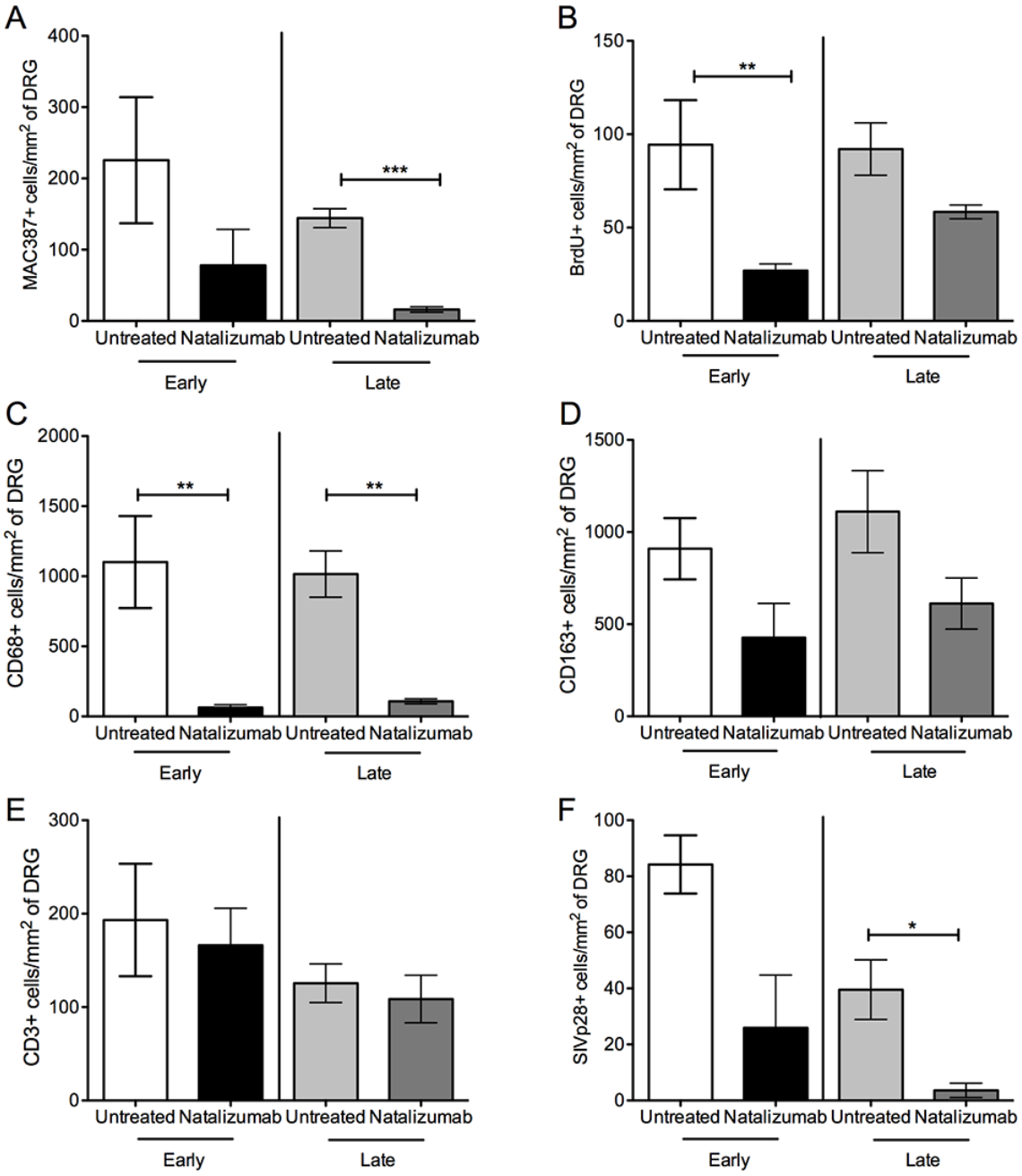
A
MAC387+ cells/mm2 of DRG
400
300
200
100
0
***
Untreated Natalizumab Untreated Natalizumab
Early
Late
B
BrdU+ cells/mm2 of DRG
150
100
50
0
**
Untreated Natalizumab Untreated Natalizumab
Early
Late
C
CD68+ cells/mm2 of DRG
2000
1500
1000
500
0
**
**
Untreated Natalizumab Untreated Natalizumab
Early
Late
D
CD163+ cells/mm2 of DRG
1500
1000
500
0
Untreated Natalizumab Untreated Natalizumab
Early
Late
E
CD3+ cells/mm2 of DRG
300
200
100
0
Untreated Natalizumab Untreated Natalizumab
Early
Late
F
SIVp28+ cells/mm2 of DRG
100
80
60
40
20
0
*
Untreated Natalizumab Untreated Natalizumab
Early
Late

Figure 4.2: Natalizumab treatment results in a decrease in monocyte traffic, macrophage activation, SIV infection, but not numbers of $CD3^+$ T cells in DRGs.

In DRG tissues from early untreated, early natalizumab-treated, late untreated and late natalizumab-treated SIV-infected CD8-depleted rhesus macaques the absolute number of (A) $MAC387^+$ monocytes/mm^2 of DRG (B) $BrdU^+$ cells/mm^2 of DRG (C) $CD68^+$ macrophages/mm^2 of DRG (D) $CD163^+$ macrophages/mm^2 of DRG (E) $CD3^+$ T cells/mm^2 of DRG and (F) SIV $p28^+$ cells/mm^2 of DRG was quantitated. At least eight non-overlapping fields at 200x magnification were quantitated per DRG tissue. The absolute number of cells was calculated by dividing the number of positively stained cells (DAB+ brown cells) by the area of tissue examined (cells/mm^2). Data were expressed as mean ± standard error of the mean (SEM). Student t test was used to detect variation in cell numbers between untreated and natalizumab treated rhesus macaques. *P< 0.05, **P< 0.01, ***P< 0.001

Figure 4.3

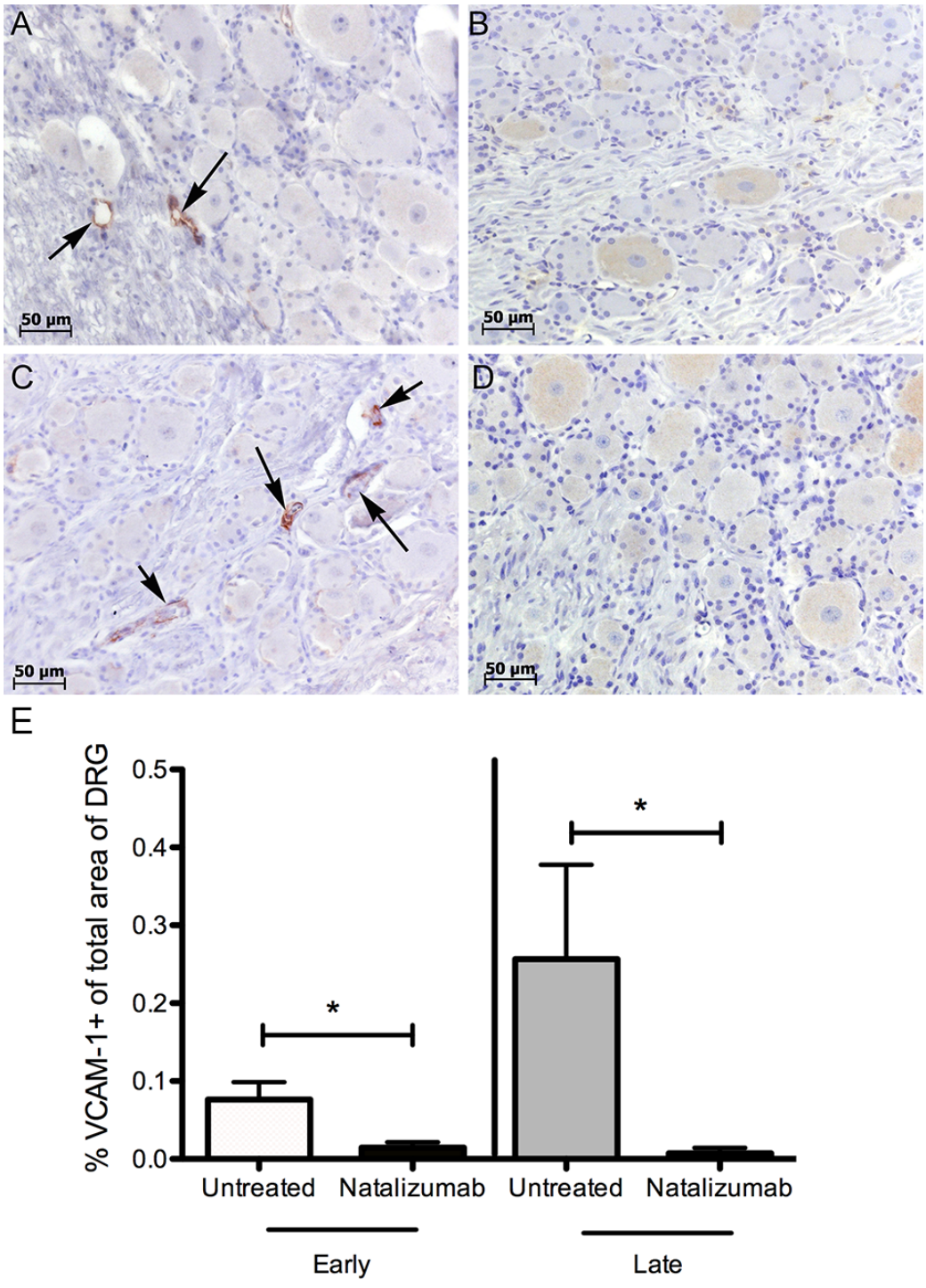
A
50 µm
B
50 µm
C
50 µm
D
50 µm
E
% VCAM-1+ of total area of DRG
0.5
0.4
0.3
0.2
0.1
0.0
*
*
Untreated
Natalizumab
Untreated
Natalizumab
Early
Late

Figure 4.3: Natalizumab treatment reduces VCAM-1 expression on surface of blood vessels in DRGs.

Representative images of DRG tissues stained with anti-VCAM-1 from (A) an early untreated, (B) an early natalizumab-treated, (C) late untreated, (D) and late natalizumab-treated SIV-infected CD8-depleted rhesus macaque. Black arrows show VCAM-1^{+} blood vessels. (E) VCAM-1 expression was quantitated in DRG tissues from early untreated, early natalizumab-treated, late untreated and late natalizumab-treated SIV-infected CD8-depleted rhesus macaques. Eight random, non-overlapping fields at 200x magnification were imaged and the percent of VCAM-1+ area of total DRG tissue area was calculated. The area of VCAM-1+ tissue was quantified using ImageJ analysis software (v1.45s, National Institutes of Health). Percent of VCAM-1+ area of total tissue was calculated by dividing the total DAB+ area by the total area of tissue and multiplying by 100. Data were expressed as mean ± standard error of the mean (SEM). Student t test was used to detect variation in cell numbers between untreated and natalizumab treated rhesus macaques. *P< 0.05, **P< 0.01, ***P< 0.001

REFERENCES:

1. Cashman, C.R. and A. Hoke, *Mechanisms of distal axonal degeneration in peripheral neuropathies.* Neurosci Lett, 2015. **596**: p. 33-50.
2. Lakritz, J.R., A. Bodair, N. Shah, R. O'Donnell, M.J. Polydefkis, A.D. Miller, and T.H. Burdo, *Monocyte Traffic, Dorsal Root Ganglion Histopathology, and Loss of Intraepidermal Nerve Fiber Density in SIV Peripheral Neuropathy.* Am J Pathol, 2015. **185**(7): p. 1912-23.
3. Polman, C.H., P.W. O'Connor, E. Havrdova, M. Hutchinson, L. Kappos, D.H. Miller, J.T. Phillips, F.D. Lublin, G. Giovannoni, A. Wajgt, M. Toal, F. Lynn, M.A. Panzara, A.W. Sandrock, and A. Investigators, *A randomized, placebo-controlled trial of natalizumab for relapsing multiple sclerosis.* N Engl J Med, 2006. **354**(9): p. 899-910.
4. Sandborn, W.J. and T.A. Yednock, *Novel approaches to treating inflammatory bowel disease: targeting alpha-4 integrin.* Am J Gastroenterol, 2003. **98**(11): p. 2372-82.
5. Campbell, J.H., E.M. Ratai, P. Autissier, D.J. Nolan, S. Tse, A.D. Miller, R.G. Gonzalez, M. Salemi, T.H. Burdo, and K.C. Williams, *Anti-alpha4 Antibody Treatment Blocks Virus Traffic to the Brain and Gut Early, and Stabilizes CNS Injury Late in Infection.* PLoS Pathog, 2014. **10**(12): p. e1004533.
6. Walker, J.A., G.A. Beck, J.H. Campbell, A.D. Miller, T.H. Burdo, and K.C. Williams, *Anti-alpha4 Integrin Antibody Blocks Monocyte/Macrophage Traffic to the Heart and Decreases Cardiac Pathology in a SIV Infection Model of AIDS.* J Am Heart Assoc, 2015. **4**(7).
7. Lackner, A.A., *Pathology of simian immunodeficiency virus induced disease.* Curr Top Microbiol Immunol, 1994. **188**: p. 35-64.
8. Sasseville, V.G. and A.A. Lackner, *Neuropathogenesis of simian immunodeficiency virus infection in macaque monkeys.* J Neurovirol, 1997. **3**(1): p. 1-9.
9. Schmitz, J.E., M.J. Kuroda, S. Santra, V.G. Sasseville, M.A. Simon, M.A. Lifton, P. Racz, K. Tenner-Racz, M. Dalesandro, B.J. Scallon, J. Ghrayeb, M.A. Forman, D.C. Montefiori, E.P. Rieber, N.L. Letvin, and K.A. Reimann, *Control of viremia in simian immunodeficiency virus infection by CD8+ lymphocytes.* Science, 1999. **283**(5403): p. 857-60.
10. Westmoreland, S.V., E. Halpern, and A.A. Lackner, *Simian immunodeficiency virus encephalitis in rhesus macaques is associated with rapid disease progression.* J Neurovirol, 1998. **4**(3): p. 260-8.
11. Williams, K., S. Westmoreland, J. Greco, E. Ratai, M. Lentz, W.K. Kim, R.A. Fuller, J.P. Kim, P. Autissier, P.K. Sehgal, R.F. Schinazi, N. Bischofberger, M. Piatak, J.D. Lifson, E. Masliah, and R.G. Gonzalez, *Magnetic resonance spectroscopy reveals that activated monocytes contribute to neuronal injury in SIV neuroAIDS.* J Clin Invest, 2005. **115**(9): p. 2534-45.

12. Williams, K.C. and W.F. Hickey, *Central nervous system damage, monocytes and macrophages, and neurological disorders in AIDS.* Annu Rev Neurosci, 2002. **25**: p. 537-62.
13. Wehner, N.G., C. Gasper, G. Shopp, J. Nelson, K. Draper, S. Parker, and J. Clarke, *Immunotoxicity profile of natalizumab.* J Immunotoxicol, 2009. **6**(2): p. 115-29.
14. Burdo, T.H., C. Soulas, K. Orzechowski, J. Button, A. Krishnan, C. Sugimoto, X. Alvarez, M.J. Kuroda, and K.C. Williams, *Increased Monocyte Turnover from Bone Marrow Correlates with Severity of SIV Encephalitis and CD163 Levels in Plasma.* PLoS Pathog, 2010. **6**(4): p. e1000842.
15. Burdo, T.H., K. Orzechowski, H.L. Knight, A.D. Miller, and K. Williams, *Dorsal root ganglia damage in SIV-infected rhesus macaques: an animal model of HIV-induced sensory neuropathy.* Am J Pathol, 2012. **180**(4): p. 1362-9.
16. Laast, V.A., C.A. Pardo, P.M. Tarwater, S.E. Queen, T.A. Reinhart, M. Ghosh, R.J. Adams, M.C. Zink, and J.L. Mankowski, *Pathogenesis of simian immunodeficiency virus-induced alterations in macaque trigeminal ganglia.* J Neuropathol Exp Neurol, 2007. **66**(1): p. 26-34.
17. Lakritz, J.R., A. Bodair, N. Shah, R. O'Donnell, M.J. Polydefkis, A.D. Miller, and T.H. Burdo, *Monocyte Traffic, Dorsal Root Ganglion Histopathology, and Loss of Intraepidermal Nerve Fiber Density in SIV Peripheral Neuropathy.* The American journal of pathology, 2015. **185**(7): p. 1912-23.
18. Hessian, P.A. and L. Fisher, *The heterodimeric complex of MRP-8 (S100A8) and MRP-14 (S100A9). Antibody recognition, epitope definition and the implications for structure.* Eur J Biochem, 2001. **268**(2): p. 353-63.
19. Goebeler, M., J. Roth, F. Burwinkel, E. Vollmer, W. Bocker, and C. Sorg, *Expression and complex formation of S100-like proteins MRP8 and MRP14 by macrophages during renal allograft rejection.* Transplantation, 1994. **58**(3): p. 355-61.
20. Goebeler, M., J. Roth, S. Teigelkamp, and C. Sorg, *The monoclonal antibody MAC387 detects an epitope on the calcium-binding protein MRP14.* J Leukoc Biol, 1994. **55**(2): p. 259-61.
21. Odink, K., N. Cerletti, J. Bruggen, R.G. Clerc, L. Tarcsay, G. Zwadlo, G. Gerhards, R. Schlegel, and C. Sorg, *Two calcium-binding proteins in infiltrate macrophages of rheumatoid arthritis.* Nature, 1987. **330**(6143): p. 80-2.
22. Mitroulis, I., V.I. Alexaki, I. Kourtzelis, A. Ziogas, G. Hajishengallis, and T. Chavakis, *Leukocyte integrins: Role in leukocyte recruitment and as therapeutic targets in inflammatory disease.* Pharmacol Ther, 2015. **147C**: p. 123-135.
23. Lakritz, J.R., J.A. Robinson, M.J. Polydefkis, A.D. Miller, and T.H. Burdo, *Loss of intraepidermal nerve fiber density during SIV peripheral neuropathy is mediated by monocyte activation and elevated monocyte chemotactic proteins.* J Neuroinflammation, 2015. **12**(1): p. 237.

24. Polydefkis, M., C.T. Yiannoutsos, B.A. Cohen, H. Hollander, G. Schifitto, D.B. Clifford, D.M. Simpson, D. Katzenstein, S. Shriver, P. Hauer, A. Brown, A.B. Haidich, L. Moo, and J.C. McArthur, *Reduced intraepidermal nerve fiber density in HIV-associated sensory neuropathy.* Neurology, 2002. **58**(1): p. 115-9.
25. You, C., K. Zhu, X. Liu, C. Xi, Z. Zhang, G. Xu, and J. Yan, *Tumor necrosis factor-alpha-dependent infiltration of macrophages into the dorsal root ganglion in a rat disc herniation model.* Spine (Phila Pa 1976), 2013. **38**(23): p. 2003-7.
26. Segond von Banchet, G., M.K. Boettger, N. Fischer, M. Gajda, R. Brauer, and H.G. Schaible, *Experimental arthritis causes tumor necrosis factor-alpha-dependent infiltration of macrophages into rat dorsal root ganglia which correlates with pain-related behavior.* Pain, 2009. **145**(1-2): p. 151-9.
27. Soulas, C., C. Conerly, W.K. Kim, T.H. Burdo, X. Alvarez, A.A. Lackner, and K.C. Williams, *Recently infiltrating MAC387(+) monocytes/macrophages a third macrophage population involved in SIV and HIV encephalitic lesion formation.* Am J Pathol, 2011. **178**(5): p. 2121-35.
28. Campbell, J.H., A.C. Hearps, G.E. Martin, K.C. Williams, and S.M. Crowe, *The importance of monocytes and macrophages in HIV pathogenesis, treatment, and cure.* AIDS, 2014. **28**(15): p. 2175-87.
29. Mehraj, V., M.A. Jenabian, K. Vyboh, and J.P. Routy, *Immune Suppression by Myeloid Cells in HIV Infection: New Targets for Immunotherapy.* Open AIDS J, 2014. **8**: p. 66-78.
30. Wilkin, T.J. and R.M. Gulick, *CCR5 antagonism in HIV infection: current concepts and future opportunities.* Annu Rev Med, 2012. **63**: p. 81-93.
31. Funderburg, N.T., Y. Jiang, S.M. Debanne, N. Storer, D. Labbato, B. Clagett, J. Robinson, M.M. Lederman, and G.A. McComsey, *Rosuvastatin treatment reduces markers of monocyte activation in HIV-infected subjects on antiretroviral therapy.* Clin Infect Dis, 2014. **58**(4): p. 588-95.
32. Walker, A., C. Watson, S.T. Alexopoulos, B. Deniz, R. Arnold, and D. Bates, *A benefit-risk analysis of natalizumab in the treatment of patients with multiple sclerosis when considering the risk of progressive multifocal leukoencephalopathy.* Curr Med Res Opin, 2014. **30**(4): p. 629-35.

CHAPTER V

Title: An oral form of methylglyoxal-bis-guanylhydrazone reduces monocyte activation and traffic to the dorsal root ganglia in a primate model of HIV-peripheral neuropathy.

Adapted from:
"An oral form of methylglyoxal-bis-guanylhydrazone reduces monocyte activation and traffic to the dorsal root ganglia in a primate model of HIV-peripheral neuropathy."

by Jessica R. Lakritz, Samshita Yalamanchili, Michael J. Polydefkis, Andrew D. Miller, Michael S. McGrath, Kenneth C. Williams, and Tricia H. Burdo

Author contributions:

JRL, MSM, KCW, and THB conceived and designed the experiments. JRL, SY,

MJP, and ADM performed the experiments. JRL and THB analyzed the data.

JRL and THB wrote the paper. All authors carried out paper revisions.

ABSTRACT

Peripheral neuropathy (PN) is a major comorbidity of HIV infection that is caused in part by chronic immune activation. HIV-PN is associated with infiltration of monocytes/macrophages to the dorsal root ganglia (DRG) causing neuronal loss and formation of Nageotte nodules. Here, we used an oral form of methylglyoxal-bis-guanylhydrazone (MGBG), a polyamine biosynthesis inhibitor, to specifically reduce activation of myeloid cells. MGBG has been shown to be selectively taken up by monocyte/macrophages *in vitro* and inhibit HIV p24 expression and viral integration in macrophages. MGBG was administered to nine SIV-infected, CD8-depleted rhesus macaques at 21 days post-infection (DPI). An additional nine SIV-infected, CD8-depleted rhesus macaques were used as untreated controls. Cell traffic to tissues was measured by *in vivo* BrdU-pulse labeling. MGBG treatment significantly diminished DRG histopathology and reduced the number of CD68+ and CD163+ macrophages in DRG tissue. The number of recently trafficked BrdU+ cells in the DRG was significantly reduced with MGBG treatment. Despite diminished DRG pathology, intraepidermal nerve fiber density (IENFD) did not recover after treatment with MGBG. These data suggest that MGBG may be a valuable adjunctive therapy for HIV inflammatory-mediated neuropathies.

INTRODUCTION

Methyl-bis-guanylhydrazone (MGBG) is a polyamine analog that interferes with polyamine biosynthesis by inhibiting S-adenosine-methionine decarboxylase (SAMDC) [1]. This process is required for cell differentiation and proliferation and thus, MGBG has been studied as an anti-tumor cell proliferation drug [2]. It was recently shown that MGBG is selectively taken up by monocyte/macrophages and decreases HIV expression in these cell types. Virally infected macrophages treated with MGBG *in vitro* displayed reduced integration of proviral DNA compared to control macrophages, although the levels of total intracellular DNA were unchanged [3]. MGBG also selectively targets and inhibits macrophage activation *in vitro* by depleting the intracellular pool of spermine and spermidine [4, 5]. Depletion of these intracellular polyamines results in prevention of alternatively-activated M2 macrophage induction and also inhibits LPS induced cytokine production from M1 macrophages [6]. Thus, MGBG could function to reduce viral replication in monocytes/macrophages through blocking viral integration and will reduce alternative activation of these cells through polyamine depletion *in vivo*.

In this study, we aimed to specifically target monocytes and macrophages with MGBG in a primate model of HIV-peripheral neuropathy (PN) in an attempt to reduce DRG pathology associated with macrophage differentiation and trafficking [7]. Eighteen rhesus macaques were infected with SIVmac251 and CD8 depleted to allow for rapid disease progression. Nine animals received an oral form of MGBG and the remaining nine animals were untreated controls.

Here, we show that MGBG treatment results in less severe DRG pathology by reducing numbers of macrophages in tissue.

MATERIALS and METHODS

Ethical Statement

All animals used in this study were handled in strict accordance with American Association for Accreditation of Laboratory Animal Care with the approval of the Institutional Animal Care and Use Committee of Harvard University (protocol number 04420) and Tulane University (protocol numbers P0066 and P0263). Animals were housed at the New England Primate Research Center (NERPC, Southborough, MA) or Tulane National Primate Research Center (TNPRC, Covington, LA).

Animals, viral infection, and CD8 lymphocyte depletion

Eighteen rhesus macaques (*Macaca mulatta*) were utilized in this study. All animals were inoculated intravenously with SIVmac251 (a generous gift from Dr. Ronald Desrosiers, University of Miami) and administered 10 mg/kg of anti-CD8 antibody subcutaneously at day 6 after infection, and 5 mg/kg intravenously at days 8 and 12 after infection in order to achieve rapid AIDS. The human anti-CD8 antibody was provided by the NIH Non-human Primate Reagent Resource (RR016001, AI040101). Animals were sacrificed between 55 and 89 days post-infection (DPI) based on progression of disease or termination of the study. They were anesthetized with ketamine-HCl and euthanized by an intravenous

pentobarbital overdose and exsanguinated. The diagnosis of simian AIDS was determined post-mortem by the presence of opportunistic infections.

MGBG administration

Nine animals received 30mg/kg of MGBG (provided by Pathologica, LLC; formulated as flavored syrup by Wedgewood Pharmacy, Swedesboro, NJ) daily beginning at 21 DPI. Previous experiments demonstrated that a daily dose of 30mg/kg of MGBG was able to achieve an effective concentration of 0.7μM in tissue and plasma (data not shown).

Bromodeoxyuridine (BrdU) administration

BrdU was administered as a slow bolus intravenous injection at a dose of 60mg/kg body weight as previously described (Chapter 3) [8]. BrdU was administered on 7, 19, 56 DPI, and 24 hours prior to necropsy.

Plasma viral load quantification

Plasma SIV-RNA was quantified using real-time polymerase chain reaction (PCR) for all animals used in this study, as previously described (Walker, in review). EDTA plasma (500μL) was collected and SIV virions were pelleted by centrifugation at 20,000 g for 1 hour. The threshold sensitivity was 100 copy Eq/mL, with an average interassay coefficient variation of less than 25%.

Intraepidermal nerve fiber density measurements

Skin biopsies (3mm) were taken in all SIV+ animals at 20 DPI (pre-drug) and at necropsy (post-drug) as previously described (Chapter 2). Quantification of intraepidermal nerve fiber density (IENFD) was performed as previously described (Chapter 2) [7, 9].

Necropsy and Histopathology

Animals were necropsied immediately following death and representative sections of all major organs were collected and preserved as previously described (Chapter 2). DRG pathology was evaluated on H&E stained DRG slides as previously described (Chapter 2) [7, 10].

Immunohistochemistry and quantification of satellite cells in DRGs

DRG sections were stained with either the pan-macrophage marker anti-CD68 (Clone KP1, Dako, Carpinteria, CA), the scavenger receptor anti-CD163 (Clone MCA1853, Serotec, Raleigh, NC), the early inflammatory marker anti-MAC387 (Clone M0747, Dako, Carpinteria, CA), anti-BrdU (Clone M0744, Dako, Carpinteria, CA), or the T lymphocyte marker anti-CD3 (Clone A0452, Dako, Carpinteria, CA) as previously described (Chapter 3) [7, 10]. For quantitation of monocyte/macrophage and T cell populations by immunohistochemical analyses, at least eight non-overlapping fields at 200x magnification were quantitated per DRG tissue as previously described (Chapter 3) [7, 10]. Data were expressed as mean ± standard error of the mean (SEM).

Statistical methods

Prism version 5.0f (GraphPad Software, Inc., San Diego, CA) software was used for statistical analyses. Mann-Whitney t tests were used to detect variation in cell numbers between untreated and MGBG treated rhesus macaques. Wilcoxon matched-pairs signed rank test was used to detect a change of IENFD within an individual over time. A P value of <0.05 was considered significant for all analysis performed.

RESULTS

MGBG treatment diminishes overall DRG pathology

Eighteen SIV-infected, CD8-depleted rhesus macaques were used in this study (Table 5.1). Nine of the animals received MGBG starting at 21 DPI. The remaining nine animals were untreated SIV-infected controls. All animals were sacrificed between 55 and 89 DPI. The viral load at necropsy in the MGBG treated group (7.28 ± 0.26 log copies/ml) was not significantly different from the viral load (7.65 ± 0.08 log copies/ml) in the control group ($p= 0.66$; data not shown).

Histopathology of lumbar, sacral, and thoracic dorsal root ganglia were assessed for the presence and degree of satellitosis, neuronophagia, and Nageotte nodules and are reported in Table 5.1. Overall DRG pathology was ranked on a scale of zero to three as previously described (Chapter 2) [7, 9] with a score of zero indicating no significant findings and a score of three indicating

severe pathology. Treatment with MGBG significantly reduced the overall DRG pathology from an average score of 1.4 ± 0.2 in control animals to 0.9 ± 0.1 ($p < 0.05$; Figure 5.1). Notably, none of the MGBG treated animals developed Nageotte nodules. Additionally, the degree of satellitosis and neuronophagia never reached a pathology score above 1.5 (mild-moderate) in MGBG treated animals compared to untreated which ranged from a score of 1 (mild) to 2.5 (moderate-severe).

MGBG treatment decreases the number of macrophages in the dorsal root ganglia

We sought to determine if MGBG affected immune activation in the DRG and the composition of macrophages that surround the DRG. We have previously shown that the numbers of CD68+, CD163+, and MAC387+ macrophages are increased in DRG tissue of SIV-infected animals compared to uninfected animals (Chapter 3). Additionally, elevated numbers of CD68+ and MAC387+ macrophages in the tissue was associated with severe pathology (Chapter 3) [7]. Here, we sought to determine if MGBG treatment would affect resident and recently trafficked macrophages. We investigated the number of CD68+, CD163+, and MAC387+ macrophages in the DRG. CD163 is a hemoglobin-haptoglobin scavenger receptor that is associated with an M2 (alternative-activation) phenotype and can also overlap with the CD68+ macrophage population, which is considered to be a marker of mature tissue macrophages [11]. MAC387 is expressed by recently infiltrated, inflammatory

M1-like (classically-activated) monocytes/macrophages and does not co-localize with CD68 or CD163 [12]. Here, we found that the number of CD68+ macrophages in the DRG decreased significantly with MGBG treatment (784.3± 86.8 versus 473.9± 44.2 cells/mm^2; p< 0.01; Figure 5.2A-C). Additionally, MGBG reduced the number of CD163+ macrophages in DRG (789± 107.5 versus 369.5± 45.7 cells/mm^2; p< 0.01; Figure 5.2D-F). The number of MAC387+ macrophages, while not statistically significant, did trend towards a decrease with MGBG treatment (133.0± 15.6 versus 91.9± 11.4 cells/mm^2; p= 0.06; Figure 5.2G-I).

Next, we assessed cell traffic to the DRG using BrdU labeling [13]. We have previously shown that increased monocyte traffic to the DRG was associated with severe pathology and a loss of IENFD (Chapter 3). The majority (78.1%) of BrdU+ cells in the DRGs were found to be MAC387+ macrophages [7]. Here, we found that MGBG significantly reduced traffic of BrdU+ cells (78.3± 6.3 versus 41.9± 4.3 cells/mm^2; p< 0.0001; Figure 5.2J-L).

Finally, we examined the number of CD3+ T lymphocytes in the DRG in both MGBG-treated and untreated groups. We have previously shown that the number of T cells in the DRG did not increase with SIV infection (compared to uninfected animals) (Chapter 3) [7, 10]. We found that there was no change in the number of CD3+ T cells with MGBG treatment (168.1±18.1 versus 122.9±11.1 cells/mm^2; p=0.08; Figure 5.2M-O), suggesting that MGBG had no effect on T cells.

There is no regeneration of IENFD with MGBG treatment.

All animals received skin biopsy punches before MGBG treatment (20 DPI) and at necropsy to assess if MGBG treatment would allow for or prevent regeneration of IENFD. We have previously reported an early decline in IENFD following SIV infection that never recovers to baseline levels (Chapter 2) [7]. As expected, IENFD in SIV-infected untreated animals did not change between 20 DPI and necropsy (298.8± 50.9 IENFD at 20 DPI versus 304.8± 47.1 IENFD at necropsy; $p= 0.84$; Figure 5.3A). Interestingly, MGBG treated animals had a significant additional loss of IENFD after drug treatment was initiated at 21 DPI. IENFD in the MGBG treated group decreased from 551.8± 73.3 IENFD at 20 DPI to 387.8± 53.0 IENFD at necropsy ($p< 0.05$; Figure 5.3B). We suspect that this is because macrophages are required for peripheral nerve regeneration and MGBG targets these M2 repair macrophages [14, 15]. MGBG treatment in the absence of SIV infection did not significantly affect the IENFD (369.3± 108.0 IENFD at pre-drug versus 291.7± 113.3 IENFD at necropsy; $p= 0.75$; data not shown). This demonstrates that MGBG is not neurotoxic and that the drug's effect on macrophages combined with SIV infection is the cause of IENFD reduction.

DISCUSSION

Here, we found that MGBG administration in a rhesus model of HIV-PN diminished DRG pathology with reduced numbers of CD68+ and CD163+ macrophages. We have previously shown that the number of CD68+ and

CD163+ macrophages in DRG tissue increases after SIV infection (Chapter 3). Additionally, we have shown that cell traffic to the DRG is associated with severe DRG pathology and a greater loss of IENFD (Chapter 3) [7]. Monocyte traffic to the DRG appears to be a driving force of formation of Nageotte nodules and neuronophagia. When cell traffic was blocked with an anti-VLA-4 antibody, natalizumab, on the day of infection there was a reduction in these lesions. However, blocking cell traffic during late infection did not completely prevent formation of Nageotte nodules suggesting that these lesions form during early infection (Chapter 4) [16]. Here, we found that MGBG treatment reduced BrdU+ cell traffic to the DRG and as expected, reduced tissue pathology.

However, despite reduction of cell traffic and pathology in the DRGs, we did not observe regeneration of IENFD in the footpad. It has been previously shown that IENFD can regenerate in the setting of HIV infection [17]. Additionally, loss of IENFD occurs early after infection and never recovers in our model (Chapter 2) [7]. Because MGBG was not administered until 21 DPI, reversible damage to the nerve fibers had most likely already occurred. Macrophages also play a role in tissue remodeling and peripheral nerve regeneration [18]. We suspect that the diminished numbers of alternatively activated macrophages in MGBG-treated animals prevented peripheral nervous system (PNS) recovery. Polyamines, which are depleted with MGBG treatment, have been shown to aid in sciatic nerve regeneration *in vivo* and promote axonal regeneration in vitro [19, 20]. Additionally, macrophage accumulation around injured PNS nerves is an important step in regeneration. Macrophages are

responsible for removing myelin and axonal debris from the injury site. Depleting macrophages delays both Wallerian degeneration and regeneration of axons, demonstrating that macrophages play a multitude of roles in PNS injury and recovery [14, 15, 18, 21]. The lack of IENFD regeneration in MGBG-treated animals implies an additional impairment (secondary to SIV infection) that consists of a lack of tissue-regenerative macrophages, depleted polyamides, and/or ongoing injury due to sustained viral load and cytokines despite MGBG-treatment.

Few drugs specifically target monocyte and macrophage activation as therapy for HIV-PN. One drug that may improve PNS pathology in HIV+ patients is maraviroc. Maraviroc is a CCR5 inhibitor that blocks viral entry into CCR5+ cells [22]. RANTES (the ligand for CCR5) and CCR5+ cells in the DRG are elevated after SIV infection and are associated with SIV-PN pathologies [9]. Additionally, *in vitro* maraviroc treatment to DRG neurons inhibited gp120-induced tumor necrosis factor-alpha expression and thus reduced neurotoxicity [23]. Cenicriviroc (CVC), which is currently in clinical trials for HIV treatment, targets both CCR5 and CCR2 [24, 25]. The ligand for CCR2 is CCL2 or monocyte chemoattractant protein-1 (MCP-1) is elevated in SIV+ DRG [9] and most likely plays a role in recruiting inflammatory CCR2+ monocytes to the tissue. Additionally, CCR2-CCL2 interaction has been implicated in models of neuropathic pain [26, 27]. It is unclear if CVC treatment will have a beneficial effect on PNS nerve pathologies.

MGBG is specifically taken up by monocytes and macrophages [3]. It was recently shown that MGBG inhibits HIV expression and integration in macrophages in vitro, although the mechanism of this phenomenon is not clear [3]. MGBG has been well studied as a potent inhibitor of SAMDC and therefore depletes the intracellular polyamine pool [1, 28]. Polyamines are regulators of macrophage activation. They are needed for alternative macrophage (M2) polarization and can also inhibit M1-cytokine production [6]. In this study, we found that MGBG significantly reduced the number of CD163+ (M2) macrophages, but not the number of MAC387+ (M1) macrophages in the DRG, supporting the mechanism that MGBG inhibits M2-activation.

Identifying drugs that target myeloid cells to reduce their traffic into tissues and over-activation during HIV and SIV disease pathogenesis is important to prevent these comorbidities. However, one must be careful to not completely block macrophage function, as they can play essential roles in innate immunity and tissue remodeling, as demonstrated by the lack of IENFD regeneration in this study. Future studies should seek to understand the diverse role of different macrophage phenotypes and identify drugs that specifically target destructive and overly inflammatory macrophages. Treatment with MGBG before PNS damage begins would likely have a greater preventative impact on the development of PN. Additionally, using MGBG in conjunction with antiretroviral therapy (ART) to reduce viral replication and monocyte/macrophage activation may also be beneficial. In this study, we did not see an effect on plasma viral load, only on monocyte traffic and activation. Thus, suppressing viral replication

with ART and reducing monocyte activation with MGBG may be a successful drug cocktail to control disease progression and prevent inflammation-induced comorbidities (experiments currently underway).

A**CKNOWLEDGEMENTS**

This work was funded by NIH/NINDS RO1 NS040237 (awarded to KC Williams), R01 NS082116 (awarded to TH Burdo), and U19MH08183 (awarded to MS McGrath). We would like to thank Pathologica for providing MGBG and Wedgwood Pharmacy for formulating MGBG and the placebo. We would also like to thank the veterinary staff at the NEPRC and TNRPC for the animal care and for assisting with necropsies and tissue collection.

Table 5.1: SIV+ rhesus macaques used in this study and DRG pathology.

Animal group	ID	Survival (days)	Overall pathology	Overall DRG pathology	Satellitosis	Neuronophagia	Nageotte nodules
Control (n=9)	C1	63	AIDS	Mild	Moderate	Rare	None
	C2	70	Severe SIVE	Mild	Mild	Mild	None
	C3	77	Severe SIVE	Mild	Mild-Mod	Mild	None
	C4	83*	AIDS	Mild	Mild	Mild	None
	C5	84*	AIDS	Mild	Mild	Mild	Rare
	C6	77	SIVE	Mod-Severe	Severe	Mod-Severe	Severe
	C7	77	SIVE	Moderate	Moderate	Moderate	Rare
	C8	89	SIVE	Moderate	Moderate	Moderate	Rare
	C9	55	SIVE	Mild-mod	Moderate	Mild	Rare
MGBG (n=9)	M1	63	SIV, no AIDS	Mild	Mild	None	None
	M2	70*	SIV, no AIDS	NSF	Rare	Rare	None
	M3	70	SIV, no AIDS	Mild	Mild-Mod	Mild	None
	M4	77*	SIV, no AIDS	Mild	Mild	Mild	None
	M5	83*	SIV, no AIDS	Mild	Mild-Mod	Mild	None
	M6	84*	SIV, no AIDS	Mild	Mild-Mod	Mild	None
	M7	63	AIDS	Mild	Mild	None	None
	M8	77	AIDS	Mild	Mild-Mod	Mild	None
	M9	83*	AIDS	Mild	Mild	Mild	None

* = timed or paired sacrificed; SIVE = SIV encephalitis; Mod = Moderate.

Figure 5.1

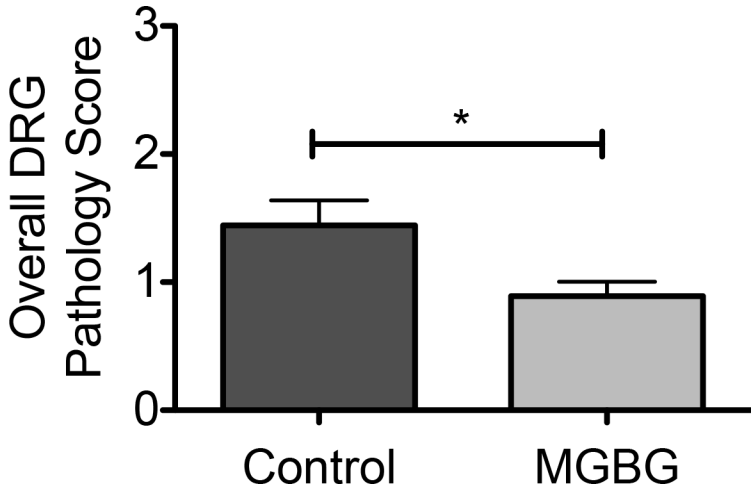

Figure 5.1: Overall DRG pathology is reduced in MGBG-treated animals compared to controls.

Overall DRG pathology was scored on a scale of zero (no significant findings) to three (severe pathology) at increments of 0.5 in lumbar, sacral, and thoracic regions and were averaged in each animal. Pathology was scored based on the degree and presence of satellitosis, neuronophagia, and Nageotte nodules. Bars represent the average overall DRG pathology mean ± SEM. Groups were compared with a Mann-Whitney T-test. *P<0.05.

Figure 5.2

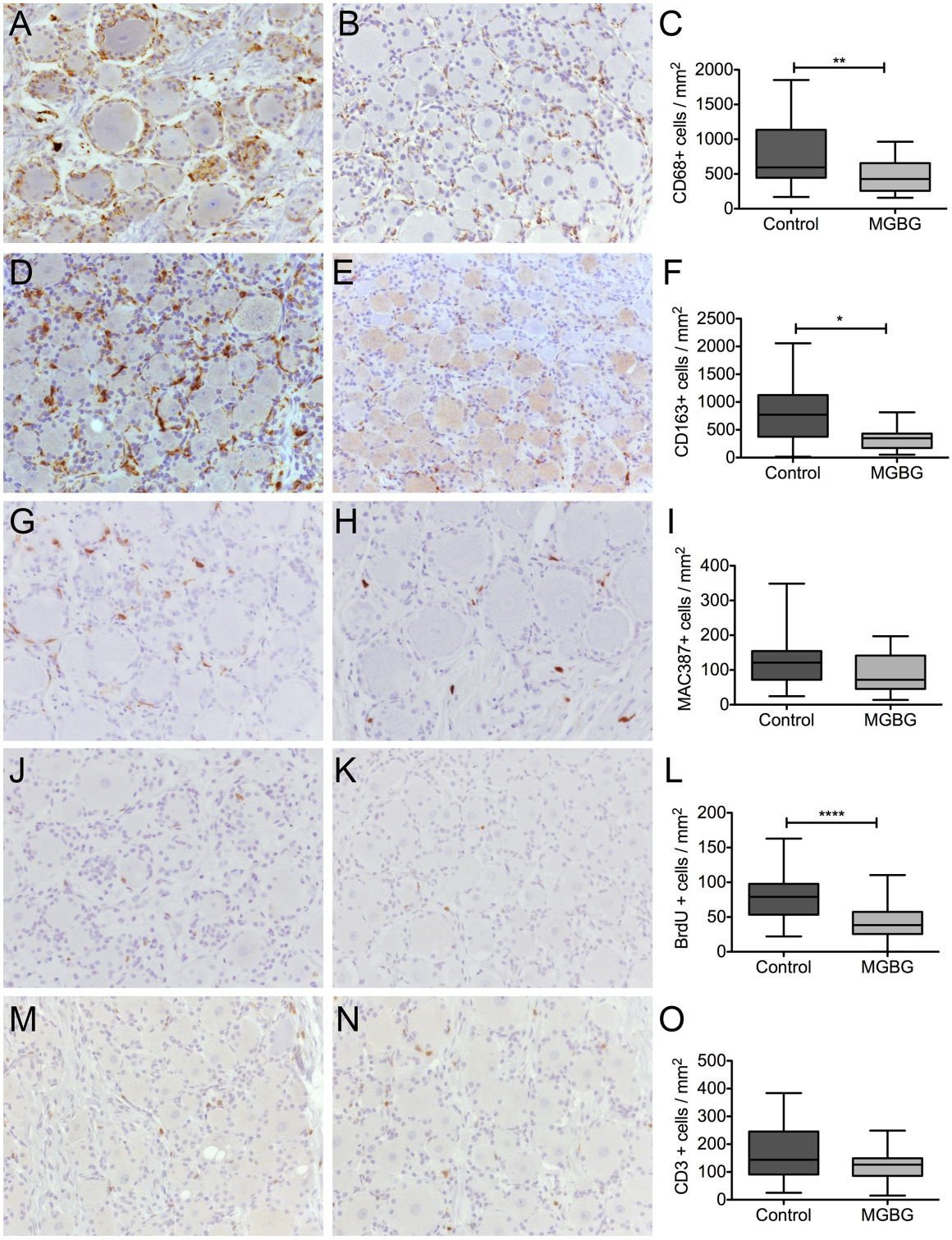
A
B
C
CD68+ cells / mm2
2000
1500
1000
500
0
**
Control
MGBG
D
E
F
CD163+ cells / mm2
2500
2000
1500
1000
500
0
*
Control
MGBG
G
H
I
MAC387+ cells / mm2
400
300
200
100
0
Control
MGBG
J
K
L
BrdU + cells / mm2
200
150
100
50
0
****
Control
MGBG
M
N
O
CD3 + cells / mm2
500
400
300
200
100
0
Control
MGBG

Figure 5.2: MGBG treatment reduces the number of macrophages in and cell traffic to the DRG.

The numbers of CD68+ (A-C), CD163+ (D-F), MAC387+ (G-I), BrdU+ (J-L), and CD3+ (M-O) cells per mm^2 of tissue were counted in DRG from control animals and MGBG-treated animals. Representative images of DRG from control animals (A, D, G, J, M) and MGBG-treated animals (B, E, H, K, N) are shown. Data are shown as mean ± SEM (C, F, I, L, O). Groups were compared with a Mann-Whitney T-test. *P<0.05; **P<0.01; ****P<0.0001.

Figure 5.3

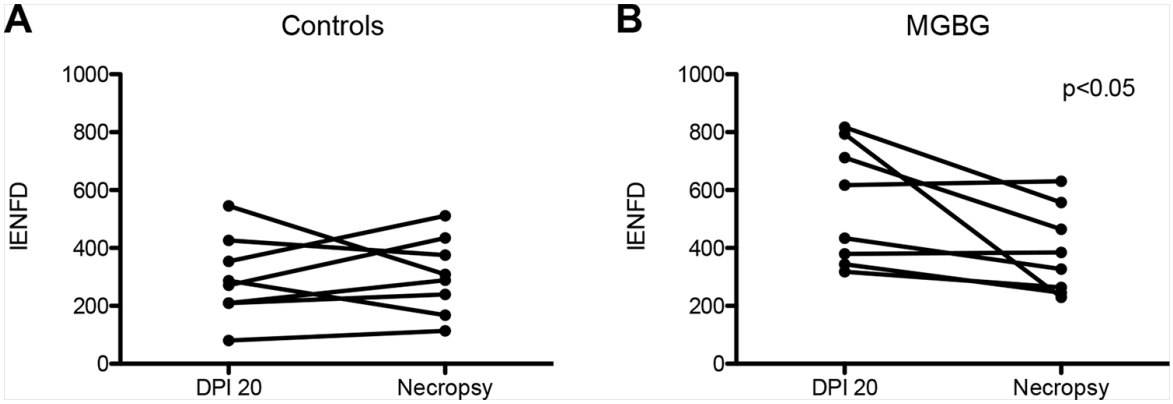
A
Controls
IENFD
1000
800
600
400
200
0
DPI 20
Necropsy
B
MGBG
p<0.05
IENFD
1000
800
600
400
200
0
DPI 20
Necropsy

Figure 5.3: MGBG treatment does not allow for regeneration of peripheral nerves.

IENFD was measured at 20 dpi and at necropsy in control (A) and in MGBG-treated (B) groups. Changes in IENFD between time points assessed with a Wilcoxon matched-pairs signed rank test. A p value less than 0.05 was considered significant.

REFERENCES:

1. Williams-Ashman, H.G. and A. Schenone, *Methyl glyoxal bis(guanylhydrazone) as a potent inhibitor of mammalian and yeast S-adenosylmethionine decarboxylases.* Biochemical and biophysical research communications, 1972. **46**(1): p. 288-95.
2. Janne, J., L. Alhonen-Hongisto, P. Nikula, and H. Elo, *S-adenosylmethionine decarboxylase as target of chemotherapy.* Advances in enzyme regulation, 1985. **24**: p. 125-39.
3. Jin, X., M.S. McGrath, and H. Xu, *Inhibition of HIV Expression and Integration in Macrophages by Methylglyoxal-Bis-Guanylhydrazone.* Journal of virology, 2015. **89**(22): p. 11176-89.
4. Messina, L., G. Spampinato, A. Arcidiacono, L. Malaguarnera, M. Pagano, B. Kaminska, L. Kaczmarek, and A. Messina, *Polyamine involvement in functional activation of human macrophages.* Journal of leukocyte biology, 1992. **52**(6): p. 585-7.
5. Kaczmarek, L., B. Kaminska, L. Messina, G. Spampinato, A. Arcidiacono, L. Malaguarnera, and A. Messina, *Inhibitors of polyamine biosynthesis block tumor necrosis factor-induced activation of macrophages.* Cancer research, 1992. **52**(7): p. 1891-4.
6. Van den Bossche, J., W.H. Lamers, E.S. Koehler, J.M. Geuns, L. Alhonen, A. Uimari, S. Pirnes-Karhu, E. Van Overmeire, Y. Morias, L. Brys, L. Vereecke, P. De Baetselier, and J.A. Van Ginderachter, *Pivotal Advance: Arginase-1-independent polyamine production stimulates the expression of IL-4-induced alternatively activated macrophage markers while inhibiting LPS-induced expression of inflammatory genes.* Journal of leukocyte biology, 2012. **91**(5): p. 685-99.
7. Lakritz, J.R., A. Bodair, N. Shah, R. O'Donnell, M.J. Polydefkis, A.D. Miller, and T.H. Burdo, *Monocyte Traffic, Dorsal Root Ganglion Histopathology, and Loss of Intraepidermal Nerve Fiber Density in SIV Peripheral Neuropathy.* The American journal of pathology, 2015. **185**(7): p. 1912-23.
8. Burdo, T.H., C. Soulas, K. Orzechowski, J. Button, A. Krishnan, C. Sugimoto, X. Alvarez, M.J. Kuroda, and K.C. Williams, *Increased monocyte turnover from bone marrow correlates with severity of SIV encephalitis and CD163 levels in plasma.* PLoS pathogens, 2010. **6**(4): p. e1000842.
9. Lakritz, J.R., J.A. Robinson, M.J. Polydefkis, A.D. Miller, and T.H. Burdo, *Loss of intraepidermal nerve fiber density during SIV peripheral neuropathy is mediated by monocyte activation and elevated monocyte chemotactic proteins.* Journal of neuroinflammation, 2015. **12**(1): p. 237.
10. Burdo, T.H., K. Orzechowski, H.L. Knight, A.D. Miller, and K. Williams, *Dorsal root ganglia damage in SIV-infected rhesus macaques: an animal*

model of HIV-induced sensory neuropathy. The American journal of pathology, 2012. **180**(4): p. 1362-9.
11. Etzerodt, A. and S.K. Moestrup, *CD163 and inflammation: biological, diagnostic, and therapeutic aspects.* Antioxidants & redox signaling, 2013. **18**(17): p. 2352-63.
12. Soulas, C., C. Conerly, W.K. Kim, T.H. Burdo, X. Alvarez, A.A. Lackner, and K.C. Williams, *Recently infiltrating MAC387(+) monocytes/macrophages a third macrophage population involved in SIV and HIV encephalitic lesion formation.* The American journal of pathology, 2011. **178**(5): p. 2121-35.
13. Goto, Y., J.C. Hogg, T. Suwa, K.B. Quinlan, and S.F. van Eeden, *A novel method to quantify the turnover and release of monocytes from the bone marrow using the thymidine analog 5'-bromo-2'-deoxyuridine.* American journal of physiology. Cell physiology, 2003. **285**(2): p. C253-9.
14. Niemi, J.P., A. DeFrancesco-Lisowitz, L. Roldan-Hernandez, J.A. Lindborg, D. Mandell, and R.E. Zigmond, *A critical role for macrophages near axotomized neuronal cell bodies in stimulating nerve regeneration.* The Journal of neuroscience : the official journal of the Society for Neuroscience, 2013. **33**(41): p. 16236-48.
15. Barrette, B., M.A. Hebert, M. Filali, K. Lafortune, N. Vallieres, G. Gowing, J.P. Julien, and S. Lacroix, *Requirement of myeloid cells for axon regeneration.* The Journal of neuroscience : the official journal of the Society for Neuroscience, 2008. **28**(38): p. 9363-76.
16. Lakritz, J.R., D. Thibault, J.A. Robinson, J. Campbell, A.D. Miller, K. Williams, and T.H. Burdo, *alpha4-Integrin Antibody Treatment Blocks Monocyte/Macrophage Traffic to, Vascular Cell Adhesion Molecule-1 Expression in, and Pathology of the Dorsal Root Ganglia in an SIV Macaque Model of HIV-Peripheral Neuropathy.* The American journal of pathology, 2016.
17. Hahn, K., A. Triolo, P. Hauer, J.C. McArthur, and M. Polydefkis, *Impaired reinnervation in HIV infection following experimental denervation.* Neurology, 2007. **68**(16): p. 1251-6.
18. Gaudet, A.D., P.G. Popovich, and M.S. Ramer, *Wallerian degeneration: gaining perspective on inflammatory events after peripheral nerve injury.* Journal of neuroinflammation, 2011. **8**: p. 110.
19. Kauppila, T., *Polyamines enhance recovery after sciatic nerve trauma in the rat.* Brain research, 1992. **575**(2): p. 299-303.
20. Deng, K., H. He, J. Qiu, B. Lorber, J.B. Bryson, and M.T. Filbin, *Increased synthesis of spermidine as a result of upregulation of arginase I promotes axonal regeneration in culture and in vivo.* The Journal of neuroscience : the official journal of the Society for Neuroscience, 2009. **29**(30): p. 9545-52.
21. Chen, P., X. Piao, and P. Bonaldo, *Role of macrophages in Wallerian degeneration and axonal regeneration after peripheral nerve injury.* Acta neuropathologica, 2015. **130**(5): p. 605-18.

22. Piotrowska, A., K. Kwiatkowski, E. Rojewska, W. Makuch, and J. Mika, *Maraviroc reduces neuropathic pain through polarization of microglia and astroglia - Evidence from in vivo and in vitro studies.* Neuropharmacology, 2016.
23. Moss, P.J., W. Huang, J. Dawes, K. Okuse, S.B. McMahon, and A.S. Rice, *Macrophage-sensory neuronal interaction in HIV-1 gp120-induced neurotoxicitydouble dagger.* British journal of anaesthesia, 2015. **114**(3): p. 499-508.
24. Kramer, V.G., S. Hassounah, S.P. Colby-Germinario, M. Oliveira, E. Lefebvre, T. Mesplede, and M.A. Wainberg, *The dual CCR5 and CCR2 inhibitor cenicriviroc does not redistribute HIV into extracellular space: implications for plasma viral load and intracellular DNA decline.* The Journal of antimicrobial chemotherapy, 2015. **70**(3): p. 750-6.
25. Thompson, M., M. Saag, E. DeJesus, J. Gathe, J. Lalezari, A.L. Landay, J. Cade, J. Enejosa, E. Lefebvre, and J. Feinberg, *A 48-week randomized phase 2b study evaluating cenicriviroc versus efavirenz in treatment-naive HIV-infected adults with C-C chemokine receptor type 5-tropic virus.* AIDS, 2016. **30**(6): p. 869-78.
26. Biber, K. and E. Boddeke, *Neuronal CC chemokines: the distinct roles of CCL21 and CCL2 in neuropathic pain.* Frontiers in cellular neuroscience, 2014. **8**: p. 210.
27. Thacker, M.A., A.K. Clark, T. Bishop, J. Grist, P.K. Yip, L.D. Moon, S.W. Thompson, F. Marchand, and S.B. McMahon, *CCL2 is a key mediator of microglia activation in neuropathic pain states.* European journal of pain, 2009. **13**(3): p. 263-72.
28. Corti, A., C. Dave, H.G. Williams-Ashman, E. Mihich, and A. Schenone, *Specific inhibition of the enzymic decarboxylation of S-adenosylmethionine by methylglyoxal bis(guanylhydrazone) and related substances.* The Biochemical journal, 1974. **139**(2): p. 351-7.

CHAPTER VI

Title: Loss of intraepidermal nerve fiber density during SIV peripheral neuropathy is mediated by monocyte activation and elevated monocyte chemotactic proteins

Adapted from:
"Loss of intraepidermal nerve fiber density during SIV peripheral neuropathy is mediated by monocyte activation and elevated monocyte chemotactic proteins"

by Jessica R. Lakritz, Jake A. Robinson, Michael J. Polydefkis, Andrew D. Miller, and Tricia H. Burdo

Journal of Neuroinflammation. 2015 Dec 18; 12:237.

Author contributions:

JRL and THB conceived and designed the experiments. JRL, JAR, MJP, and ADM performed the experiments. JRL and THB analyzed the data. JRL and THB wrote the paper. All authors carried out paper revisions.

ABSTRACT

Increased monocyte traffic to the dorsal root ganglia (DRG) has previously been associated with severe DRG pathology, as well as a loss in intraepidermal nerve fiber density (IENFD) (Chapter 3). Here, we sought to characterize the molecular signals associated with monocyte activation and trafficking to the DRGs. 11 SIV-infected CD8 depleted rhesus macaques were compared to 4 uninfected control animals. sCD14, sCD163, sCD137, RANTES, and MCP-1 were measured in plasma and the latter three proteins were also quantified in DRG tissue lysates. All SIV-infected animals received serial skin biopsies to measure IENFD loss as well as bromodeoxyuridine (BrdU) inoculations to measure monocyte turnover during the course of infection. The number of BrdU+ and CD14+CD16+ peripheral blood monocytes was determined by flow cytometry. The number of MAC387+, CCR2+, CCR5+, and CD137+ cells in DRG tissue was quantified by immunohistochemistry. sCD14, sCD163, MCP-1, and sCD137 increased significantly in plasma from pre-infection to necropsy. Plasma sCD163 and RANTES inversely correlated with IENFD. Additionally, sCD137 in DRG tissue lysate was elevated with severe DRG pathology and associated with the recruitment of MAC387+ cells to DRG. Elevated numbers of CCR5+ and CCR2+ satellite cells in the DRG were found, suggesting a chemotactic role of their ligands, RANTES and MCP-1 in recruiting monocytes to the tissue. We characterized the role of systemic (plasma) and tissue-specific (DRG) monocyte activation and associated cytokines in the pathogenesis of SIV-PN. We identified

sCD163 and RANTES as potential biomarkers for HIV-PN, as these were associated with a loss of IENFD. Additionally, we identified CD137 signaling to play a role in MAC387+ cell traffic to DRG and possibly contribute to severe pathology. These studies highlight the role of monocyte activation and traffic in the pathogenesis of SIV-PN, while identifying specific signaling proteins for future pharmacological blockade.

INTRODUCTION

Cytokines have a large impact on the nervous system, in addition to regulating the immune response. Dorsal root ganglia (DRG) neurons express cytokine receptors on their surfaces so they can appropriately respond to cytokines in their environment [1, 2]. CCR5, the receptor for RANTES (Regulated on Activation, Normal T cell Expressed and Secreted)/CCL5 can be expressed on DRG neuronal cell bodies. Gp120 can bind to CCR5 resulting in neuronal excitation [3]. CCR2, another chemokine receptor expressed on DRG neurons, can also facilitate neuronal excitation when it binds to monocyte chemoattractant protein-1 (MCP-1/CCL2) [4]. Various rodent models of neuropathic pain have demonstrated that blocking the MCP-1-CCR2 interaction via neutralizing antibodies or gene knockout can block pain sensation [5-9]. Neuronal cell bodies in the DRG can also upregulate inflammatory cytokines following peripheral nerve injury [10-12]. Thus, cytokines can transmit pain signals from the periphery to the central nervous system (CNS) via interactions with cytokine receptors on DRG neurons [8, 13]. Additionally, MCP-1 and RANTES might increase recruitment of monocytes to the DRG causing further neuronal damage and activation [1, 14, 15],

Other signaling pathways besides CCR2 and CCR5 are likely involved in neuronal damage during SIV-DSP. One potential signaling protein of interest is CD137, which is a member of TNF superfamily that can be expressed on T cells, monocytes, other immune cells, as well as endothelial cells [16, 17]. CD137 cross-linking on monocytes induces activation and production of pro-

inflammatory cytokines [18]. CD137 expression on endothelial cells facilitates migration of monocytes out of blood vessels and into tissues [17, 19]. Additionally, CD137 reverse signaling is involved in myelopoiesis [20, 21]. Elevated sCD137 in plasma, a splice variant of CD137, has been associated with several inflammation-linked diseases [22-24], but its role in monocyte activation during HIV infection has not been studied.

We used a CD8-depleted, SIV-infected macaque model to recapitulate HIV-DSP in humans, where animals show a loss of intraepidermal nerve fiber density (IENFD) and DRG pathology [25-27]. We have previously demonstrated an influx of activated MAC387+ macrophages to the DRG as well as an increase in CD163+ macrophages (Chapter 3). Importantly, we found that increased cell traffic was associated with severe DRG pathology and a greater loss of IENFD (Chapter 3) [28]. This study sought to investigate the role of monocyte activation in HIV-distal sensory polyneuropathy (DSP), as well as identify cytokines that are associated with monocyte activation and neuronal loss in plasma and in DRG tissue.

MATERIALS and METHODS

Ethical Statement

All animals used in this study were handled in strict accordance with American Association for Accreditation of Laboratory Animal Care with the approval of the Institutional Animal Care and Use Committee of Harvard

University and the Institutional Animal Care and Use Committee of Tulane University.

Animals, viral infection, and CD8 lymphocyte depletion

Fifteen rhesus macaques (*Macaca mulatta*) were utilized in this study. Eleven animals were inoculated intravenously with SIVmac251 (a generous gift from Dr. Ronald Desrosiers, University of Miami). Four uninfected rhesus macaques served as uninfected controls. All infected animals were administered 10 mg/kg of anti-CD8 antibody subcutaneously at day 6 after infection and 5 mg/kg intravenously at days 8 and 12 after infection in order to achieve rapid progression to AIDS. The human anti-CD8 antibody was provided by the NIH Non-human Primate Reagent Resource (RR016001, AI040101). SIV-infected animals were sacrificed at the onset of terminal AIDS. Animals were housed at either the New England Primate Research Center (NEPRC; Southborough, MA) or Tulane University's National Primate Research Center (TNPRC; Covington, LA) in strict accordance with standards of the American Association for Accreditation of Laboratory Animal Care.

Necropsy and Histopathology

Tissue collection and preservation was performed as previously described (Chapter 2). DRG tissue sections were stained with hematoxylin and eosin and were evaluated for pathology as previously described (Chapter 2) [26, 28, 29].

BrdU Administration

BrdU was administered as previously described (Chapter 3) [28, 31, 32]. BrdU was administered at 8 and 21 DPI in animals A01-A07. Additionally, animals A04-A11 received BrdU 42, 63 DPI, and 24 hours prior to necropsy.

Immunohistochemistry

DRG sections were deparafinized with xylene and hydrated in a series of graded alcohols. Sections were stained with antibodies against MAC387 (clone M0747; Dako), CCR5 (rabbit polyclonal; Novus Biologicals) or CCR2 (clone 7A7; Abcam). Frozen DRG sections were used for CD137 staining (clone BBK-2). Sections were counterstained with hematoxylin, dehydrated, and mounted using VectaMount permanent mounting medium (Vector Labs). Tissues were visualized using a Zeiss Axio Imager M1 microscope (Carl Zeiss MicroImaging). Quantification of the absolute number and percent of positive satellite cells were performed as previously described (Chapter 3) [28]. For each animal, eight non-overlapping fields of view at 200x magnification were quantified by manually counting the number of positive cells in the field and dividing by the total area of DRG tissue. The average number of positive cells per mm^2 was used.

Skin Punch and IENFD Measurement

Skin punch biopsy and IENFD measurement was performed as previously described (Chapter 2) [28, 30].

Flow Cytometry

Flow cytometric analyses were performed with 100 µl aliquots of EDTA-coagulated whole blood. Erythrocytes were lysed using ImmunoPrep Reagent System (Beckman Coulter), washed twice with PBS containing 2% FBS, then incubated for 15 minutes at room temperature with fluorochrome-conjugated surface antibodies including anti-HLA-DR-PerCp-Cy5.5 (clone L243), anti-CD16-PE-Cy7 (clone 3G8), anti-CD3-APC (clone SP34-2), and CD8-APC (clone RPA-T8), anti-CD20 (APC (clone 2H7) and anti-CD14-Pacific blue (clone M5E2). For intracellular staining, cells were fixed and permeabilized with BD Cytofix/Cytoperm™ buffer (BD Biosciences) for 30 mins at room temperature. Cells were again washed and incubated with BD Cytoperm Plus™ buffer for 10 mins on ice, then washed and incubated with DNase (30mg) for 1hr at 37°C, washed and then stained for intracellular antigen with anti-BrdU-FITC (clone 3D4; BD Biosciences) and anti-Ki-67-PE (clone B56; BD Biosciences) for 20 mins at room temperature. Samples were acquired on a BD FACS Aria (BD Biosciences) and analyzed with Tree Star Flow Jo version 9.6. Identification and quantitation of BrdU+ monocytes and CD14+CD16+ monocytes was performed as previously described [32].

Preparation of DRG lysate

Frozen lumbar DRG was mechanically homogenized in Tissue Extraction Reagent I (Invitrogen, Waltham, MA) containing 1x protease inhibitor (Sigma-Aldrich). For every 1g of tissue, 10mL of lysis buffer was used. Lysate was

centrifuged and supernatant containing protein was stored at -80°C. Protein was quantified using a BCA protein assay kit (Thermo Scientific) according to the manufacturer's instructions.

Enzyme-linked immunosorbent assays (ELISAs)

sCD14 and RANTES were quantified in plasma (diluted 1:200 and 1:4; respectively) using ELISA kits (R&D Systems) . sCD163 was quantified in plasma (diluted 1:500) using an ELISA kit (Trillium Diagnostics). All ELISAs were carried out according to the manufacturer's instructions and as previously described [32].

Luminex Multiplex Assays

RANTES, MCP-1 and sCD137 were quantified in DRG tissue lysates and MCP-1 and sCD137 were quantified in plasma using Multiplex Luminex Technology (EMD Millipore). Non-human Primate Cytokine/Chemokine Panels 1 and 2 were used according to the manufacturer's instructions with the following modifications. For DRG tissue lysate protein quantification, 10µg of protein (in 25µl of lysis buffer) from each sample was loaded onto the plate. Tissue lysis buffer was used as the matrix for dilution of standards and quality control samples. For the plasma sample analysis, plasma samples were diluted 2-fold in the assay buffer provided. The provided serum matrix was used for dilution of standards and quality control samples. All samples were performed in duplicate

and plates were incubated overnight at 4°C on a rocker. Samples were analyzed using MAGPIX System (EMD Millipore).

Statistical Analysis

All statistical analysis was performed using Prism Software (Version 5.0d). A Wilcoxon matched-pairs signed rank test was used to determine increase in markers from pre-infection to necropsy. A Mann-Whitney U test was used to detect variation between infected and uninfected samples. ANOVA was used to detect variance among different pathology groups followed by a Dunn's post-test if the ANOVA was significant. Non-parametric Spearman correlation was used for all correlations. A p value of <0.05 was considered significant for all tests performed.

RESULTS

Animals used for the study

Eleven rhesus macaques were infected with SIVmac251 and were administered with a CD8-depletion antibody 6, 8, and 12 days post-infection (DPI) in order to rapidly progress to AIDS. All SIV-infected animals developed mild to severe lumbar DRG pathology, as well as a loss of IENFD (Table 6.1).

Plasma markers of monocyte egress and activation during SIV infection

Monocyte egress from the bone marrow was measured by BrdU pulse labeling [32]. We also measured CD14+CD16+ monocytes by multi-color flow cytometry and found that this population of activated monocytes was expanded during SIV infection (data not shown). We investigated soluble monocyte activation markers sCD14 (Figure 6.1A-C) and sCD163 (Figure 6.1D-F) in plasma and their correlation to the rate of peripheral monocyte turnover and the number of CD14+CD16+ activated peripheral monocytes. Both of these markers increased significantly in from pre-infection to necropsy using Wilcoxon matched-pairs signed rank test (sCD14 $p< 0.05$; sCD163 $p< 0.01$). sCD14 was also associated with the number of BrdU+ monocytes (Figure 6.1B, $p< 0.05$) and the percent of CD14+CD16+ monocytes out of the total number of circulating monocytes (Figure 6.1C, $p< 0.05$). sCD163 did not significantly correlate to the absolute number of BrdU+ or CD14+CD16+ monocytes (Figure 6.1E-F), in contrast to previously published data where percentages and not absolute numbers were examined [32].

Next, we examined the correlation of RANTES (Figure 6.1G-I), MCP-1 (Figure 6.1J-L), and sCD137 (Figure 6.1M-O) to monocyte egress and activation. We identified sCD137 as a novel signaling protein that may also play an important role in SIV-DSP pathogenesis because of its role in myelopoiesis, monocyte extravasation, and monocyte activation [17-21]. When we compared pre-infection plasma concentrations of RANTES, MCP-1, and sCD137 to necropsy plasma concentrations using the Wilcoxon matched-pairs signed rank

test, we found that MCP-1 and sCD137 both increased significantly during infection (MCP-1, P< 0.001; sCD137, p< 0.01). RANTES was not increased significantly during infection, but it correlated with the percent of activated CD14+CD16+ monocytes in circulation at matched time points (p< 0.05, Figure 6.1I). Additionally, necropsy plasma concentrations of RANTES and MCP-1 were associated with more severe DRG pathology (p< 0.05, Figures 6.1G, 2J). MCP-1 was also associated with monocyte egress from the bone marrow (p< 0.001, Figure 6.1K) and with CD14+CD16+ monocytes (p< 0.05, Figure 6.1L). sCD137 did not significantly correlate with either BrdU+ or CD14+CD16+ blood monocytes (Figure 6.1N-O). These data suggest that the rate of monocyte activation and egress from the bone marrow is likely controlled by several soluble factors. Because of this complexity and likely redundancy of pathways, suppressing elevated rates of myelopoiesis is unlikely to be a successful pharmacologic target. In addition, we found that three out of five of our examined proteins to be correlated with the percent of CD14+CD16+ monocytes, which are typically considered to be the most activated monocyte population, but it is unclear if this population of monocytes is activated by these proteins or producing these signaling factors.

Correlates of reduced IENFD

We hypothesized that monocyte activation and chemokines responsible for monocyte traffic to the DRG may facilitate neurodegeneration resulting in a reduced density of nerve fibers in the periphery. To test this, we correlated

sCD14 (Figure 6.2A), sCD163 (Figure 6.2B), RANTES (Figure 6.2C), MCP-1 (Figure 6.2D), and sCD137 (Figure 6.2E) with absolute IENFD at matched time points. sCD163 ($p< 0.0001$) and RANTES ($p< 0.0001$) in plasma negatively correlated with absolute IENFD values. No significant correlation was found for sCD14, MCP-1, and sCD137. Thus, increased monocyte activation and possibly chemotaxis are involved in the dying-back of axons during SIV infection.

Elevated monocyte chemoattractants in DRG tissue during SIV infection

Next, we sought to investigate which chemokines are associated with monocyte traffic to the DRG. We have previously shown that an influx of mononuclear cells to the DRG during SIV infection is associated with severe tissue pathology [28]. Thus, we hypothesized that monocyte chemoattractants are elevated in DRG tissue. Whole DRG tissue, consisting of neurons, satellite cells, and vasculature were homogenized and proteins were extracted and analyzed by multiplex assay. There was no detectable difference in RANTES between uninfected and infected DRG tissues, but there was a trend for elevated RANTES in SIV+ DRG with more severe pathology, although this did not reach statistical significance (Figure 6.3A). MCP-1 was elevated in SIV+ DRG compared to uninfected control tissue (Figure 6.3B; $P< 0.05$). sCD137 was only above the detection level in the three DRG examined with severe pathology (Figure 6.3C; ANOVA< 0.001).

To determine if the levels of these chemoattractants in DRGs correlated with the absolute number of MAC387+ recently recruited monocytes in DRGs, we

correlated the protein concentrations of RANTES, MCP-1 and sCD137 with the number of MAC387+ monocytes in tissue determined by immunohistochemistry. No significant correlation was found for RANTES or MCP-1 for recruitment of MAC387+ cells (Figure 6.3D-E). The amount of sCD137 in DRGs positively correlated with the number of MAC387+ cells in matched DRG tissue (Figure 6.3F, $p < 0.05$). These results point to a potential role in sCD137 recruiting MAC387+ monocytes to DRG tissue and facilitating severe tissue damage. Alternatively, MAC387+ cells could be releasing sCD137.

The chemotactic role of RANTES and MCP-1 is well established. MAC387+ cells in the brain of SIV+ macaques are CCR2 negative. Instead, CCR2 was expressed on perivascular macrophages [33]. Thus, we sought to demonstrate the likely role RANTES and MCP-1 play in recruiting monocytes to DRG. We found increased numbers of CCR5+ (Figure 6.4A-C) and CCR2+ (Figure 6.4D-F) satellite cells in infected tissue (Figure 6.4E and H) compared to uninfected (Figure 6.4D and G) controls. The increase of CCR5+ and CCR2+ with SIV infection in DRG was quantitated and found to be statistically significant (Figure 6.4C and F; $p < 0.05$ and $p < 0.05$).

sCD137 is generated by alternative splicing [24]. Membrane-bound CD137 is expressed on a wide range of cell types, including monocytes and expression of CD137 facilitates monocyte extravasation into tissue [17, 19, 34]. Thus, we chose to examine membrane-bound CD137 expression on satellite cells in DRGs of SIV- (Figure 6.4G) and SIV+ (Figure 6.4H) animals. We found that the number of CD137+ cells in SIV+ DRG tissue correlates to tissue

pathology (Figure 6.4I, ANOVA< 0.05). Because CD137 is not unique to myeloid cells, we performed double immunohistochemistry stains. We found that 16.1% of CD137+ cells were T cells (CD3+) and 33.5% of CD137+ cells expressed CD68, a pan-macrophage marker (data not shown). However, because MAC387+ macrophages do not co-express CD68, we suspect the remainder of the CD137+ cells in DRG tissue to be MAC387+ macrophages. However, the MAC387 and CD137 antibodies required different tissue preparation for immunohistochemistry and were incompatible with each other to perform a double stain. Despite this technical pitfall, the correlation of sCD137 to MAC387+ satellite cells in DRG and increased CD137+ satellite cells in DRG with severe pathology highlight a novel potential role of CD137 signaling during SIV infection and DSP pathogenesis.

DISCUSSION

To investigate the systemic inflammation that is causing neuronal damage, both in the DRG and in the extremities, we examined five soluble proteins in plasma, which are associated with monocyte activation and traffic. Here, we found that plasma sCD14 and MCP-1 were correlated to the number of BrdU+ monocytes in blood. We also found that sCD14, RANTES, and MCP-1 were correlated to the percent of CD14+CD16+ monocytes out of total blood monocytes. CD14+CD16+ monocytes are an activated population of monocytes that highly express CCR2, the receptor for MCP-1, and CD163 [35, 36]. Elevated

levels of RANTES and MCP-1 in plasma were associated with moderate or severe DRG pathology, compared to mild pathology. These findings confirm these soluble factors in plasma are associated with monocyte activation and traffic during SIV-PN.

Because the blood-nerve barrier is more promiscuous (or leakier) than the blood-brain barrier [37], we assumed that neurons were exposed to all proteins found in plasma. Several inflammatory cytokines have been found to be neurotoxic *in vitro* [38, 39], but this direct causation is difficult to prove *in vivo.* We found a significant inverse correlation between sCD163 and IENFD. Thus, sCD163 may be useful as a plasma biomarker of IENFD loss in HIV+ patients. While sCD163 and sCD14 are both markers of monocyte activation, they are shed by different mechanisms. CD163 is highly expressed on M2- polarized macrophages and CD14+CD16+ monocytes, while CD14 is present on all populations of monocytes and is shed in the setting of non-specific activation [40] and CD163 is shed due to cell-surface TLR activation [41]. Plasma RANTES/CCL5 also correlated to a reduction in IENFD. Other studies have demonstrated that the supernatant of macrophages exposed to gp120, presumably containing proteins such as sCD163 and RANTES, is capable of damaging neurons *in vitro* [38]. Even though sCD163 and RANTES strongly correlated to a reduction of IENFD, the dying back of axons is likely caused by several signals.

To investigate the local signals in the DRG responsible for monocyte traffic, we analyzed DRG tissue homogenate using a multiplex assay that

allowed for quantification of many proteins with a small amount of tissue homogenate available. The limitation of this method is that it is unknown which cell types are producing the proteins that were detected. Endothelial cells, neurons, Schwann cells, and immune cells (including macrophages and T cells) in the DRG are all capable of secreting cytokines and chemokines. However, this method still affords us the opportunity to investigate the local signals responsible for monocyte traffic and neuronal damage at the DRG. We found that MCP-1 in DRG tissue was significantly increased in DRG from SIV+ animals compared to uninfected control tissue. Because MCP-1 is a potent monocyte chemoattractant and is produced by activated macrophages, it is likely that MCP-1 is partially responsible for increased monocyte traffic to the DRG.

In addition to the proteins we reported on in detail here, we also investigated other known monocyte chemoattractants, both in the DRG and in plasma. We did not find a significant increase in macrophage inflammatory protein (MIP)-1α, MIP-1β, and MIP-3α in plasma, nor were these proteins elevated in SIV+ DRG tissue lysate. In fact, these proteins were below detection level for many of the DRG samples tested. However, monocyte activation and traffic is a complex process, likely to be controlled by several signaling molecules that were not included on the two cytokine/chemokine panels we utilized.

sCD137/CD137 (formally called 4-1BB or tumor necrosis factor receptor superfamily member 9 (TNFRSF9)) has not been extensively studied in the context of monocyte activation during HIV infection, although its known functions in other diseases are relevant to HIV pathogenesis. Here, CD137 was found to

potentially play a role in SIV-DSP pathogenesis. The soluble form of CD137 (sCD137) is generated by alternative splicing and was found to significantly increase in plasma from pre-infection to terminal AIDS. Additionally, sCD137 was only detectable in DRG lysate with severe pathology, and it correlated with the number of MAC387+ cells in DRG tissue. CD137 is expressed on a wide range of cell types, although most of the research on this protein focuses on T cell activation [16-18]. However, CD137 signaling has been shown to play a role in myelopoiesis, monocyte activation, and monocyte extravasation into inflamed tissue [17, 18, 21]. The known roles of CD137 in regards to monocyte activity are also highly deregulated during HIV/SIV infection. Additional research needs to be conducted in order to further define the role of CD137 signaling in HIV/SIV disease progression. CD137 activation, through the use of agnostic monoclonal antibodies, has proven to have potential for cancer treatment by stimulating the immune system to target cancer cells [42]. Blocking CD137 may ameliorate chronic immune activation seen during HIV/SIV infection.

Our findings presented here demonstrate the complexity of the neuro-immune interaction that occurs during the pathogenesis of SIV-DSP. Neurons are capable of producing cytokines, and express cytokine receptors. Stimulation through these receptors has been shown to modulate pain signaling [13, 39]. However, targeting a single cytokine or a receptor is likely not to reverse or prevent nerve damage due to redundancy of immune signaling. No single protein that was investigated in this study was found to associate with all the factors we know to be important in nerve damage during SIV infection. However, sCD163

and RANTES were identified as potential biomarkers for loss of IENFD. Additionally, elevated sCD137 in DRG tissue lysate was found to be associated with MAC387+ cell recruitment and severe pathology. The role of CD137 signaling during SIV-PN pathogenesis warrants further investigation. Future studies should focus on blockade of multiple signals, which may dampen monocyte activation and traffic to the DRG, and thus prevent a loss of IENFD and DRG damage.

ACKNOWLEDGEMENTS

This worked was supported by NIH/NINDS R01 NS082116 (awarded to THB). The *in vivo* CD8 T lymphocyte depletion antibodies used in these studies were provided by the NIH Nonhuman Primate Reagent Resource (RR016001, AI040101). We thank the veterinary staff at the NEPRC and TNRPC for animal care, pathology residents, and staff for assisting with necropsies and tissue collection.

Table 6.1: Animals used in the study.

Animal Treatment	Animal ID	Survival (days)	% Loss of IENFD at necropsy from pre-infection	Lumbar DRG Pathology
SIV-infected CD8 depleted	A01	84	-43.3%	Severe (3)
	A02	96	-13.0%	Mild (1)
	A03	106	-74.5%	Moderate (2)
	A04	89	-36.8%	Moderate-Severe (2.5)
	A05	55	-43.1%	Mild-Moderate (1.5)
	A06	174	-82.5%	Severe (3)
	A07	146	-51.5%	Severe (3)
	A08	77	-57.4%	Moderate-Severe (2.5)
	A09	77	-18.4%	Moderate (2)
	A10	168	-20.4%	Mild (1)
	A11	97	-51.6%*	Mild (1)

IENFD= intraepidermal nerve fiber density; * = percent change from pre-infection to 63 DPI.

Figure 6.1

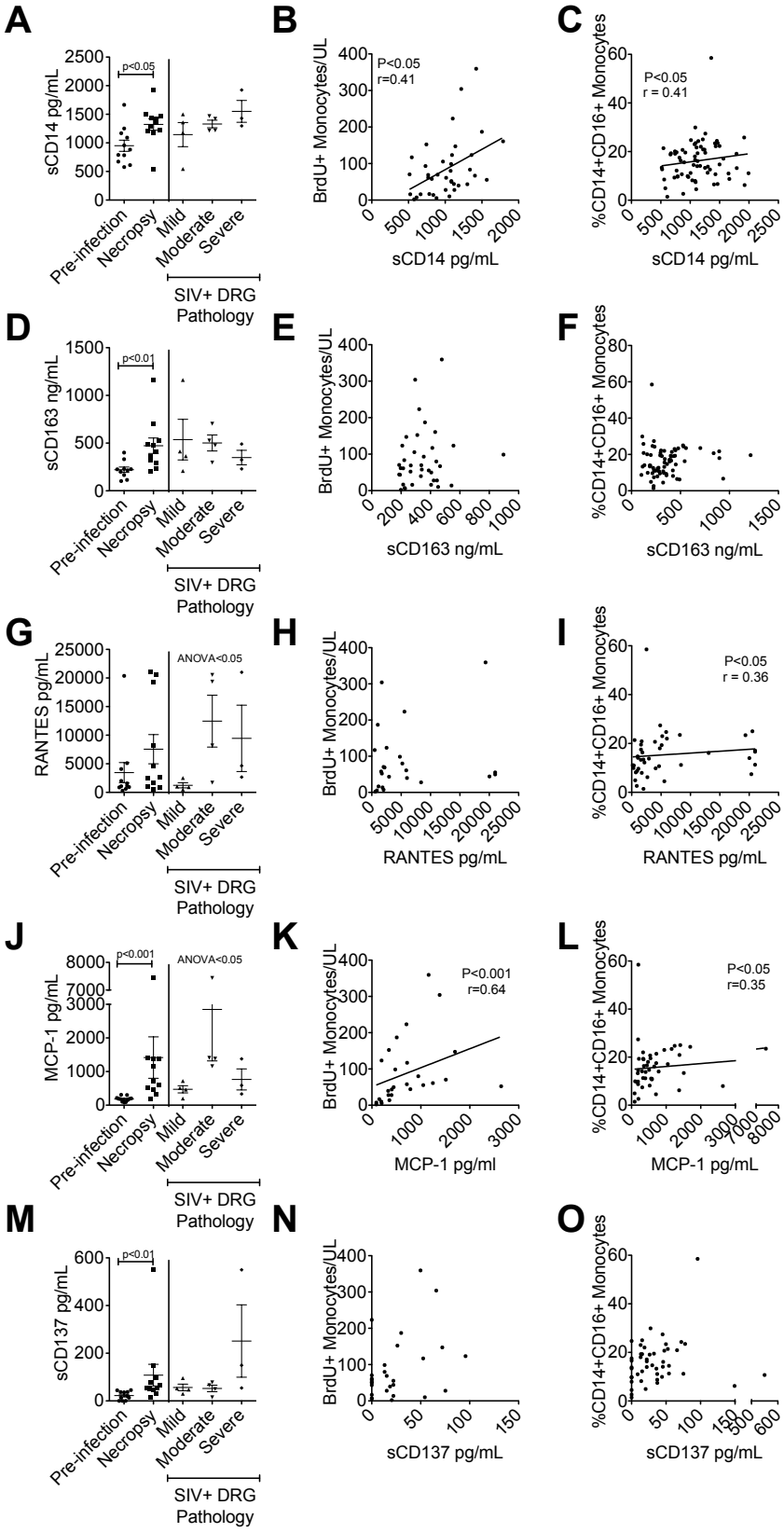
A
sCD14 pg/mL
p<0.05
Pre-infection
Necropsy
Mild
Moderate
Severe
SIV+ DRG Pathology
B
BrdU+ Monocytes/UL
P<0.05
r=0.41
sCD14 pg/mL
C
%CD14+CD16+ Monocytes
P<0.05
r = 0.41
sCD14 pg/mL
D
sCD163 ng/mL
p<0.01
E
BrdU+ Monocytes/UL
sCD163 ng/mL
F
%CD14+CD16+ Monocytes
sCD163 ng/mL
G
RANTES pg/mL
ANOVA<0.05
H
BrdU+ Monocytes/UL
RANTES pg/mL
I
%CD14+CD16+ Monocytes
P<0.05
r = 0.36
RANTES pg/mL
J
MCP-1 pg/mL
p<0.001
ANOVA<0.05
K
BrdU+ Monocytes/UL
P<0.001
r=0.64
MCP-1 pg/ml
L
%CD14+CD16+ Monocytes
P<0.05
r=0.35
MCP-1 pg/mL
M
sCD137 pg/mL
p<0.01
N
BrdU+ Monocytes/UL
sCD137 pg/mL
O
%CD14+CD16+ Monocytes
sCD137 pg/mL

Figure 6.1: Correlates of plasma markers of monocyte activation and monocyte chemoattractants.

sCD14 (A-C), sCD163 (D-F), RANTES (G-I), MCP-1 (J-L), and sCD137 (M-O) were measured in plasma at multiple time points throughout infection. (A, D, G, J, M) Pre-infection and necropsy plasma concentrations were compared using a Wilcoxon matched-pairs signed rank test. Necropsy plasma concentrations were grouped according to lumbar DRG pathology and compared using a Kruskal-Wallis test. The number of BrdU+ monocytes in blood (B, E, H, K, N) and the percent of CD14+CD16+ monocytes of the total monocyte population (C, F, I, L, O) was determined by flow cytometry and correlated to the plasma soluble protein concentrations at matched time points. A Spearman correlation test was used for all correlations. P value of < 0.05 was considered significant.

Figure 6.2

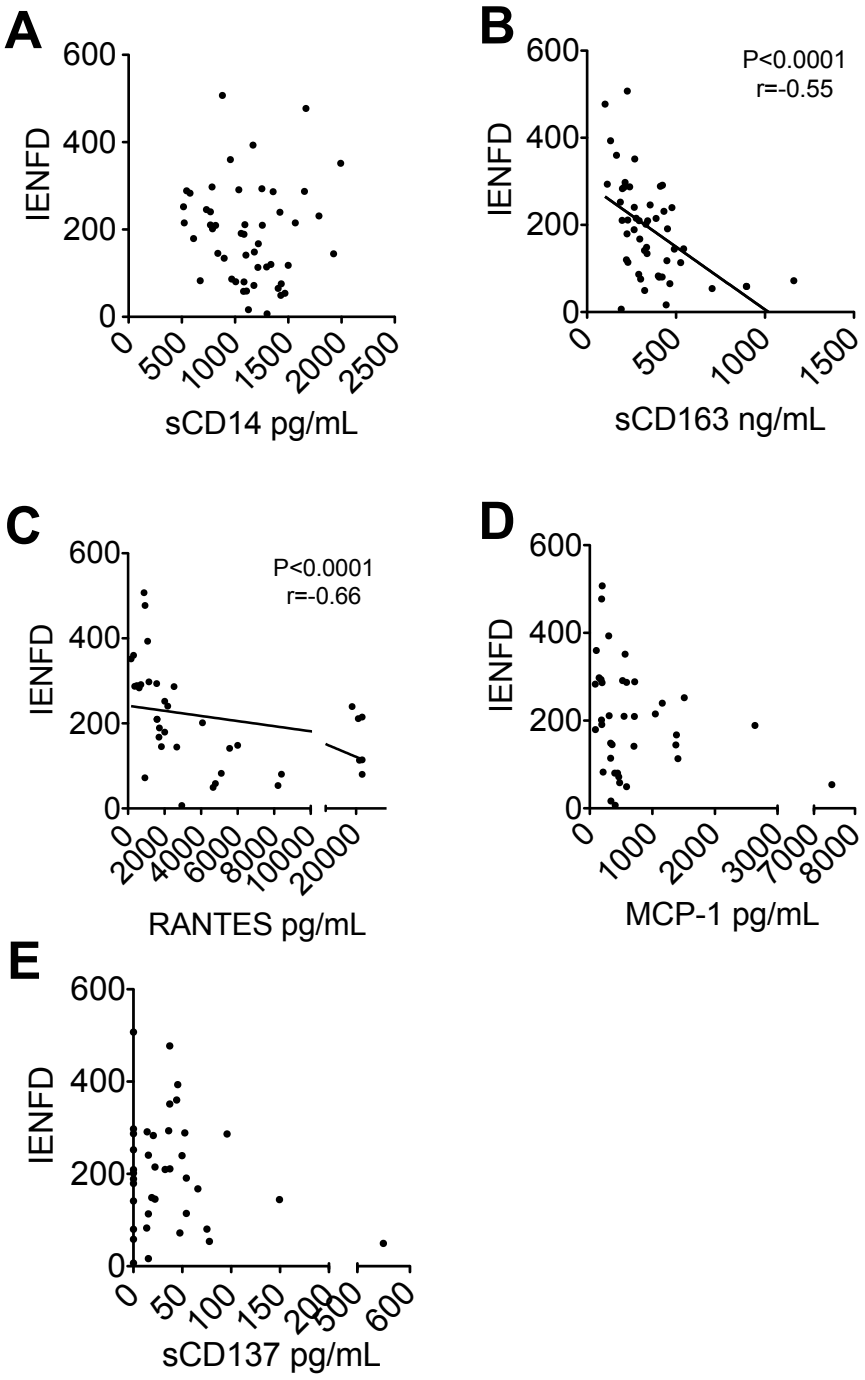
A
IENFD
600
400
200
0
0
500
1000
1500
2000
2500
sCD14 pg/mL
B
P<0.0001
r=-0.55
IENFD
600
400
200
0
0
500
1000
1500
sCD163 ng/mL
C
P<0.0001
r=-0.66
IENFD
600
400
200
0
0
2000
4000
6000
8000
10000
20000
RANTES pg/mL
D
IENFD
600
400
200
0
0
1000
2000
3000
7000
8000
MCP-1 pg/mL
E
IENFD
600
400
200
0
0
50
100
150
200
500
600
sCD137 pg/mL

Figure 6.2: sCD163 and RANTES in plasma negatively correlated to IENFD. IENFD was measured at multiple time points throughout infection in all SIV+ animals. sCD14 (A), sCD163 (B), RANTES (C), MCP-1 (D), and sCD137 (E) in plasma were correlated to IENFD at matched time points using a Spearman correlation test. P value of < 0.05 was considered significant.

Figure 6.3

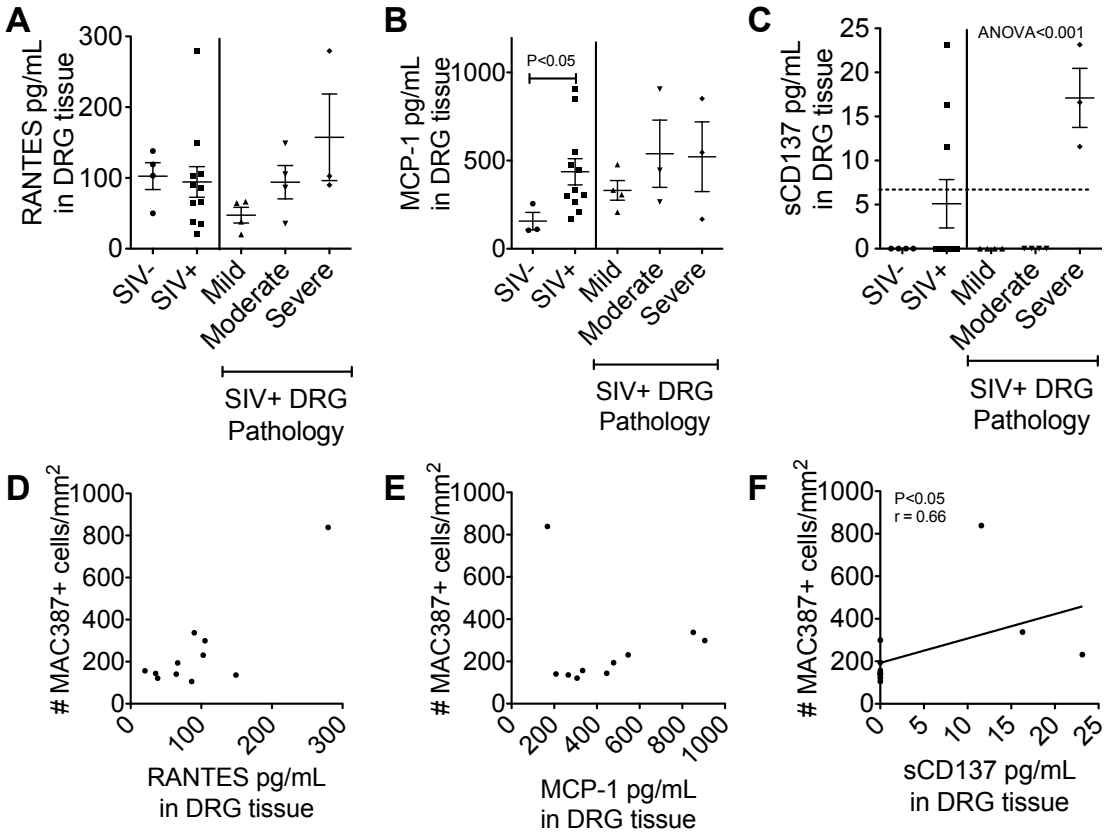
A
RANTES pg/mL in DRG tissue
300
200
100
0
SIV-
SIV+
Mild
Moderate
Severe
SIV+ DRG Pathology
B
MCP-1 pg/mL in DRG tissue
P<0.05
1000
500
0
SIV-
SIV+
Mild
Moderate
Severe
SIV+ DRG Pathology
C
sCD137 pg/mL in DRG tissue
ANOVA<0.001
25
20
15
10
5
0
SIV-
SIV+
Mild
Moderate
Severe
SIV+ DRG Pathology
D
MAC387+ cells/mm2
1000
800
600
400
200
0
0
100
200
300
RANTES pg/mL in DRG tissue
E
MAC387+ cells/mm2
1000
800
600
400
200
0
0
200
400
600
800
1000
MCP-1 pg/mL in DRG tissue
F
MAC387+ cells/mm2
P<0.05
r = 0.66
1000
800
600
400
200
0
0
5
10
15
20
25
sCD137 pg/mL in DRG tissue

Figure 6.3: RANTES, MCP-1, and sCD137 protein levels in DRG tissue.

RANTES (A), MCP-1 (B), and sCD137 (C) were detected by Luminex multiplex assay in DRG tissue lysate. Differences in protein concentrations in SIV- and SIV+ DRG tissue were analyzed using a Mann-Whitney test. SIV+ DRGs were grouped according to tissue pathology. Differences between SIV+ tissue pathology groups were analyzed using a Kruskal-Wallis test, followed by a Dunn's post-test. The amount of RANTES (D), MCP-1 (E), and sCD137 (F) in DRG tissue lysate were correlated to the number of MAC387+ cells/mm^2 determined by immunohistochemistry using a Spearman correlation test. P value of < 0.05 was considered significant.

Figure 6.4

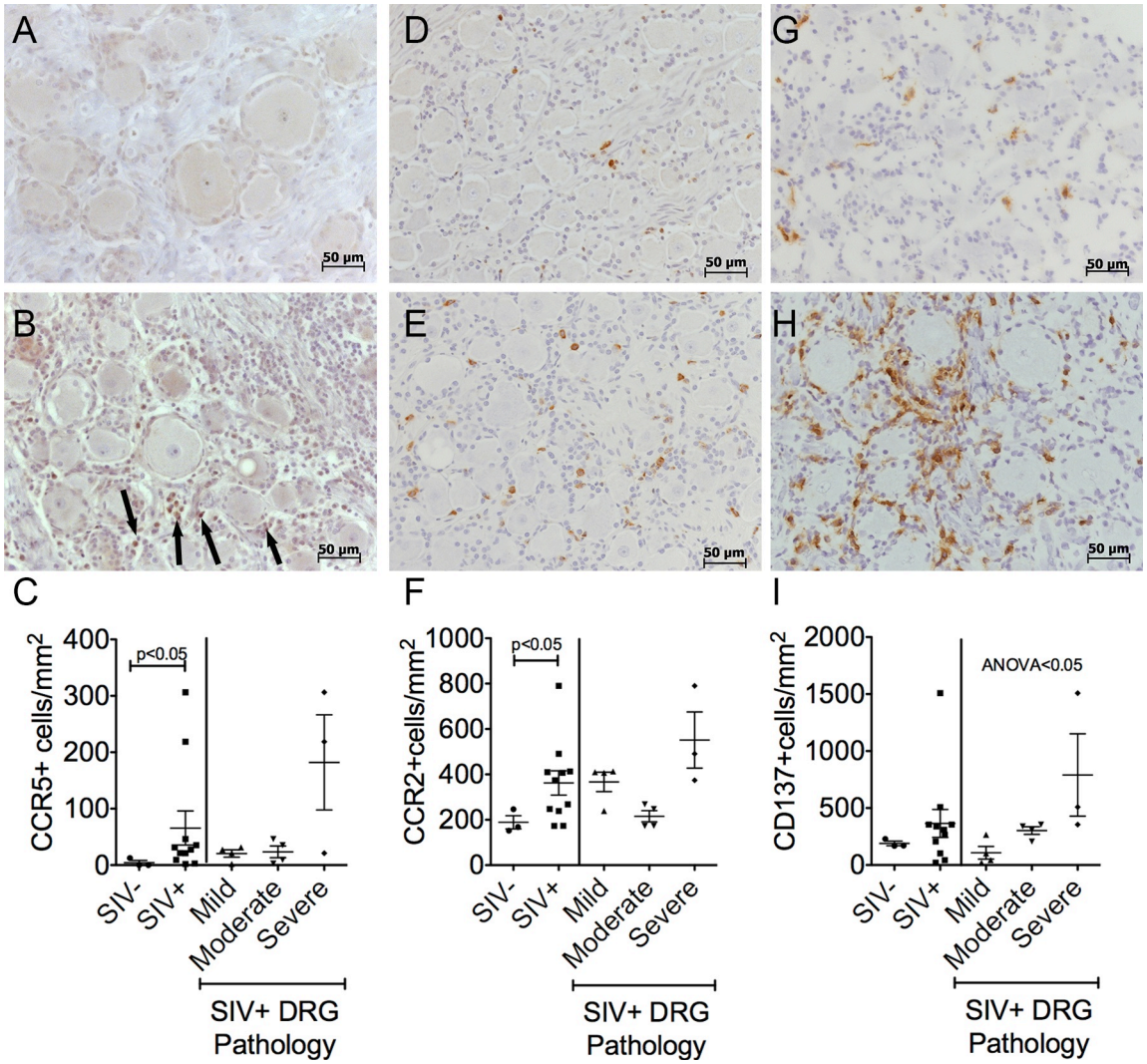
A
D
G
B
E
H
50 µm
C
F
I
CCR5+ cells/mm2
CCR2+cells/mm2
CD137+cells/mm2
p<0.05
ANOVA<0.05
SIV-
SIV+
Mild
Moderate
Severe
SIV+ DRG Pathology

Figure 6.4: CCR5, CCR2, and CD137 expression on DRG satellite cells.

The number of CCR5 (A-C), CCR2 (D-F) and CD137 (G-I) positive satellite cells in DRG tissue was determined by immunohistochemistry in uninfected (A, D, G) and SIV-infected animals. (B, E, H). Arrows show CCR5+ cells in SIV+ DRG tissue. For each animal, eight non-overlapping fields of view at 200x magnification were quantified by manually counting the number of positive cells in the field and dividing by the total area of DRG tissue. The average number of positive cells per mm^2 is plotted for each animal (C, F, I). Analysis in SIV- and SIV+ DRG tissue was determined using a Mann-Whitney test. SIV+ DRGs were grouped according to tissue pathology. Differences between pathology groups determined using a Kruskal-Wallis test, followed by a Dunn's post-test. P value of < 0.05 was considered significant.

REFERNCES:

1. Thacker, M.A., A.K. Clark, T. Bishop, J. Grist, P.K. Yip, L.D. Moon, S.W. Thompson, F. Marchand, and S.B. McMahon, *CCL2 is a key mediator of microglia activation in neuropathic pain states.* European journal of pain, 2009. **13**(3): p. 263-72.
2. Hahn, K., B. Robinson, C. Anderson, W. Li, C.A. Pardo, S. Morgello, D. Simpson, and A. Nath, *Differential effects of HIV infected macrophages on dorsal root ganglia neurons and axons.* Experimental neurology, 2008. **210**(1): p. 30-40.
3. Oh, S.B., P.B. Tran, S.E. Gillard, R.W. Hurley, D.L. Hammond, and R.J. Miller, *Chemokines and glycoprotein120 produce pain hypersensitivity by directly exciting primary nociceptive neurons.* The Journal of neuroscience : the official journal of the Society for Neuroscience, 2001. **21**(14): p. 5027-35.
4. Sun, J.H., B. Yang, D.F. Donnelly, C. Ma, and R.H. LaMotte, *MCP-1 enhances excitability of nociceptive neurons in chronically compressed dorsal root ganglia.* Journal of neurophysiology, 2006. **96**(5): p. 2189-99.
5. Van Steenwinckel, J., C. Auvynet, A. Sapienza, A. Reaux-Le Goazigo, C. Combadiere, and S. Melik Parsadaniantz, *Stromal cell-derived CCL2 drives neuropathic pain states through myeloid cell infiltration in injured nerve.* Brain, behavior, and immunity, 2015. **45**: p. 198-210.
6. Zhang, J., X.Q. Shi, S. Echeverry, J.S. Mogil, Y. De Koninck, and S. Rivest, *Expression of CCR2 in both resident and bone marrow-derived microglia plays a critical role in neuropathic pain.* The Journal of neuroscience : the official journal of the Society for Neuroscience, 2007. **27**(45): p. 12396-406.
7. Zhu, X., S. Cao, M.D. Zhu, J.Q. Liu, J.J. Chen, and Y.J. Gao, *Contribution of chemokine CCL2/CCR2 signaling in the dorsal root ganglion and spinal cord to the maintenance of neuropathic pain in a rat model of lumbar disc herniation.* The journal of pain : official journal of the American Pain Society, 2014. **15**(5): p. 516-26.
8. Biber, K. and E. Boddeke, *Neuronal CC chemokines: the distinct roles of CCL21 and CCL2 in neuropathic pain.* Frontiers in cellular neuroscience, 2014. **8**: p. 210.
9. Gao, Y.J. and R.R. Ji, *Targeting astrocyte signaling for chronic pain.* Neurotherapeutics : the journal of the American Society for Experimental NeuroTherapeutics, 2010. **7**(4): p. 482-93.
10. White, F.A., J. Sun, S.M. Waters, C. Ma, D. Ren, M. Ripsch, J. Steflik, D.N. Cortright, R.H. Lamotte, and R.J. Miller, *Excitatory monocyte chemoattractant protein-1 signaling is up-regulated in sensory neurons after chronic compression of the dorsal root ganglion.* Proceedings of the National Academy of Sciences of the United States of America, 2005. **102**(39): p. 14092-7.

11. Bhangoo, S.K., M.S. Ripsch, D.J. Buchanan, R.J. Miller, and F.A. White, *Increased chemokine signaling in a model of HIV1-associated peripheral neuropathy.* Molecular pain, 2009. **5**: p. 48.
12. Austin, P.J. and G. Moalem-Taylor, *The neuro-immune balance in neuropathic pain: involvement of inflammatory immune cells, immune-like glial cells and cytokines.* Journal of neuroimmunology, 2010. **229**(1-2): p. 26-50.
13. Miller, R.J., H. Jung, S.K. Bhangoo, and F.A. White, *Cytokine and chemokine regulation of sensory neuron function.* Handbook of experimental pharmacology, 2009(194): p. 417-49.
14. Abbadie, C., J.A. Lindia, A.M. Cumiskey, L.B. Peterson, J.S. Mudgett, E.K. Bayne, J.A. DeMartino, D.E. MacIntyre, and M.J. Forrest, *Impaired neuropathic pain responses in mice lacking the chemokine receptor CCR2.* Proceedings of the National Academy of Sciences of the United States of America, 2003. **100**(13): p. 7947-52.
15. Tanaka, T., M. Minami, T. Nakagawa, and M. Satoh, *Enhanced production of monocyte chemoattractant protein-1 in the dorsal root ganglia in a rat model of neuropathic pain: possible involvement in the development of neuropathic pain.* Neuroscience research, 2004. **48**(4): p. 463-9.
16. Vinay, D.S. and B.S. Kwon, *4-1BB signaling beyond T cells.* Cellular & molecular immunology, 2011. **8**(4): p. 281-4.
17. Drenkard, D., F.M. Becke, J. Langstein, T. Spruss, L.A. Kunz-Schughart, T.E. Tan, Y.C. Lim, and H. Schwarz, *CD137 is expressed on blood vessel walls at sites of inflammation and enhances monocyte migratory activity.* FASEB journal : official publication of the Federation of American Societies for Experimental Biology, 2007. **21**(2): p. 456-63.
18. Kienzle, G. and J. von Kempis, *CD137 (ILA/4-1BB), expressed by primary human monocytes, induces monocyte activation and apoptosis of B lymphocytes.* International immunology, 2000. **12**(1): p. 73-82.
19. Quek, B.Z., Y.C. Lim, J.H. Lin, T.E. Tan, J. Chan, A. Biswas, and H. Schwarz, *CD137 enhances monocyte-ICAM-1 interactions in an E-selectin-dependent manner under flow conditions.* Molecular immunology, 2010. **47**(9): p. 1839-47.
20. Tang, Q., D. Jiang, S. Alonso, A. Pant, J.M. Martinez Gomez, D.M. Kemeny, L. Chen, and H. Schwarz, *CD137 ligand signaling enhances myelopoiesis during infections.* European journal of immunology, 2013. **43**(6): p. 1555-67.
21. Tang, Q., D. Jiang, Z. Harfuddin, K. Cheng, M.C. Moh, and H. Schwarz, *Regulation of myelopoiesis by CD137L signaling.* International reviews of immunology, 2014. **33**(6): p. 454-69.
22. Dongming, L., L. Zuxun, X. Liangjie, W. Biao, and Y. Ping, *Enhanced levels of soluble and membrane-bound CD137 levels in patients with acute coronary syndromes.* Clinica chimica acta; international journal of clinical chemistry, 2010. **411**(5-6): p. 406-10.
23. Hentschel, N., M. Krusch, P.A. Kiener, H.J. Kolb, H.R. Salih, and H.M. Schmetzer, *Serum levels of sCD137 (4-1BB) ligand are prognostic factors*

for progression in acute myeloid leukemia but not in non-Hodgkin's lymphoma. European journal of haematology, 2006. **77**(2): p. 91-101.
24. Michel, J., J. Langstein, F. Hofstadter, and H. Schwarz, *A soluble form of CD137 (ILA/4-1BB), a member of the TNF receptor family, is released by activated lymphocytes and is detectable in sera of patients with rheumatoid arthritis.* European journal of immunology, 1998. **28**(1): p. 290-5.
25. Burdo, T.H. and A.D. Miller, *Animal models of HIV peripheral neuropathy.* Future virology, 2014. **9**(5): p. 465-474.
26. Burdo, T.H., K. Orzechowski, H.L. Knight, A.D. Miller, and K. Williams, *Dorsal root ganglia damage in SIV-infected rhesus macaques: an animal model of HIV-induced sensory neuropathy.* The American journal of pathology, 2012. **180**(4): p. 1362-9.
27. Westmoreland, S.V., E. Halpern, and A.A. Lackner, *Simian immunodeficiency virus encephalitis in rhesus macaques is associated with rapid disease progression.* Journal of neurovirology, 1998. **4**(3): p. 260-8.
28. Lakritz, J.R., A. Bodair, N. Shah, R. O'Donnell, M.J. Polydefkis, A.D. Miller, and T.H. Burdo, *Monocyte Traffic, Dorsal Root Ganglion Histopathology, and Loss of Intraepidermal Nerve Fiber Density in SIV Peripheral Neuropathy.* The American journal of pathology, 2015. **185**(7): p. 1912-23.
29. Laast, V.A., C.A. Pardo, P.M. Tarwater, S.E. Queen, T.A. Reinhart, M. Ghosh, R.J. Adams, M.C. Zink, and J.L. Mankowski, *Pathogenesis of simian immunodeficiency virus-induced alterations in macaque trigeminal ganglia.* Journal of neuropathology and experimental neurology, 2007. **66**(1): p. 26-34.
30. Liu, Y., J. Billiet, G.J. Ebenezer, B. Pan, P. Hauer, J. Wei, and M. Polydefkis, *Factors influencing sweat gland innervation in diabetes.* Neurology, 2015. **84**(16): p. 1652-9.
31. Walker, J.A., M.L. Sulciner, K.D. Nowicki, A.D. Miller, T.H. Burdo, and K.C. Williams, *Elevated numbers of CD163+ macrophages in hearts of simian immunodeficiency virus-infected monkeys correlate with cardiac pathology and fibrosis.* AIDS research and human retroviruses, 2014. **30**(7): p. 685-94.
32. Burdo, T.H., C. Soulas, K. Orzechowski, J. Button, A. Krishnan, C. Sugimoto, X. Alvarez, M.J. Kuroda, and K.C. Williams, *Increased monocyte turnover from bone marrow correlates with severity of SIV encephalitis and CD163 levels in plasma.* PLoS pathogens, 2010. **6**(4): p. e1000842.
33. Soulas, C., C. Conerly, W.K. Kim, T.H. Burdo, X. Alvarez, A.A. Lackner, and K.C. Williams, *Recently infiltrating MAC387(+) monocytes/macrophages a third macrophage population involved in SIV and HIV encephalitic lesion formation.* The American journal of pathology, 2011. **178**(5): p. 2121-35.

34. Choi, J.W., H.W. Lee, G.S. Roh, H.H. Kim, and K. Kwack, *CD137 induces adhesion and cytokine production in human monocytic THP-1 cells.* Experimental & molecular medicine, 2005. **37**(2): p. 78-85.
35. Williams, D.W., D. Byrd, L.H. Rubin, K. Anastos, S. Morgello, and J.W. Berman, *CCR2 on CD14(+)CD16(+) monocytes is a biomarker of HIV-associated neurocognitive disorders.* Neurology(R) neuroimmunology & neuroinflammation, 2014. **1**(3): p. e36.
36. Burdo, T.H., M.R. Lentz, P. Autissier, A. Krishnan, E. Halpern, S. Letendre, E.S. Rosenberg, R.J. Ellis, and K.C. Williams, *Soluble CD163 made by monocyte/macrophages is a novel marker of HIV activity in early and chronic infection prior to and after anti-retroviral therapy.* The Journal of infectious diseases, 2011. **204**(1): p. 154-63.
37. Kanda, T., *Biology of the blood-nerve barrier and its alteration in immune mediated neuropathies.* Journal of neurology, neurosurgery, and psychiatry, 2013. **84**(2): p. 208-12.
38. Moss, P.J., W. Huang, J. Dawes, K. Okuse, S.B. McMahon, and A.S. Rice, *Macrophage-sensory neuronal interaction in HIV-1 gp120-induced neurotoxicitydouble dagger.* British journal of anaesthesia, 2015. **114**(3): p. 499-508.
39. Ramesh, G., A.G. MacLean, and M.T. Philipp, *Cytokines and chemokines at the crossroads of neuroinflammation, neurodegeneration, and neuropathic pain.* Mediators of inflammation, 2013. **2013**: p. 480739.
40. Shive, C.L., W. Jiang, D.D. Anthony, and M.M. Lederman, *Soluble CD14 is a nonspecific marker of monocyte activation.* AIDS, 2015. **29**(10): p. 1263-5.
41. Weaver, L.K., K.A. Hintz-Goldstein, P.A. Pioli, K. Wardwell, N. Qureshi, S.N. Vogel, and P.M. Guyre, *Pivotal advance: activation of cell surface Toll-like receptors causes shedding of the hemoglobin scavenger receptor CD163.* Journal of leukocyte biology, 2006. **80**(1): p. 26-35.
42. Ascierto, P.A., E. Simeone, M. Sznol, Y.X. Fu, and I. Melero, *Clinical experiences with anti-CD137 and anti-PD1 therapeutic antibodies.* Seminars in oncology, 2010. **37**(5): p. 508-16.

CHAPTER VII

Title*:* Conclusion

Discussion

Great strides have been made in the treatment of HIV infection since the start of the worldwide epidemic over 30 years ago. Patient mortality has greatly decreased due to advances in antiretroviral therapy (ART) [1]. However, non-AIDS related comorbidities in the HIV+ population remain problematic. Diseases and conditions that typically appear with advanced age appear at a younger age in HIV+ individuals due to accelerated aging of the immune system [2-5]. Understanding the mechanism underlying advanced aging in HIV+ individuals with controlled viral load is key to further closing the gap between the life span of the HIV+ and the general populations.

Neurologic complications were identified during the early years of the HIV epidemic. Patients had severe neuropathic pain, as well as neurocognitive impairments and encephalitis [6, 7]. While the severity of central nervous system (CNS) complications has decreased (although milder forms still remain prevalent) [8, 9], peripheral neuropathy (PN) continues to be the most frequent neurologic complication of HIV infection [10]. Rates of antiretroviral neurotoxicity (ATN) have decreased because of knowledge of neurotoxicity of d-drugs, but distal sensory polyneuropathy (DSP) persists in patients despite reductions in viral loads and increased CD4 counts [11]. The greatest risk factor for HIV-PN is increased age [10, 11]. Therefore, with an aging HIV population, it is expected that the prevalence of HIV-PN will only increase.

This thesis sought to understand the immunologic mechanisms associated with HIV-PN. The central hypothesis of this thesis was that monocyte traffic and

activation drives pathologies associated with HIV-PN, including damage to the dorsal root ganglia (DRG) and a loss of intraepidermal nerve fiber density (IENFD) (Figure 7.1). To test this hypothesis we defined pathologies of the peripheral nervous system (PNS) in our model, identified immune cell types and phenotypes associated with tissue damage, and identified signaling proteins associated with damage to be used as biomarkers and future drug targets. We also directly examined if cell traffic to tissues and monocyte/macrophage activation were necessary for SIV-PN using pharmacological blockade of specific pathways.

Where does damage happen first?

Multiple regions of the PNS are affected during HIV-PN pathogenesis. Sensory information travels from peripheral nerves to the DRG and then to the spinal cord. Neurologic damage in any of these regions could potentially result in neuropathic pain. When we first began these studies, it was unknown where damage occurs first, or even if multiple PNS regions are linked in severity due to the inability to repeatedly sample different PNS regions in humans. Post-mortem analysis on the human DRG samples revealed a loss of neurons, formation of Nageotte nodules, and an increase in activated macrophages and satellite cells in the DRG [12-14]. Other studies have found that measuring IENFD in distal skin strongly correlates with pain and thus is a reliable diagnostic tool for HIV-PN [15].

Using an animal model, we were able to study the order of events in the pathogenesis of SIV-PN by repeatedly sampling the footpad in longitudinal

analysis and time-sacrificing animals at 21 days post-infection (DPI) to determine when damage to the DRG occurs. We were also able to use bromodeoxyuridine (BrdU) dosing time points to determine when monocytes traffic to the DRG.

In Chapter 2, we found that a loss of IENFD occurs during early infection (before 21 DPI) [16]. This is consistent with findings that Laast, et al found using a different primate model of SIV-PN. They found reduced IENFD at 6 and 8 weeks post-infection (although not significant until 8 weeks post-infection, probably due to cross-sectional sampling instead of longitudinal sampling). IENFD was not measured earlier than 6 weeks post-infection in this study [17]. They also observed that the decline in IENFD occurred before the decline in C-fiber nerve conduction velocity. They hypothesized that this was because longer fibers are affected the most by SIV infection [17].

Laast and colleagues, and our studies found that DRG neuronal density declines during late infection. We found a decrease in neuronal density at terminal disease (Chapter 2), while Laast, et al observed a decrease in DRG neurons at 12 weeks post-infection, and no significant decrease at 6 weeks post-infection. Our studies demonstrated that only small-diameter neurons are lost with SIV infection. Small-diameter DRG neurons give rise to unmyelinated C-fibers [18]. Thus, long, unmyelinated C-fibers in distal tissues are probably the most vulnerable to viral protein and cytokine-induced neurotoxity during early infection. The loss of C-fibers in the epidermis may relay signals to DRG neurons associated with these fibers causing small diameter neuronal loss (Figure 7.1).

This thesis was also able to evaluate the role of cell traffic to the DRG. Natalizumab, an anti-VLA4 (very late antigen-4) antibody, is used to block traffic of leukocytes to tissues. It is used as a therapy for multiple sclerosis and Crohn's disease by blocking the traffic of T cells and monocytes to the brain and the gut, respectively [19, 20]. In Chapter 4, we used natalizumab, in a proof-of-concept manner to directly investigate the impact of bone marrow-derived monocytes trafficking to the DRG on the development of tissue pathology [21]. Natalizumab treatment improved overall DRG pathologies in both early and late treated groups. Blocking cell traffic early (at the day of infection), completely prevented formation of Nageotte nodules at day 22. However, it is not known if these animals would have gone on to develop Nageotte nodules if they were allowed to continue to progress to AIDS. We predict that severe lesions in the DRG would not form if animals were treated with natalizumab at the day of infection, and treatment continued until sacrifice with AIDS. Pathology in the DRG during early infection is mild to moderate, compared to moderate to severe pathology seen with AIDS. Blocking cell traffic beginning at 28 DPI, did not completely prevent formation of Nageotte nodules, suggesting that damage to the DRG may be initiated during early infection (before loss of neurons (Chapter 2)), but disease progression is not completely halted by stopping cell traffic (Figure 7.1). We have also observed that BrdU+ monocytes traffic in the largest numbers during late infection (unpublished data).

Thus, we hypothesize that a loss of IENFD is the initiating event in SIV-PN disease pathogenesis, likely due to viral protein toxicity or from an early

inflammatory response that is typical of acute infection. Because these fibers are unmyelinated, they may be more sensitive to neurotoxic products in plasma during acute infection. Monocytes likely traffic to injured axons and the DRG in response to stress signals and chemokines released from Schwann cells, activated resident macrophages, or the injured neurons. An influx of inflammatory monocytes/macrophages to the DRG likely perpetuates inflammation and neuronal damage. Chronic immune activation and an inability for inflammation to resolve is a hallmark of HIV infection [22]. Our natalizumab study suggested that monocyte traffic and macrophage activation is not the initiating factor driving tissue histopathology, but it does seem to exacerbate and perpetuate ongoing damage (Figure 7.1).

What role do M1 and M2 macrophages play in SIV-PN pathogenesis?

Macrophages have a diverse array of functions such as pathogen sensing, tissue remodeling, and development [23]. In 2000, an M1-M2 macrophage polarization paradigm was proposed [24]. M1 macrophages are associated with antigen presentation and pathogen killing, along with producing pro-inflammatory cytokines that promote a Th1 response. In contrast M2 macrophages are highly phagocytic, produce anti-inflammatory cytokines and promote a Th2 response. Typical wound healing consists of an influx of M1 macrophages during acute inflammation. M2 macrophages then enter the injury site to resolve inflammation and remodel the tissue. However, in states of chronic inflammation, this process is disrupted [25]. Recently, evidence has emerged that M1 and M2 polarization

states represent two extremes of a continuous spectrum of transcriptional profiles [26]. Additionally, polarized macrophages are not terminally differentiated, but can be re-programmed by the cytokine milieu and other local environmental factors [27].

Increased numbers of macrophages and elevated macrophage activation have previously been observed in HIV+ and SIV+ DRG tissues [17, 28]. However, no studies had previously investigated the source of and phenotypes of macrophages in the DRG. In chapter 3, we used three different macrophage markers to identify different populations of macrophages. CD68 is expressed on mature tissue macrophages. CD163 is expressed on M2-polarized macrophages, while MAC387 is expressed on M1 macrophages. However, these macrophage markers are not exclusive. There is significant overlap between CD68 and CD163 in the CNS, which we have also observed in the PNS (data not shown) [29]. MAC387 is not coexpressed with CD163 or CD68. MAC387 recognizes recently infiltrated monocytes/macrophages [29, 30]. CD163 is a typical marker of M2 polarized macrophages [31]. Thus, in our studies we used CD163 and MAC387 to identify M2 and M1 macrophages, respectively. All three populations were significantly increased in the DRG of infected animals, compared to uninfected. Interestingly, the number of M1-like MAC387+ macrophages correlated to the severity of tissue pathology, while M2-like CD163+ macrophages were present in the same amount across different pathology severity groups. We would expect M1 macrophages to contribute to severe pathology due to their pro-inflammatory nature. Others have found that there is

an increase in M1 macrophages during acute infection and M2 macrophages dominate during chronic infection [32]. Because we used a rapid progression model, we may not have captured the phenotypic shift that occurs during late stages of disease in non-CD8 depleted animals or in HIV disease progression.

We found that a majority of BrdU+ cells are MAC387+, meaning that M1-macrophages in the DRG are bone-marrow derived and have trafficked to tissues [16]. Thus, when we blocked cell traffic with natalizumab treatment in Chapter 4, there was a decrease in MAC387+ cells in late-treated animals. There was no significant decrease in CD163+ M2-like macrophages in late-treated animals, suggesting that resident macrophages (that have not recently trafficked to the tissue) can become M2-activated [21]. However, there was a significant decrease in CD68+ macrophages when cell traffic was blocked. This may be because MAC387+ cells that traffic into tissues, eventually mature into CD68+ macrophages and no longer express MAC387. This is evidenced by a small percentage of CD68+BrdU+ macrophages that we observed in Chapter 3 [16]. Macrophage polarization and activation states are dynamic, and thus phenotypic shifts are likely occurring throughout infection [26].

In chapter 5, we reduced monocyte/macrophage activation with methylglyoxal-bis-guanylhydrazone (MGBG) oral administration. MGBG is a polyamine synthesis-inhibitor and depletes the intracellular pool of polyamines which are needed for M2-polarization [33, 34]. MGBG blocks S-adenosyl methionine decarboxlyase (SAMDC), an enzyme that converts S-adenosyl methionine (SAM) to dcSAM, which then feeds into the synthesis polyamines

(spermidine and spermine). Upstream in this synthesis pathway, Arginase-1 (Arg-1) is needed to convert arginine to ornithine. Expression of Arg-1 is a hallmark of M2 activation, along with production of polyamines. Thus, when MGBG interrupts this pathway and depletes polyamines, M2 polarization is reduced [34]. In our study, MGBG (given daily on starting at 21 DPI) treatment reduced the number of M2 macrophages in the DRG, but not M1 macrophages. Treatment also reduced CD16 expression on blood monocytes (data not shown), which is significant because CD16+ monocytes highly express CD163, while CD16- monocytes do not. Interestingly, a reduction in M2 polarized macrophages resulted in improved DRG pathology, but a worsened outcome for a recovery of IENFD. MGBG-treated animals continued to have a decrease in IENFD after drug administration on 21 DPI, while untreated animals had no significant change in IENFD from 21 DPI to necropsy. This supports what others have reported that M2 macrophages are needed for peripheral nerve regeneration [35, 36].

Based on the outcomes of these studies, we propose that M1-macrophages secrete inflammatory cytokines and chemokines that assist in neuronal loss, both in the skin and in the DRG. In Chapter 6, we found increased MCP-1/CCL2 and CCR2+ macrophages in the DRG of SIV+ animals, both of which are associated with an M1 phenotype [37]. In our rapid progression model, there is a failure to resolve M1 inflammation. In non-depleted animals, or during chronic HIV infection, a switch to M2 polarization may halt severe M1-induced damage. However, based on the progressive nature of HIV-PN in HIV+ patients on cART, we hypothesize that proper neural regeneration fails to take place in

the context of HIV infection [38]. Continued M1 activation due to microbial translocation, viral blipping, or co-infections most likely prevents full peripheral nerve regeneration in the context of chronic HIV infection [32].

Why do monocytes traffic to the DRG?

Increased presence of macrophages in the DRG was one of the earliest observations of the DRG in patients with HIV-PN [14]. Monocytes traffic to tissues for a multitude of reasons, which range from routine immune surveillance to tissue damage or presence of pathogens [39]. Monocyte traffic and macrophage accumulation in tissues is linked to CNS and cardiac pathologies during HIV infection [40]. In addition, increased monocyte egress from the bone marrow is correlated with a rapid progression to AIDS [41]. We therefore, hypothesized that BrdU+ monocyte traffic plays a role in SIV-PN pathogenesis (Figure 7.1).

In Chapter 3, we found that the number of MAC387+BrdU+ cells in the DRG correlated to the severity of pathology. Additionally, the number of BrdU+ cells in the DRG also correlated to a greater loss of IENFD. Interestingly, no other cell population in the DRG examined in this study was correlated to a loss of IENFD. This finding demonstrated the important role of ongoing monocyte traffic in development of pathology both in the DRG and in distal peripheral nerves (Figure 7.1).

This finding led us to ask what was causing an increase in monocyte traffic to the DRG. Monocytes could be recruited due to pathogen (e.g., SIV)

presence, to phagocytose dying neurons, or due to increased cytokines and chemokines secreted from activated, resident satellite cells or the neurons themselves. The amount of virus in the DRG did not correlate to pathology nor to monocyte recruitment. In addition, HIV-PN occurs in patients with undetectable viral loads [10]. Thus, we hypothesized that monocyte recruitment occurs in response to dying neurons and/or increased cytokines and chemokines in the region (Figure 7.1). Understanding the chemotactic signals that are responsible for monocyte traffic are important to both understand the cause of the pathology, and to identify pathways for future pharmacological targeting.

In Chapter 6 we performed a multiplex screen to identify cytokines and chemokines that are upregulated in infected DRG tissues. We found that MCP-1 was significantly upregulated in the DRG of infected animals. Injured neurons have previously been shown to secrete MCP-1 [42-44]. MCP-1 is a potent monocyte chemoattractant and in plasma correlated to a greater egress of monocytes from the bone marrow and high number of activated CD14+CD16+ circulating monocytes. The ligand of MCP-1, CCR2, is expressed on M1 polarized macrophages. CCR2+ macrophages were also present in greater numbers in DRG of SIV+ animals. Thus, CCR2 expression and MCP-1 gradient likely plays a role in M1 macrophage recruitment to the DRG.

How to target monocyte activation and traffic to prevent and treat HIV-PN?

There is currently no FDA-approved treatment for HIV-PN. Attempts to treat HIV-PN with “off label” medications such as analgesics and treatments for

other types of chronic pain prove to be ineffective or have only a transient relief of symptoms [45]. Failure to find an effective treatment is in part due to a lack of understanding of the underlying mechanism of HIV-PN. In this thesis, we used two different drugs to target monocyte activation and traffic to attempt to understand pathogenesis and reduce pathologies associated with SIV-PN.

In Chapter 4, we used natalizumab to directly test the effect of monocyte traffic. We demonstrated that continuous monocyte traffic exacerbates ongoing pathology, but mild pathology is still present after traffic is stopped. Long-term use of natalizumab is not recommended in HIV patients due to risk of developing progressive multifocal leukoencephalopathy (PML) caused by JC virus and other opportunistic infections [46]. Treatment with natalizumab has been shown to be safe for long durations when there is no risk of PML [46]. Even short-term usage may be beneficial to slow inflammation-induced damage to the PNS. It is not known if damage would continue to progress after stopping treatment with natalizumab. In addition, natalizumab does not specifically target monocytes or differentiate between M1 and M2 polarization. Thus, beneficial effects from M2 polarized macrophages on peripheral nerve regeneration would be thwarted by use of natalizumab.

In Chapter 5, we used MGBG to specifically target myeloid cells. MGBG reduced BrdU+ cell traffic and reduced the number of CD163+ and CD68+ cells in the DRG. Because MGBG is a polyamine synthesis inhibitor, it reduced M2 activation. MGBG slowed the progression to AIDS and improved DRG pathology scores. However, reducing M2 polarization did not allow for regeneration of nerve

fibers in the footpad. Our study with MGBG demonstrates both the beneficial and potentially disadvantageous effects targeting monocyte/macrophage activation. While we have linked monocyte and macrophage over-activation to SIV-PN, these cell types still play a vital role in tissue remodeling and homeostasis. Thus, one must be cautious when using immunologic agents that target myeloid cells.

Combining therapeutics that target monocyte activation and ART will likely show a greater effect in our model than simply reducing monocyte activation and traffic alone. Our natalizumab and MGBG drug studies were done in the absence of ART. It is likely that even greater therapeutic benefit would be observed by reducing viral loads with ART and targeting monocyte activation and traffic. Maraviroc is a CCR5 viral entry inhibitor. Because CCR5 serves as both a viral entry receptor and has immune functions, blocking CCR5 has been shown to both block viral entry and reduce monocyte activation [47]. Maraviroc has been shown to reduce monocyte chemotaxis in vitro [48] and improve cardiac and neurologic outcomes in vivo [49, 50]. Macrophages serve as a viral reservoir that is difficult to target with conventional ART drugs [51]. Cenicriviroc (CVC), another CCR5 entry inhibitor, which is currently in clinical trials, also blocks CCR2 [52, 53]. Dual targeting of CCR2 and CCR5 may be a successful strategy to target monocytes and macrophages and block viral entry simultaneously. In Chapter 6, we highlighted the roles of CCR2 and CCR5 and their ligands in SIV-PN. Treatment with CVC in conjunction with other ART drugs may be of benefit to patients who suffer from HIV-PN and are at risk of other monocyte activation induced comorbidities, such as neurocognitive disorders and atherosclerosis.

Summary

In conclusion, this thesis elucidated potential mechanisms underlying HIV and SIV-PN (Figure 7.1). We described and investigated the cause of damage to the DRG and a loss of nerve fibers in the footpad of SIV-infected monkeys. We found that monocyte traffic to the DRG was linked to both a loss of IENFD and DRG pathology. We investigated the molecular signals associated with monocyte traffic to the DRG and systemic monocyte activation and highlighted the potential roles of MCP-1, RANTES, sCD137, sCD14, and sCD163 in monocyte traffic and activation, and PNS pathologies. We found that when cell traffic was blocked with natalizumab treatment, DRG pathology was improved. In addition, reducing myeloid cell activation with MGBG also improved DRG pathology. Future studies should aim to identify drugs to be used in conjunction with ART that specifically target inflammatory monocytes and macrophages.

Figure 7.1

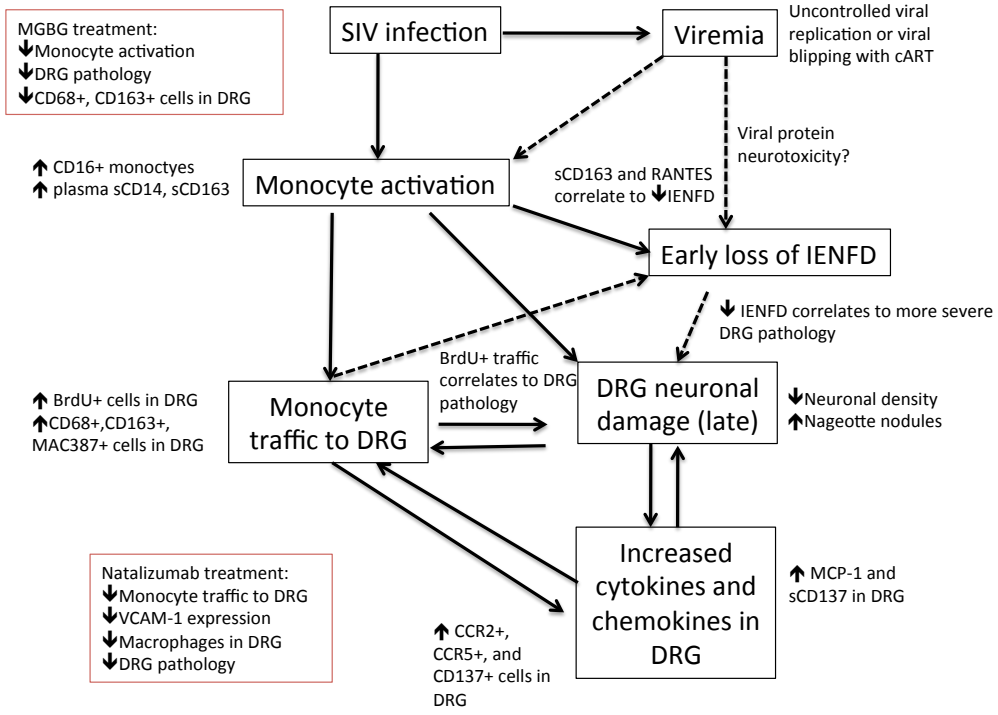
MGBG treatment:
↓Monocyte activation
↓DRG pathology
↓CD68+, CD163+ cells in DRG
SIV infection
Viremia
Uncontrolled viral replication or viral blipping with cART
↑ CD16+ monoctyes
↑ plasma sCD14, sCD163
Monocyte activation
sCD163 and RANTES correlate to ↓IENFD
Viral protein neurotoxicity?
Early loss of IENFD
↓ IENFD correlates to more severe DRG pathology
BrdU+ traffic correlates to DRG pathology
↑ BrdU+ cells in DRG
↑CD68+,CD163+, MAC387+ cells in DRG
Monocyte traffic to DRG
DRG neuronal damage (late)
↓Neuronal density
↑Nageotte nodules
Natalizumab treatment:
↓Monocyte traffic to DRG
↓VCAM-1 expression
↓Macrophages in DRG
↓DRG pathology
Increased cytokines and chemokines in DRG
↑ MCP-1 and sCD137 in DRG
↑ CCR2+, CCR5+, and CD137+ cells in DRG

Figure 7.1: Pathways involved in SIV-PN pathogenesis

The initial insult to the PNS is unknown. There is an early loss of IENFD, followed by damage to the DRG during late infection. Both a loss of IENFD and DRG neuronal damage is associated monocyte activation that occurs following SIV infection, either with or without viremia. Monocyte traffic in the DRG is associated with DRG pathology and a loss of IENFD. Inflammatory monocytes that traffic to the DRG release cytokines and chemokines which further damage tissue and recruit additional monocytes to the tissue. Reducing monocyte activation with MGBG and blocking cell traffic with natalizumab reduces DRG pathology and cell traffic, but does not completely resolve PNS damage. Thus monocyte traffic and activation perpetuate ongoing PNS damage.

REFERENCES:

1. *Life expectancy of individuals on combination antiretroviral therapy in high-income countries: a collaborative analysis of 14 cohort studies.* Lancet, 2008. **372**(9635): p. 293-9.
2. Effros, R.B., C.V. Fletcher, K. Gebo, J.B. Halter, W.R. Hazzard, F.M. Horne, R.E. Huebner, E.N. Janoff, A.C. Justice, D. Kuritzkes, S.G. Nayfield, S.F. Plaeger, K.E. Schmader, J.R. Ashworth, C. Campanelli, C.P. Clayton, B. Rada, N.F. Woolard, and K.P. High, *Aging and infectious diseases: workshop on HIV infection and aging: what is known and future research directions.* Clinical infectious diseases : an official publication of the Infectious Diseases Society of America, 2008. **47**(4): p. 542-53.
3. Warriner, A.H., G.A. Burkholder, and E.T. Overton, *HIV-related metabolic comorbidities in the current ART era.* Infectious disease clinics of North America, 2014. **28**(3): p. 457-76.
4. Nasi, M., S. De Biasi, L. Gibellini, E. Bianchini, S. Pecorini, V. Bacca, G. Guaraldi, C. Mussini, M. Pinti, and A. Cossarizza, *Aging and inflammation in patients with HIV infection.* Clinical and experimental immunology, 2016.
5. Marin, B., R. Thiebaut, H.C. Bucher, V. Rondeau, D. Costagliola, M. Dorrucci, O. Hamouda, M. Prins, S. Walker, K. Porter, C. Sabin, and G. Chene, *Non-AIDS-defining deaths and immunodeficiency in the era of combination antiretroviral therapy.* AIDS, 2009. **23**(13): p. 1743-53.
6. Parry, G.J., *Peripheral neuropathies associated with human immunodeficiency virus infection.* Annals of neurology, 1988. **23 Suppl**: p. S49-53.
7. Snider, W.D., D.M. Simpson, S. Nielsen, J.W. Gold, C.E. Metroka, and J.B. Posner, *Neurological complications of acquired immune deficiency syndrome: analysis of 50 patients.* Annals of neurology, 1983. **14**(4): p. 403-18.
8. Brew, B.J., S.M. Crowe, A. Landay, L.A. Cysique, and G. Guillemin, *Neurodegeneration and ageing in the HAART era.* Journal of neuroimmune pharmacology : the official journal of the Society on NeuroImmune Pharmacology, 2009. **4**(2): p. 163-74.
9. Ellis, R., D. Langford, and E. Masliah, *HIV and antiretroviral therapy in the brain: neuronal injury and repair.* Nature reviews. Neuroscience, 2007. **8**(1): p. 33-44.
10. Ellis, R.J., D. Rosario, D.B. Clifford, J.C. McArthur, D. Simpson, T. Alexander, B.B. Gelman, F. Vaida, A. Collier, C.M. Marra, B. Ances, J.H. Atkinson, R.H. Dworkin, S. Morgello, and I. Grant, *Continued high prevalence and adverse clinical impact of human immunodeficiency virus-associated sensory neuropathy in the era of combination antiretroviral therapy: the CHARTER Study.* Archives of neurology, 2010. **67**(5): p. 552-8.

11. Evans, S.R., R.J. Ellis, H. Chen, T.M. Yeh, A.J. Lee, G. Schifitto, K. Wu, R.J. Bosch, J.C. McArthur, D.M. Simpson, and D.B. Clifford, *Peripheral neuropathy in HIV: prevalence and risk factors.* AIDS, 2011. **25**(7): p. 919-28.
12. Esiri, M.M., C.S. Morris, and P.R. Millard, *Sensory and sympathetic ganglia in HIV-1 infection: immunocytochemical demonstration of HIV-1 viral antigens, increased MHC class II antigen expression and mild reactive inflammation.* Journal of the neurological sciences, 1993. **114**(2): p. 178-87.
13. Rizzuto, N., T. Cavallaro, S. Monaco, M. Morbin, B. Bonetti, S. Ferrari, S. Galiazzo-Rizzuto, G. Zanette, and L. Bertolasi, *Role of HIV in the pathogenesis of distal symmetrical peripheral neuropathy.* Acta neuropathologica, 1995. **90**(3): p. 244-50.
14. Pardo, C.A., J.C. McArthur, and J.W. Griffin, *HIV neuropathy: insights in the pathology of HIV peripheral nerve disease.* Journal of the peripheral nervous system : JPNS, 2001. **6**(1): p. 21-7.
15. Polydefkis, M., C.T. Yiannoutsos, B.A. Cohen, H. Hollander, G. Schifitto, D.B. Clifford, D.M. Simpson, D. Katzenstein, S. Shriver, P. Hauer, A. Brown, A.B. Haidich, L. Moo, and J.C. McArthur, *Reduced intraepidermal nerve fiber density in HIV-associated sensory neuropathy.* Neurology, 2002. **58**(1): p. 115-9.
16. Lakritz, J.R., A. Bodair, N. Shah, R. O'Donnell, M.J. Polydefkis, A.D. Miller, and T.H. Burdo, *Monocyte Traffic, Dorsal Root Ganglion Histopathology, and Loss of Intraepidermal Nerve Fiber Density in SIV Peripheral Neuropathy.* The American journal of pathology, 2015. **185**(7): p. 1912-23.
17. Laast, V.A., B. Shim, L.M. Johanek, J.L. Dorsey, P.E. Hauer, P.M. Tarwater, R.J. Adams, C.A. Pardo, J.C. McArthur, M. Ringkamp, and J.L. Mankowski, *Macrophage-mediated dorsal root ganglion damage precedes altered nerve conduction in SIV-infected macaques.* The American journal of pathology, 2011. **179**(5): p. 2337-45.
18. Eilers, H. and M.A. Schumacher, *Mechanosensitivity of Primary Afferent Nociceptors in the Pain Pathway*, in *Mechanosensitivity in Cells and Tissues*, A. Kamkin and I. Kiseleva, Editors. 2005: Moscow.
19. Sandborn, W.J. and T.A. Yednock, *Novel approaches to treating inflammatory bowel disease: targeting alpha-4 integrin.* The American journal of gastroenterology, 2003. **98**(11): p. 2372-82.
20. Polman, C.H., P.W. O'Connor, E. Havrdova, M. Hutchinson, L. Kappos, D.H. Miller, J.T. Phillips, F.D. Lublin, G. Giovannoni, A. Wajgt, M. Toal, F. Lynn, M.A. Panzara, and A.W. Sandrock, *A randomized, placebo-controlled trial of natalizumab for relapsing multiple sclerosis.* The New England journal of medicine, 2006. **354**(9): p. 899-910.
21. Lakritz, J.R., D. Thibault, J.A. Robinson, J. Campbell, A.D. Miller, K. Williams, and T.H. Burdo, *alpha4-Integrin Antibody Treatment Blocks Monocyte/Macrophage Traffic to, Vascular Cell Adhesion Molecule-1 Expression in, and Pathology of the Dorsal Root Ganglia in an SIV*

Macaque Model of HIV-Peripheral Neuropathy. The American journal of pathology, 2016.
22. Paiardini, M. and M. Muller-Trutwin, *HIV-associated chronic immune activation.* Immunological reviews, 2013. **254**(1): p. 78-101.
23. Gordon, S. and P.R. Taylor, *Monocyte and macrophage heterogeneity.* Nature reviews. Immunology, 2005. **5**(12): p. 953-64.
24. Mills, C.D., K. Kincaid, J.M. Alt, M.J. Heilman, and A.M. Hill, *M-1/M-2 macrophages and the Th1/Th2 paradigm.* Journal of immunology, 2000. **164**(12): p. 6166-73.
25. Sica, A., M. Erreni, P. Allavena, and C. Porta, *Macrophage polarization in pathology.* Cellular and molecular life sciences : CMLS, 2015. **72**(21): p. 4111-26.
26. Martinez, F.O. and S. Gordon, *The M1 and M2 paradigm of macrophage activation: time for reassessment.* F1000prime reports, 2014. **6**: p. 13.
27. Wynn, T.A., A. Chawla, and J.W. Pollard, *Macrophage biology in development, homeostasis and disease.* Nature, 2013. **496**(7446): p. 445-55.
28. Keswani, S.C., C.A. Pardo, C.L. Cherry, A. Hoke, and J.C. McArthur, *HIV-associated sensory neuropathies.* AIDS, 2002. **16**(16): p. 2105-17.
29. Soulas, C., C. Conerly, W.K. Kim, T.H. Burdo, X. Alvarez, A.A. Lackner, and K.C. Williams, *Recently infiltrating MAC387(+) monocytes/macrophages a third macrophage population involved in SIV and HIV encephalitic lesion formation.* The American journal of pathology, 2011. **178**(5): p. 2121-35.
30. Geissmann, F., S. Jung, and D.R. Littman, *Blood monocytes consist of two principal subsets with distinct migratory properties.* Immunity, 2003. **19**(1): p. 71-82.
31. Roszer, T., *Understanding the Mysterious M2 Macrophage through Activation Markers and Effector Mechanisms.* Mediators of inflammation, 2015. **2015**: p. 816460.
32. Herbein, G. and A. Varin, *The macrophage in HIV-1 infection: from activation to deactivation?* Retrovirology, 2010. **7**: p. 33.
33. Williams-Ashman, H.G. and A. Schenone, *Methyl glyoxal bis(guanylhydrazone) as a potent inhibitor of mammalian and yeast S-adenosylmethionine decarboxylases.* Biochemical and biophysical research communications, 1972. **46**(1): p. 288-95.
34. Van den Bossche, J., W.H. Lamers, E.S. Koehler, J.M. Geuns, L. Alhonen, A. Uimari, S. Pirnes-Karhu, E. Van Overmeire, Y. Morias, L. Brys, L. Vereecke, P. De Baetselier, and J.A. Van Ginderachter, *Pivotal Advance: Arginase-1-independent polyamine production stimulates the expression of IL-4-induced alternatively activated macrophage markers while inhibiting LPS-induced expression of inflammatory genes.* Journal of leukocyte biology, 2012. **91**(5): p. 685-99.
35. Niemi, J.P., A. DeFrancesco-Lisowitz, L. Roldan-Hernandez, J.A. Lindborg, D. Mandell, and R.E. Zigmond, *A critical role for macrophages near axotomized neuronal cell bodies in stimulating nerve regeneration.*

The Journal of neuroscience : the official journal of the Society for Neuroscience, 2013. **33**(41): p. 16236-48.
36. Barrette, B., M.A. Hebert, M. Filali, K. Lafortune, N. Vallieres, G. Gowing, J.P. Julien, and S. Lacroix, *Requirement of myeloid cells for axon regeneration.* The Journal of neuroscience : the official journal of the Society for Neuroscience, 2008. **28**(38): p. 9363-76.
37. Lakritz, J.R., J.A. Robinson, M.J. Polydefkis, A.D. Miller, and T.H. Burdo, *Loss of intraepidermal nerve fiber density during SIV peripheral neuropathy is mediated by monocyte activation and elevated monocyte chemotactic proteins.* Journal of neuroinflammation, 2015. **12**: p. 237.
38. Evans, S.R., A.J. Lee, R.J. Ellis, H. Chen, K. Wu, R.J. Bosch, and D.B. Clifford, *HIV peripheral neuropathy progression: protection with glucose-lowering drugs?* Journal of neurovirology, 2012. **18**(5): p. 428-33.
39. Ingersoll, M.A., A.M. Platt, S. Potteaux, and G.J. Randolph, *Monocyte trafficking in acute and chronic inflammation.* Trends in immunology, 2011. **32**(10): p. 470-7.
40. Burdo, T.H., J. Walker, and K.C. Williams, *Macrophage Polarization in AIDS: Dynamic Interface between Anti-Viral and Anti-Inflammatory Macrophages during Acute and Chronic Infection.* Journal of clinical & cellular immunology, 2015. **6**(3).
41. Burdo, T.H., C. Soulas, K. Orzechowski, J. Button, A. Krishnan, C. Sugimoto, X. Alvarez, M.J. Kuroda, and K.C. Williams, *Increased monocyte turnover from bone marrow correlates with severity of SIV encephalitis and CD163 levels in plasma.* PLoS pathogens, 2010. **6**(4): p. e1000842.
42. White, F.A., J. Sun, S.M. Waters, C. Ma, D. Ren, M. Ripsch, J. Steflik, D.N. Cortright, R.H. Lamotte, and R.J. Miller, *Excitatory monocyte chemoattractant protein-1 signaling is up-regulated in sensory neurons after chronic compression of the dorsal root ganglion.* Proceedings of the National Academy of Sciences of the United States of America, 2005. **102**(39): p. 14092-7.
43. Tanaka, T., M. Minami, T. Nakagawa, and M. Satoh, *Enhanced production of monocyte chemoattractant protein-1 in the dorsal root ganglia in a rat model of neuropathic pain: possible involvement in the development of neuropathic pain.* Neuroscience research, 2004. **48**(4): p. 463-9.
44. Thacker, M.A., A.K. Clark, T. Bishop, J. Grist, P.K. Yip, L.D. Moon, S.W. Thompson, F. Marchand, and S.B. McMahon, *CCL2 is a key mediator of microglia activation in neuropathic pain states.* European journal of pain, 2009. **13**(3): p. 263-72.
45. Stavros, K. and D.M. Simpson, *Understanding the etiology and management of HIV-associated peripheral neuropathy.* Current HIV/AIDS reports, 2014. **11**(3): p. 195-201.
46. Planas, R., R. Martin, and M. Sospedra, *Long-term safety and efficacy of natalizumab in relapsing-remitting multiple sclerosis: impact on quality of life.* Patient related outcome measures, 2014. **5**: p. 25-33.

47. Ndhlovu, L.C., T. Umaki, G.M. Chew, D.C. Chow, M. Agsalda, K.J. Kallianpur, R. Paul, G. Zhang, E. Ho, N. Hanks, B. Nakamoto, B.T. Shiramizu, and C.M. Shikuma, *Treatment intensification with maraviroc (CCR5 antagonist) leads to declines in CD16-expressing monocytes in cART-suppressed chronic HIV-infected subjects and is associated with improvements in neurocognitive test performance: implications for HIV-associated neurocognitive disease (HAND).* Journal of neurovirology, 2014. **20**(6): p. 571-82.
48. Rossi, R., M. Lichtner, A. De Rosa, I. Sauzullo, F. Mengoni, A.P. Massetti, C.M. Mastroianni, and V. Vullo, *In vitro effect of anti-human immunodeficiency virus CCR5 antagonist maraviroc on chemotactic activity of monocytes, macrophages and dendritic cells.* Clinical and experimental immunology, 2011. **166**(2): p. 184-90.
49. Kelly, K.M., C.G. Tocchetti, A. Lyashkov, P.M. Tarwater, D. Bedja, D.R. Graham, S.E. Beck, K.A. Metcalf Pate, S.E. Queen, R.J. Adams, N. Paolocci, and J.L. Mankowski, *CCR5 inhibition prevents cardiac dysfunction in the SIV/macaque model of HIV.* Journal of the American Heart Association, 2014. **3**(2): p. e000874.
50. Gates, T.M., L.A. Cysique, K.J. Siefried, J. Chaganti, K.J. Moffat, and B.J. Brew, *Maraviroc-intensified combined antiretroviral therapy improves cognition in virally suppressed HIV-associated neurocognitive disorder.* AIDS, 2016. **30**(4): p. 591-600.
51. Kumar, A. and G. Herbein, *The macrophage: a therapeutic target in HIV-1 infection.* Molecular and cellular therapies, 2014. **2**: p. 10.
52. Kramer, V.G., S. Hassounah, S.P. Colby-Germinario, M. Oliveira, E. Lefebvre, T. Mesplede, and M.A. Wainberg, *The dual CCR5 and CCR2 inhibitor cenicriviroc does not redistribute HIV into extracellular space: implications for plasma viral load and intracellular DNA decline.* The Journal of antimicrobial chemotherapy, 2015. **70**(3): p. 750-6.
53. Visseaux, B., C. Charpentier, G. Collin, M. Bertine, G. Peytavin, F. Damond, S. Matheron, E. Lefebvre, F. Brun-Vezinet, and D. Descamps, *Cenicriviroc, a Novel CCR5 (R5) and CCR2 Antagonist, Shows In Vitro Activity against R5 Tropic HIV-2 Clinical Isolates.* PloS one, 2015. **10**(8): p. e0134904.